Faculty of Natural Science and Technology
Department of Physics

MASTER'S THESIS FOR

JACOB B. KRYVI

TIME DEPENDENT STUDY OF QUANTUM DOTS

Trondheim, June 2009

Supervisor: Jon Andreas Støvneng
Co-Supervisor: Morten Hjorth-Jensen (UiO)

Acknowledgements

This Master's thesis has been written at the Department of Physics at the Norwegian University of Science and Technology (NTNU).

First of all, I would like to thank my supervisors: Jon Andreas Støvneng, at NTNU, for his patience, support and encouragement. Morten Hjorth-Jensen at the University of Oslo, for suggesting the topic of the thesis, and for inviting me to spend a week at the physics department at UiO in March.

I am deeply indebted to Simen Kvaal at the University of Oslo for all the help he has given me during the course of this thesis. He has patiently answered all of my questions, and during my stay at UiO, spent an entire work day teaching me about the relevant topics from numerical analysis I needed for my thesis.

I would like to thank my parents for their support.
And I would like to thank Christine. :-)

Trondheim, June 2009

Jacob B. Kryvi

Contents

Chapter 1

Introduction

In the first half of the 20th century physicists revealed the inner workings of nature at its smallest length and time scales. Nature was found to be described by a framework known as quantum mechanics. Quantum mechanics paints a picture of time and space that seems far removed from what our everyday experience tells us, but it is in no doubt the correct description of nature, having passed careful scrutiny for almost a century.

Driven by the need for ever smaller and more powerful electronic devices, miniaturization technology has reached a point where the structure and composition of nanometre-sized systems can be controlled. Systems of this size can only be understood properly by quantum mechanics. Of particular interest these days, are the so-called *quantum dots*. They are semiconductor devices in which a few electrons can be trapped. They are of great interest due to their potential for technological applications, but are also interesting from a more fundamental point of view, since they offer us a new method of studying many-body quantum systems.

The original aim of this thesis was to look at the dynamics of several interacting particles in a quantum dot, using an electronic structure code for quantum dots developed recently at UiO. It turned out however, that to modify this code to produce the input I needed for studying the time development of the system, would be a much more demanding task than what was originally envisaged. The focus of the thesis is therefore slightly shifted to studying the time-stepping methods themselves, and to outline how we can use these methods to study the dynamics of the charge carriers in quantum dots. A review of the necessary topics from quantum mechanics will be given, where emphasis is put on providing a pedagogical treatment of the material. As this thesis is about quantum dots, I have felt it necessary to include a numerical study of a quantum dot system, even if this system might not be as advanced as what was originally intended. A numerical study of a one-dimensional two-particle coupled quantum dot has therefore been included.

The thesis is structured in the following way: Chapter 2 gives an introduction to quan-

tum dots. Emphasis is here put on the experimental side. In Chapter 3 the quantum many-body problem is reviewed, and an introduction to the most important approximative techniques for solving the many-body problem is given. I will not use any of these methods later in the thesis, at least in the form they are presented here, so they should be considered as background material necessary to understand the literature on quantum dots. Many electronic structure calculations on quantum dots use the methods described in this chapter.

Chapter 4 is without a doubt the thickest chapter of the thesis. I review the problem of solving the time-dependent Schrödinger equation numerically, and present three of the most widely used methods for this task. Such methods are often referred to as *time stepping schemes*. Writing this chapter has been particularly difficult, since as far as I know, no comprehensive and coherent treatment of the topic exists. From a mathematical point of view, the Schrödinger equation is just a particular type of partial differential equations, for which mathematicians have devised numerous solution techniques. However, most of them are ill-suited to the Schrödinger equation due to the requirement of conservation of unitarity on the wave function. Another problem for the physicist with limited background in numerical analysis, is that much of the literature on the numerical methods that might be of interest to apply to the Schrödinger equation, is quite inaccessible to the physicist. I therefore aim to give a thorough and pedagogical introduction to the subject. I then turn the attention to a relatively new time stepping scheme, first proposed by Blanes and Moan in 1999 [1]. This scheme is of interest since it will potentially give us greater accuracy when simulating time-dependent systems at a lower computational cost. A series of numerical experiments is carried out to test whether this claim could be true.

In Chapter 5 I will once again focus the attention on quantum dots. I briefly review some of the physical models used to describe quantum dots, and explain how the time stepping schemes of Chapter 4 can be extended to study the dynamics of electrons in quantum dots. Using the new time stepping scheme of Blanes and Moan, the time evolution of a two-particle system in a quantum dot is studied. Chapter 6 contains the conclusion and suggestions for further work.

Chapter 2

Quantum Dots

Quantum dots are nanometre-sized structures made of semiconductor materials which confine the motion of electrons in all spatial directions. They have been made possible by the ever-advancing sophistication of miniaturization technology. In this chapter I briefly review some background material from solid state theory, discuss how one can manufacture quantum dots and thereby mention the most important types of quantum dots, and discuss evidence of quantum behaviour observed in quantum dots.

2.1 A Short Introduction to the Band Theory of Solids

A great deal of the properties of crystalline materials can be understood from the *band theory* of solids.

The discrete energy levels of isolated atoms give rise to bands of energies when the atoms are brought together to form a crystal. Energy levels between the bands which no electrons can occupy, are called *band gaps*. A very important consequence of the Pauli exclusion principle is that when an allowed band is completely filled with electrons, the electrons in the band cannot conduct any current. This essentially determines whether the solid is a metal, an insulator or a semiconductor. At zero temperature, semiconductors are in a condition where the electrons reside in a completely filled band called the *valence band* separated by a band gap from the so called *conduction band*. To conduct current, electrons have to be excited from the valence band into the conduction band. This can happen at nonzero temperatures by thermal excitations. In fact, it is only the size of the band gap that separates a semiconductor from an insulator. These are to be contrasted with the metal, which contains a band that is partly empty and partly filled regardless of temperature.

The properties of the electrons in solids can in principle be found by solving the Schrödinger equation for the system. For solids we are considering systems of $\sim 10^{23}$ interacting

particles, so we have to make approximations to extract the essence of the physics involved. The fact that crystalline solids are periodic simplifies matters enormously. The nuclei are considered to be fixed in position, and the Schrödinger equation is solved for the electrons moving in the background potential set up by the nuclei. The fluctuations created by lattice vibrations and scattering of electrons from other electrons are removed from the problem and treated later via perturbation theory, should this be necessary. The calculation of the electronic structure in solids is in this way reduced to a one-particle problem.

Much information about the solution itself can be found by examining the consequences of the periodicity of the potential. The solution to the Schrödinger equation for a periodic potential $U(\mathbf{r}) = U(\mathbf{r} + \mathbf{R})$, has the general form

$$\psi_{\mathbf{k}}(\mathbf{r}) = \mathrm{e}^{i\mathbf{k}\cdot\mathbf{r}} u_{\mathbf{k}}(\mathbf{r}), \qquad u_{\mathbf{k}}(\mathbf{r}) = u_{\mathbf{k}}(\mathbf{r} + \mathbf{R}) \tag{2.1}$$

which is to say, a plane wave $\mathrm{e}^{i\mathbf{k}\cdot\mathbf{r}}$ multiplied by a function $u_{\mathbf{k}}(\mathbf{r})$ of the same periodicity as the crystal. This result is known as *Bloch's theorem*. In the perfectly periodic background potential of the crystal, the electron propagates freely without scattering, regardless of the form of $U(\mathbf{r})$.

What happens then to the electron when we apply an external field to the solid? Including the time-dependent part of the Bloch wave functions of Eq. (2.1), we get $\Psi_{\mathbf{k}}(\mathbf{r}, t) = u_{\mathbf{k}}(\mathbf{r}) \exp(i(\mathbf{kr} - Et/\hbar))$, to which we can associate a frequency $\omega = E/\hbar$. By superimposing these wave functions we can represent a localized electron. The group velocity of a wave packet centered around a wave vector $\mathbf{k}$ is $\mathbf{v}_g \equiv \nabla_{\mathbf{k}}\omega = \nabla_{\mathbf{k}}E/\hbar$. The work done by the external field in the time interval Δt is $\Delta W = \mathbf{F}_{\mathrm{Ext}} \cdot \mathrm{d}\mathbf{s} = \mathbf{F}_{\mathrm{Ext}} \cdot \mathbf{v}_g \Delta t$. But we also have that $\Delta W = \Delta E = \nabla_{\mathbf{k}} E \cdot \Delta\mathbf{k} = \hbar \mathbf{v}_g \cdot \Delta\mathbf{k}$. Upon comparing the two and using that it holds for any $\mathbf{v}_g$ we have $\hbar\Delta\mathbf{k} = \mathbf{F}_{\mathrm{Ext}}\Delta t$. So, for the electron under the influence of an external field we see that

$$\hbar \frac{\mathrm{d}\mathbf{k}}{\mathrm{d}t} = \mathbf{F}_{\mathrm{Ext}}. \tag{2.2}$$

When comparing this with Newton's equation of motion we see that the electrons move under external forces as if it had the momentum $\hbar\mathbf{k}$. The quantity $\hbar\mathbf{k}$ is called *crystal momentum*, and is not the true momentum of the electrons, but a quantity that also contains the effect of the underlying lattice. The effect of all this is that the electrons in the crystal behave under external fields as if they were free particles, but of a different mass. This mass is called *effective mass*. As an example, in GaAs the effective mass is $m^* = 0.067 m_e$, where m_e is the electron mass. When investigating the effects of, say, an electric field on the electrons in a quantum dot, we may simply substitute their mass with the effective mass.

By producing thin films of layered semiconductor materials it is possible to produce situations where electrons are confined to move only in one of the layers. This quasi

two-dimensional state is often called a *quantum well*. This can be achieved by choosing materials whose band gaps line up in a certain way at the intersection. Roughly speaking, when the bottom of the conduction band of the mid layer is below the bottom of the conduction band of the surrounding layers, and the top of the valence band of the mid layer is above the top of the valence band of the surrounding layers, both electrons and holes may be confined to the mid layer. A simplified diagram of this situation is shown in Figure 2.1.

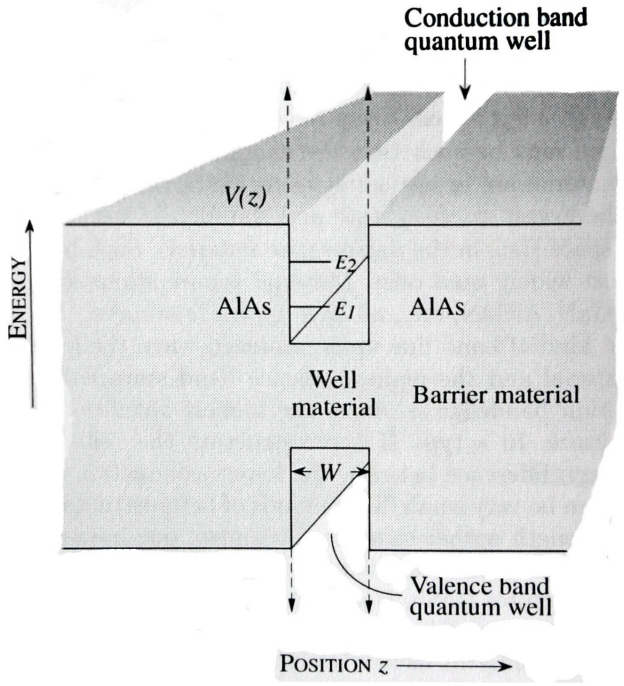

Figure 2.1: *A schematic diagram of the quantum well. Image taken from [2].*

2.2 Fabrication

2.2.1 A Top-Down Approach

The first successful way of making quantum dots was to start with a quantum well structure and using etching techniques to reduce the spatial extent of the well until the system became small enough for evidence of confinement in all directions to become visible. Quantum wells are formed in semiconductor heterostructures by having a semiconductor material sandwiched between two layers of a material with a wider bandgap. The quantum wells are made by epitaxial crystal growth on a monocrystalline substrate. Here, *substrate* refers to the base material on which the deposited

layers are said to be grown. *Epitaxial growth* means that the material is grown "layer by layer", so to speak. The substrate is made with bulk crystal growth techniques, and is then sliced into thin wafers and polished.

The two main epitaxial growth techniques used for making quantum wells are molecular beam epitaxy (MBE) and metal-organic chemical vapour deposition (MOCVD). With these techniques the growth can be controlled to monolayer precision. I will only describe the MBE technique here.

Ultra-pure samples of elements (gallium and arsenic in our case) are heated until they slowly begin to sublimate. The gaseous elements are then let into the growth chamber where they condense on the substrate. Different elements may react with each other, in the case of gallium and arsenic, forming single-crystal gallium arsenide, GaAs. The growth rate in MBE is about one monolayer per second and this slow rate allows one to modify the composition of the growing crystal with monolayer control. MBE takes place in ultra high vacuum (below 10^{-6} Pa).

While the epitaxial techniques for two-dimensional confinement are well-established and conceptually simple, confinement in the other directions involves considerably more sophisticated techniques.

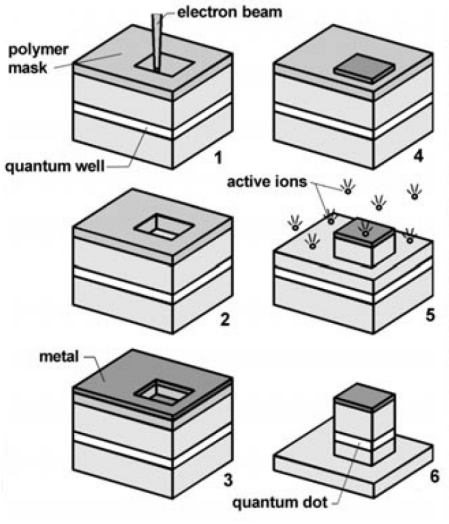

(a) The etching process.

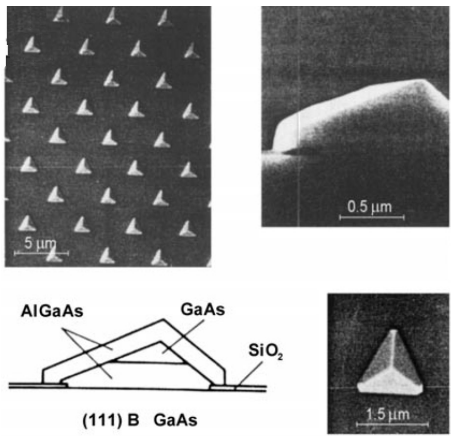

(b) Selective growth QDs

Figure 2.2: *Outline of the etching process (left), and SEM images of selective growth quantum dots created on the surface of GaAs (right). Both images are taken from [3].*

Etching Methods As mentioned, etching techniques were the first successful way of achieving confinement in all dimensions. For a schematic overview of the process, see Figure 2.2a. The surface of the heterostructure containing the quantum well is first

covered with a polymer mask. By using lithography a pattern is "burned" into the mask. Owing to the precision needed, electron or ion lithography is used instead of light lithography. The entire surface is then covered with a thin metal layer. Using a special solution, the polymer mask and metal film are removed, except for the areas exposed to the electron/ion beam where the metal still remains. Finally, by chemical etching the areas not protected by the metal film are removed, so that what remains are slim pillars of the quantum well material. The motion of the electrons which were confined to a plane by the quantum well are now further restricted to an area of $10-100$ nm in diameter. GaAs is the preferred material for creating quantum dots by etching methods. Quantum dots made this way are often called *vertical quantum dots*.

Confinement By Electric Fields Another approach to creating quantum dots by starting with a quantum well structure, is to confine the electrons by means of an electric field. Small electrodes are deposited on the surface of the quantum well using lithographic techniques. Application of a voltage to the electrodes produces an electric field which localizes the electrons in the two-dimensional electron gas. By different etching patterns we may create either a single quantum dot or a large array of quantum dots. An advantage of using this method is that by tuning the voltage we can change the properties of the quantum dots, whereas in the case of the etching method we would have to go through the complicated process of manufacturing a new sample. Quantum dots made this way are often called *lateral quantum dots*. Since they rely on an applied electric field to produce confinement their potential for applications is of course different from the other structures using physical boundaries. An example of a double quantum dot can be seen in Figure 2.3

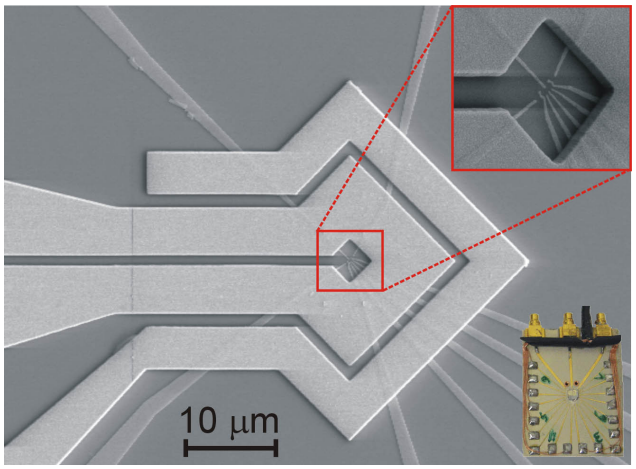

Figure 2.3: *Confinement by using electric fields: SEM picture of a double quantum dot set up by electrostatic gates applied to a sandwich of GaAs/AlGaAs/GaAs, surrounded by a loop antenna that produces a magnetic field. Image taken from [4].*

2.2.2 A Bottom-Up Approach

The etching method is an example of a "top-down" method. It can be likened to sculpting from a block of stone. A piece of base material is gradually eroded until the desired shape is achieved. Quantum dots can also be made using a "bottom-up" approach. Atom upon atom the dot is gradually built up. As millions of atoms are needed, it is vital that the dot organizes itself into the right shape.

Selective Growth One example of a bottom-up method is using selective growth. Here one covers the surface of the substrate with a mask and etches miniature geometric shapes (most often triangles) onto it. On the surface not covered by the mask the quantum dot is grown using the MOCVD method. A scannning electron micrograph of quantum dots in the shape of tetrahedral pyramids created in this way can be seen in Figure 2.2b.

Self-Organized Growth Another very promising method is self-organized growth. When the lattice spacings of the substrate and the deposited material differ considerably (roughly by more than 2.5% [2]), the growth starts out monolayer by monolayer. However, since stress builds up in the structure, at a critical thickness the spontaneous formation of randomly distributed islets of regular shape and size occurs. Both pyramid-like and cylindrical structures can be made this way. Under proper growth conditions, these self-assembled quantum dots have the important property of being defect-free. The most commonly used pair of semiconductor materials used in this method is GaAs and InAs. An AFM image of quantum dots made by self-organized growth can be found in Figure 2.4.

2.3 Possible Applications of Quantum Dots

It is not without reason that intense effort is being directed to research on quantum dots, particularly on the experimental level. They have many properties which make them suitable for use in several novel technological applications.

At the top of our wish list is the use of quantum dots as the hardware elements of quantum computers. The idea of making use of quantum mechanical phenomena, such as superposition and entanglement, to perform operations on data was conceived in the early 80s by Feynman and others. It was at that time also realised that a computer built on these principles, a so-called *quantum computer*, would be able to solve certain types of problems, such as factorization and simulation of quantum systems, much faster than a traditional computer. The "bit" in a quantum computer[1] could be realised for example

[1] Also known as the *qubit*.

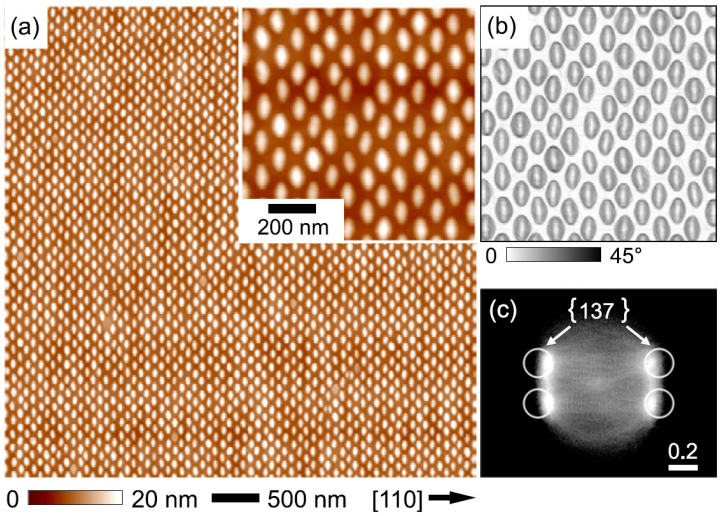

Figure 2.4: *Self-Organized growth:* ***(a)*** *An AFM image of an array of quantum dots consisting of In(Ga)As QDs grown on a QD seed layer on a patterned hole array. The pattern period is* $103\ \mathrm{nm}$ *and the image shows an area of* $5 \times 5\mu\mathrm{m}^2$ *.* ***(b)*** *The same part as the inset in (a) is shown here in grayscale corresponding to the local surface slope.* ***(c)*** *Facet plot obtained from the AFM shown in (b). The image is taken from [5].*

by utilizing the spins of coupled single-electron quantum dots [6]. A major problem which needs to be overcome before this becomes technologically feasible is that of decoherence. Due to lattice vibrations in our semiconductor at nonzero temperatures, our carefully prepared quantum state breaks down very quickly.

Another application of quantum dots which we are more likely to live to see, is their use in photovoltaic cells. Quantum dots promise to increase efficiency in solar cells by producing more than one electron-hole pair from each photon of incoming sunlight. Quantum dot photovoltaics could also theoretically be cheaper to manufacture than traditional solar panels.

Quantum dots have already found use as agents for cellular imaging in biology. They have many advantages to the fluorescent organic dyes traditionally used, being optically superior, and are much less susceptible to photobleaching. Before quantum dots become widespread in medical imaging and are approved for clinical use, much research needs to be done on the toxicology of quantum dots.

Other technological applications of quantum dots include using the sharper density of states of quantum dots to improve existing laser technology and to make new types of light-emitting diodes. But of course, the most important application of quantum dots might just turn out to be the one that nobody has thought of yet.

2.4 Quantum Mechanics and Quantum Dots

Technological applications aside, quantum dots are also interesting for studying fundamental quantum systems. In analogy with atoms, quantum dots are sometimes called *artificial atoms*, or *designer atoms*. Much of the interest in quantum dots is motivated by the fact that experiments can be carried out to investigate quantum effects inaccessible for real atoms. One example of this is the effect of an applied magnetic field on the energy levels. The effect of a 1 Tesla magnetic field on a quantum dot is comparable with the effect of a field of one million Tesla on a real atom [7]. Quantum dots can also be used to study quantum many-body effects, especially since correlation effects play a greater role in quantum dots than in atoms. One of the clearest examples of quantum effects in quantum dots is the shell structure exhibited by the energy levels in highly symmetric, vertical quantum dots. I will discuss this effect briefly, along with the main experimental methods for quantum dots.

2.4.1 Shell Structure

A major breakthrough in the study of the quantum effects in quantum dots was the discovery of shell structure in the energy spectra of small, vertical quantum dots in 1996 [8]. Shell structure is a distinguishing feature of quantum many-body systems with a high degree of symmetry, and is observed in atoms and nuclei. With this discovery, one had a clear analogy between quantum dots and atoms.

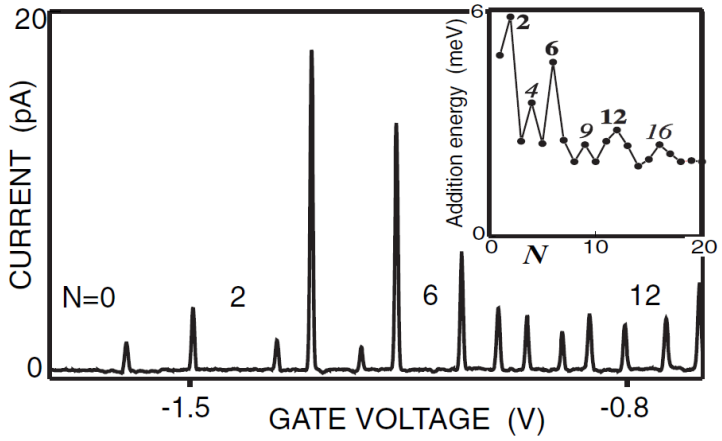

Figure 2.5: *Coulomb blockade spectroscopy on a vertical, cylindrical quantum dot: The larger image shows the current flowing through the quantum dot upon varying the gate voltage. The inset shows the addition energy of adding an electron to the dot plotted against the number of electrons in the dot. The image is taken from [9].*

Shell structure was first demonstrated by Coulomb blockade spectroscopy on vertical

quantum dots. A result from such an experiment is seen in Figure 2.5. From the inset in this figure, we see that when the number of electrons in the dot has certain values, the energy needed to add another electron to the dot is particularly large. When this electron is added, the number of electrons in the dot is a so-called *magic number*, a terminology borrowed from nuclear physics for which nuclei with the number of protons or neutrons equal to the magic numbers are particularly stable. In vertical quantum dots it is found experimentally that the lowest magic numbers are 2, 6, 12 and 20. Midway between these magic numbers, at electron numbers of 4, 9 and 16, we see that the addition energy rises as well. This substructure reflects how the interactions between electrons can influence the filling of energy states. In atomic physics these effects are formulated as Hund's rules, which state that electrons enter a shell with parallel spins until the shell is half full, and then enter with opposite spin.

For atoms the shells are demonstrated by the maxima of the ionization energies of neutral atoms for the atomic numbers $Z = 2, 10, 18 \ldots$, which correspond to the noble gases. These shells can be explained by assuming that the electrons move in a mean-field potential consisting of the Coulomb potential set up by the nucleus and the averaged attractions between the electrons. In nuclei, the lowest magic numbers are 2, 8, 20, 28 and 50. These numbers can be arrived at by assuming that the nucleons moved in a mean-field potential approximated as an isotropic harmonic oscillator plus a spin-orbit interaction term.

The question is then, in what potential do the electrons move to give rise to the magic numbers of the quantum dots? It can be shown that the magic numbers for the quantum dot are reproduced by assuming that potential is a circularly symmetric two-dimensional harmonic oscillator. The states we get when solving the Schrödinger equation with this potential in (polar coordinates) are called *Fock-Darwin states*. I will not state these explicitly here, as they are not central to this thesis, but note that they are characterized by two quantum numbers n (the nodal quantum number) and m (the azimuthal quantum number) and have the energy

$$E_{nm} = \hbar\omega_0 \left(2n + |m| + 1\right), \tag{2.3}$$

where ω_0 is the characteristic frequency of the oscillator potential. By defining the *shell number* R, by $R \equiv 2n + |m|$, we see that by including electron spin, the number of Fock-Darwin states with an energy less than or equal to that given by the shell number R is $(R + 2)(R + 1)$. This reproduces the "magic numbers" of the quantum dots.

2.4.2 Experimental Techniques

The confinement energy of the electrons in quantum dots are typically in the milli electronvolt range. To resolve such small energies experimentally, it is necessary to conduct the experiments at very low temperatures so as to avoid the signal from being obscured

by thermal fluctuations. I will briefly describe the two most prevalent techniques for stuying quantum phenomena in quantum dots.

Coulomb Blockade Spectroscopy

An important experimental technique for studying quantum many-body effects in quantum dots is based on electron tunnelling. The idea is to isolate the quantum dot from its surroundings by insulating barriers. It then confines a well-defined number of electrons N, and in view of the Pauli exclusion principle, loosely speaking, any electron entering the dot must occupy a new quantum state. The experiment aims at measuring the difference in energy between a state of N electrons and a state of $N + 1$ electrons.

A small bias voltage is set up over the vertical quantum dot, and another voltage is applied to metal gates around the dot [9]. By varying the gate voltage the diameter of the dot can effectively be adjusted, thereby shifting the quantized energy levels of the dot. By measuring the current flowing through the dot as function of gate voltage, the resulting plot shows sharp periodic peaks, between which no current will flow, see Figure 2.5. This addition energy is (unfortunately) dominated by an essentially classical effect that arises from the discrete unit of charge of the electron: The Coulomb repulsion between electrons on the dot results in a considerable energy cost for adding an extra electron charge. Extra energy is therefore needed, and no current will flow until increasing the voltage to provide this energy. This phenomenon is known as *Coulomb blockade*.

Models have been devised (see [10]) to account for the contribution to the addition energy stemming from the disrete unit of charge of the electrons. If one can obtain a very clean signal, it is possible to see evidence of quantum confinement, and in particular that of shell structure. To obtain such clean signals it is necessary to operate at very low temperatures ($T < 4$ K).

Far-Infrared Spectroscopy

The idea of far-infrared spectroscopy is to use light of a suitable wavelength to induce excitation between energy levels in the quantum dot and measure the absorption spectrum of transmitted light through the sample. To get a measurable signal, it is necessary to study arrays of quantum dots. It is difficult though, to fabricate arrays where the quantum dots are equal enough in size and shape for the quantum effects to be discernable.

Chapter 3

The Quantum Many-Body Problem and Approximation Methods

All properties of a many-body system can in principle be deduced from solving the corresponding Schrödinger equation for the system. Unfortunately, in almost all cases this equation is far too complex to allow solution. Aided by the computational power offered by modern computers, enormous progress has been made for finding approximative solutions of the Schrödinger equation for systems of several interacting particles. The practitioners of the science of many-body systems work on topics as different as nuclear physics and quantum chemistry. But they both share a common goal: To solve the Schrödinger equation for as many particles as needed, with great accuracy and for the least computational cost.

I will in this chapter give an introduction to the quantum many-body problem, and describe three of the most common approximation schemes for solving the Schrödinger equation: The Hartree-Fock method, density functional theory, and the full configuration interaction method.

3.1 Recap of the Quantum Many-Body Problem

In quantum mechanics, a system of N particles is represented by a wave function $\Psi\left(\mathbf{x}_1, \mathbf{x}_2, \ldots, \mathbf{x}_N\right)$ whose dynamics is governed by the Schrödinger equation

$$i\hbar\frac{\partial}{\partial t}\Psi\left(\mathbf{x}_1, \mathbf{x}_2, \ldots, \mathbf{x}_N, t\right) = H\Psi\left(\mathbf{x}_1, \mathbf{x}_2, \ldots, \mathbf{x}_N, t\right). \tag{3.1}$$

Here, $\mathbf{x}_j = (\mathbf{r}_j, s_j)$ represents both the position and spin coordinates of particle j. The Schrödinger equation applies to an enormous range of systems in nature. It tells us, in

principle, the properties of systems as different as electrons in a solid, to nucleons in an atomic nucleus, or even bound states of heavy quarks (quarkonium). I will here have the atomic or molecular problem in mind when discussing its applications. I will work in the non-relativistic regime, and ignore a number of spin-related effects, such as spin-orbit coupling. If the Hamiltonian is independent of time, there exist stationary-state solutions of the form

$$\Psi\left(\mathbf{x}_1, \mathbf{x}_2, \ldots, \mathbf{x}_N, t\right) = \Psi\left(\mathbf{x}_1, \mathbf{x}_2, \ldots, \mathbf{x}_N\right) \mathrm{e}^{-iEt/\hbar}. \tag{3.2}$$

The equation for the spatial part becomes

$$H\Psi\left(\mathbf{x}_1, \mathbf{x}_2, \ldots, \mathbf{x}_N\right) = E\Psi\left(\mathbf{x}_1, \mathbf{x}_2, \ldots \mathbf{x}_N\right), \tag{3.3}$$

which is the familiar time independent Schrödinger equation, but for N particles. I will use the later sections of this chapter to discuss various methods for solving this equation approximatively. For a solid, or a molecular system, the Hamiltonian is

$$\begin{aligned} H = &-\sum_i \frac{\hbar^2}{2m_e}\nabla_i^2 - \sum_I \frac{\hbar^2}{2M_I}\nabla_I^2 + \frac{1}{2}\sum_{i,j,i\neq j} \frac{1}{4\pi\epsilon_0}\frac{e^2}{|\mathbf{r}_i - \mathbf{r}_j|} \\ &- \sum_{i,I} \frac{1}{4\pi\epsilon_0}\frac{Z_I e^2}{|\mathbf{r}_i - \mathbf{R}_I|} + \frac{1}{2}\sum_{I,J,I\neq J} \frac{1}{4\pi\epsilon_0}\frac{Z_I Z_J e^2}{|\mathbf{R}_I - \mathbf{R}_J|}. \end{aligned} \tag{3.4}$$

Indices in capital letters represent the nuclei while small letters represent the electrons. Since the nuclei are much more massive than the electrons, the electron-proton mass ratio being $m_e/M_p \approx 1/1836$, it is a good approximation to consider the nuclei to be stationary compared to the electrons. This way of freezing out the degrees of freedom of the nuclei is referred to as the *Born-Oppenheimer approximation*, or the *adiabatic approximation.* The resulting Hamiltonian is

$$H = -\sum_i \frac{\hbar^2}{2m_e}\nabla_i^2 + \frac{1}{2}\sum_{i,j,i\neq j} \frac{1}{4\pi\epsilon_0}\frac{e^2}{|\mathbf{r}_i - \mathbf{r}_j|} - \sum_{i,I} \frac{1}{4\pi\epsilon_0}\frac{Z_I e^2}{|\mathbf{r}_i - \mathbf{R}_I|}. \tag{3.5}$$

The positions of the nuclei $\mathbf{R}_I$ are here considered as parameters in the Hamiltonian, so we have reduced the dimensionality of the problem by removing these degrees of freedom. As this thesis is about quantum dots it would be appropriate to give an example of a Hamiltonian of a quantum dot system. It is common to model quantum dots as electrons moving in a two-dimensional harmonic oscillator potential. The Hamiltonian for a quantum dot system, of N electrons, in the absence of external electromagnetic fields, is

$$H = \sum_{i=1}^{N} \left[-\frac{\hbar^2}{2m^*} \nabla_i^2 + \frac{1}{2} m^* \omega_0^2 \left(x_i^2 + y_i^2 \right) \right] + \frac{1}{2} \sum_{i,j,i \neq j}^{N} \frac{e^2}{4\pi\epsilon_r \epsilon_0} \frac{1}{r_{ij}}, \tag{3.6}$$

where m^* is the reduced mass of the electrons, and ϵ_r is the relative permittivity of the material. Generally, the Hamiltonian can be separated into one-particle operators $h_i = T_i + V_i$ and two-particle operators W_{ij}

$$H = \sum_{i=1}^{N} h_i + \frac{1}{2} \sum_{i,j,i \neq j} W_{ij}. \tag{3.7}$$

If there were no interaction between the particles ($W_{ij} = 0$) the Schrödinger equation then contains a sum of single-particle Hamiltonians, and is trivial to solve since the equation is separable in the coordinates of the different particles. A solution can be written on product form as

$$H\Psi\left(\mathbf{x}_1, \mathbf{x}_2, \ldots, \mathbf{x}_N\right) = E\varphi_{\alpha_1}\left(\mathbf{x}_1\right)\varphi_{\alpha_2}\left(\mathbf{x}_2\right)\ldots\varphi_{\alpha_N}\left(\mathbf{x}_N\right), \tag{3.8}$$

where $\varphi_\mu\left(\mathbf{x}_i\right)$ is an eigenfunction of the single-particle equation

$$h_i\varphi_\mu\left(\mathbf{x}_i\right) = E_\mu\varphi_\mu\left(\mathbf{x}_i\right). \tag{3.9}$$

Due to a particular peculiarity of quantum mechanics this solution never occurs in nature. In quantum mechanics there is no way of keeping track of individual particles when the wave functions of identical particles overlap. In the solution of Eq. (3.8) we are effectively saying that particle 1 is in the state φ_{α_1} while particle 2 is in the state φ_{α_2}, which in quantum mechanics makes no sense since there is no way of telling the particles apart.

We will discuss the consequences of this in a little more detail. To formalize the problem we define the permutation operator P_{ij} which interchanges the particles i and j

$$P_{ij}\Psi\left(\mathbf{x}_1, \ldots, \mathbf{x}_i, \ldots, \mathbf{x}_j, \ldots, \mathbf{x}_N\right) = \Psi\left(\mathbf{x}_1, \ldots, \mathbf{x}_j, \ldots, \mathbf{x}_i, \ldots, \mathbf{x}_N\right). \tag{3.10}$$

Because the particles are identical, the Hamiltonian must be symmetric in the interchange of any pair of particles, and so the operator P_{ij} must commute with the Hamiltonian,

$$[P_{ij}, H] = 0. \tag{3.11}$$

This implies that we can find a complete set of functions that are simultaneous eigenstates of both H and P_{ij} . Successive interchanges bring back the original configuration, that is, $P_{ij}^2 = I$. The eigenvalues of P_{ij} are therefore ± 1. The wave functions with the eigenvalue $+1$

$$P_{ij}\Psi_S(\mathbf{x}_1,\ldots,\mathbf{x}_i,\ldots,\mathbf{x}_j,\ldots,\mathbf{x}_N) = +\Psi_S(\mathbf{x}_1,\ldots,\mathbf{x}_i,\ldots,\mathbf{x}_j,\ldots,\mathbf{x}_N) \tag{3.12}$$

are said to be *symmetric*, while the wave functions with eigenvalue -1

$$P_{ij}\Psi_A(\mathbf{x}_1,\ldots,\mathbf{x}_i,\ldots,\mathbf{x}_j,\ldots,\mathbf{x}_N) = -\Psi_A(\mathbf{x}_1,\ldots,\mathbf{x}_i,\ldots,\mathbf{x}_j,\ldots,\mathbf{x}_N) \tag{3.13}$$

are said to be *antisymmetric*.

The two types of states Ψ_S and Ψ_A are thought to be sufficient to describe all systems of identical particles[1]. This is known as the *symmetrization postulate*. Particles having states described by completely symmetric wave functions are called bosons, and they are said to obey Bose-Einstein statistics. Experiment show that particles of zero or integer spin are bosons ($s = 0, 1, 2, \ldots$). On the other hand, particles having states described by totally antisymmetric functions are called fermions, and they are said to obey Fermi-Dirac statistics. Experiments shows that particles of half-odd integer spin are fermions ($s = 1/2, 3/2, 5/2, \ldots$). In non-relativistic quantum mechanics the connection between spin and statistics must be taken as a fundamental axiom. It is one of the greatest triumphs of quantum field theory that this connection can be proven to be a consequence of the theory itself.

Let us now turn to the question of how to construct a totally antisymmetric and normalized wave function for the case of N non-interacting fermions. Such a state can be constructed from the single-particle states if we take an antisymmetric sum of such products with the electronic coordinates permuted in all possible ways

$$\Psi(\mathbf{x}_1,\mathbf{x}_2,\ldots,\mathbf{x}_N) = \frac{1}{\sqrt{N!}}\sum_p (-1)^p \varphi_{\alpha_1}(\mathbf{x}_1)\varphi_{\alpha_2}(\mathbf{x}_2)\cdots\varphi_{\alpha_N}(\mathbf{x}_N). \tag{3.14}$$

This is just a compact way of writing the determinant

$$\Psi(\mathbf{x}_1,\mathbf{x}_2,\ldots,\mathbf{x}_N) = \frac{1}{\sqrt{N!}}\begin{vmatrix} \varphi_{\alpha_1}(\mathbf{x}_1) & \varphi_{\alpha_2}(\mathbf{x}_1) & \ldots & \varphi_{\alpha_N}(\mathbf{x}_1) \\ \varphi_{\alpha_1}(\mathbf{x}_2) & \varphi_{\alpha_2}(\mathbf{x}_2) & \ldots & \varphi_{\alpha_N}(\mathbf{x}_2) \\ \vdots & \vdots & & \vdots \\ \varphi_{\alpha_1}(\mathbf{x}_N) & \varphi_{\alpha_2}(\mathbf{x}_N) & \ldots & \varphi_{\alpha_N}(\mathbf{x}_N). \end{vmatrix} \tag{3.15}$$

[1]This is indeed true for elementary particles. For quasiparticles in two-dimensional systems however, Leinaas and Myrheim (1977) have shown that the statistics can vary continuously between Fermi-Dirac and Bose-Einstein statistics. These types of "particles" are called *anyons*.

This determinant is commonly referred to as the Slater determinant. It must be emphasized that the Slater determinant can only be the exact solution to the many-body problem when there is no interaction between the particles. Since a degree of statistical correlation is always present due to the antisymmetrization of the wave function, the Slater determinant is the state of minimal correlation between the particles.

3.2 Approximation Methods

For interacting particles, it is impossible to find analytic solutions for systems of more than two particles. For two particles interacting through a central potential, analytic solutions can sometimes be found by solving the problem in centre of mass and relative coordinates. For anything more complicated, approximation techniques must be used. Many ways of approximating the many-body problem is built on one, or a combination of two basic results of quantum mechanics: The variational principle, and time-independent perturbation theory.

The variational principle, or the Rayleigh-Ritz variational principle as it is sometimes called, gives us an upper bound to the ground state energy E_0. It states that for any wave function Ψ, the following inequality holds:

$$E_0 \leq \frac{\langle \Psi | H | \Psi \rangle}{\langle \Psi | \Psi \rangle} \tag{3.16}$$

For simple systems, such as He and H^-, it is possible to get very accurate results for the ground state energy by choosing suitable trial functions Ψ and varying a number of parameters. It was by this method incidentally, that the first evidence was obtained that quantum mechanics was capable of describing many-particle physics[2]. The variational principle provides the theoretical foundation for several approximation schemes for the many-body problem.

Time-independent perturbation theory, or Rayleigh-Schrödinger perturbation theory, is a way of obtaining approximate solutions to a perturbed problem, by building on the known exact solutions to the unperturbed problem. The theory is stated to second order as follows[3]: For a Hamiltonian H_0 for which the eigenvectors $|\psi_n\rangle$ and eigenvalues E_n^0 are known, when adding a perturbation H_1 to the Hamiltonian

$$H = H_0 + H_1, \tag{3.17}$$

the correction to the energy levels are given to second order as

[2] This was in fact first shown by the Norwegian physicist Egil A. Hylleraas, in 1928 [11].
[3] The eigenstates of H_0 are taken to be nondegenerate.

$$E_n = E_n^0 + \langle \psi_n^0 | H_1 | \psi_n^0 \rangle + \sum_{k(\neq n)} \frac{\left| \langle \psi_k^0 | H_1 | \psi_n^0 \rangle \right|^2}{E_n^0 - E_k^0}. \tag{3.18}$$

By for example considering H_0 to be the Hamiltonian of a system of non-interacting electrons, and H_1 to be the Coulomb interaction terms, we have a workable (but still very crude) method for calculating the energy of a many-body system.

Methods that are not based on one, or a combination of these two principles also exist. The coupled cluster method, which nowadays is one of the most powerful ways of obtaining the ground state of molecular systems [12] or nuclei, is an example of this. I will now give a short introduction to three of the most important electronic structure methods.

3.2.1 The Hartree-Fock Method

It is the electron-electron interaction term that makes solving the Schrödinger equation for the many-body problem such a difficult task. Without it, the exact wave function is given by a Slater determinant as in Eq. (3.15). Since the correlations introduced by these two-body terms are in most cases quite strong, this Slater determinant will be a poor approximation to the exact solution of the full problem. We can improve on this in methods such as configuration interaction methods, where we work in a basis of Slater determinants. The wave function will then be given as a linear combination of Slater determinants. But while a single Slater determinant is easy to visualize and provides us with a clear physical picture, linear combinations do not.

We therefore seek to approximate the exact wave function by a single Slater determinant of single-particle functions[4]. To find the optimal single-particle state we use variational calculus and minimize the expression

$$\langle \Psi | H | \Psi \rangle \,, \tag{3.19}$$

when varying over the set of normalized Slater determinants Ψ of single particle functions $\varphi_{\alpha_i}(\mathbf{x}_i)$,

$$\Psi(\mathbf{x}_1, \mathbf{x}_2, \ldots, \mathbf{x}_N) = \frac{1}{\sqrt{N!}} \sum_p (-1)^p \varphi_{\alpha_1}(\mathbf{x}_1) \varphi_{\alpha_2}(\mathbf{x}_2) \ldots \varphi_{\alpha_N}(\mathbf{x}_N) \,. \tag{3.20}$$

Approximating the exact wave function this way is known as the Hartree-Fock method. From the Rayleigh-Ritz variational principle (Eq. (3.16)), we know that this will give us

[4]The single-particle functions here are often called *spin-orbitals*.

an upper bound to the ground state energy. The single-particle functions $\varphi_{\alpha_i}(\mathbf{x}_i)$ can be found from a set of coupled equations known as the *Hartree-Fock equations* [13]

$$\left[-\frac{\hbar^2}{2m}\nabla^2 + V_{\text{ext}}(\mathbf{r})\right]\varphi_i(\mathbf{r}) + \left[\sum_{j=1,j\neq i}^{N}\frac{e^2}{4\pi\varepsilon_0}\int\frac{|\varphi_j(\mathrm{r}')|^2}{|\mathrm{r}-\mathrm{r}'|}\,\mathrm{dr}'\right]\varphi_i(\mathbf{r}) - \left[\sum_{j=1,j\neq i}^{N}\delta_{s_i s_j}\frac{e^2}{4\pi\varepsilon_0}\int\left(\varphi_j^*(\mathbf{r}')\frac{1}{|\mathbf{r}-\mathbf{r}'|}\varphi_i(\mathbf{r}')\right)\mathrm{d}\mathbf{r}'\right]\varphi_j(\mathbf{r}) = \epsilon_i\varphi_i(\mathbf{r}). \tag{3.21}$$

Here, $V_{\text{ext}}(\mathbf{r})$ is the external potential, which in case of the molecular problem is set up by the ions, or in case of a quantum dot is often taken to be that of a harmonic oscillator[5]. The Hartree-Fock equations have here been written for the position part of the single-particle wave functions $\varphi_{\alpha_i}(\mathbf{x}_i)$ (and by a slight abuse of notation we use the same symbol for the whole wave function as for the spatial part). Since the Hamiltonian used in the Hartree-Fock method does not depend explicitly on spin, we can separate the spatial and spin parts of the wave function. The Kronecker-delta symbol $\delta_{s_i s_j}$, which here depends on the spin state of the single-particle states (up or down, as they say) of the single-particle states, here has the effect that the third term cancels when the spin states of two of the single-particle states are different.

What is the physical meaning of the terms in the Hartree-Fock equations? The first term is the sum of the one-body kinetic energy and the external potential energy term, obviously. The second term is the averaged electronic repulsion of the other electrons. It is interesting to add that if we vary Eq. (3.19) over a product of single particle functions of the form $\Psi(\mathbf{x}_1,\ldots,\mathbf{x}_N) = \varphi_{\alpha_1}(\mathbf{x}_1)\cdots\varphi_{\alpha_N}(\mathbf{x}_N)$ instead of the Slater determinants, we do not get the third term on the left hand side in Eq. (3.21). This tells us that the third term contains effects of the anti-symmetrization of the wave function, and is for this reason known as the *exchange term*. It has the effect that electrons of the same spin tend to avoid one another. The exchange term is seen to be non-local, in contrast to ordinary potential operators. The Hartree-Fock method is an example of a mean-field method, where the electron-electron interactions are represented by an average particle-independent potential.

To solve the Hartree-Fock equations, we use fix-point iterations. We start by making an educated guess of the single-particle functions $\varphi_{\alpha_i}(\mathbf{x}_i)$, calculate the effective potentials in the Hartree-Fock equations, solve the Hartree-Fock equations, thus finding a new set of single-particle wave functions. The process is then repeated. When solving the Hartree-Fock equations an infinite number of eigenfunctions could in principle be found, but only the lowest are used for the next iteration. The process is repeated until we get self-consistent solutions, that is, our fix-point iteration has converged.

[5]For an example of the application of the Hartree-Fock method to parabolic quantum dots, see [14].

3.2.2 The Density Functional Method

Density functional theory (DFT) is an alternative approach to the quantum many-body problem, in which the electron density distribution rather than the many-electron wave funtion plays the central role. DFT has its conceptual roots in the Thomas-Fermi model[6] that was discovered shortly after the advent of quantum mechanics. This model gives an estimate of the electronic energy in terms of the electron density distribution, but while being useful for predicting qualitative trends, it is quite useless for the kind of precision demanded by e.g. materials science. Indeed, the model fails to even predict molecular bonding.

Density functional theory offers two big advantages over the other methods that are commonly used to attack the many-body problem. The first is in the area of fundamental understanding. To improve on the Hartree-Fock method it is common practice to work with large basis sets of Slater determinants of single particle functions. While this will increase the accuracy of the calculations, we have now lost something in terms of comprehension. DFT provides a complementary perspective, as it focuses on quantities in the real, 3-dimensional coordinate space, principally on the ground state electron density. The second contribution is that it scales better with the number of particles than traditional wave function methods. This is the principal reason for the widespread use of DFT in the electronic structure calculations. At present DFT can handle systems with up to $100 - 200$ atoms.

The theory is based on two theorems first given by Hohenberg and Kohn [15]:

Theorem 1 (The basic lemma of DFT): The ground state density $n(\mathbf{r})$ of a bound system of interacting electrons in some external potential V_{ext} determines this potential uniquely, except for an additive constant.

Theorem 2 (The Hohenberg-Kohn Variational Principle): A universal functional for the energy, $E[n]$, in terms of the density $n(\mathbf{r})$ can be defined, valid for any external potential V_{ext}. For any particular V_{ext}, the exact ground state energy of the system is the global minimum value of this functional, and the density $n(\mathbf{r})$ that minimizes the functional is the exact ground state density.

The proofs of these theorems are surprisingly simple, and can be found in Ref. [15]. We can define a functional for the energy in terms for the density $n(\mathbf{r})$ for an interacting system of electrons as

$$E[n] = \int V_{\text{ext}}(\mathbf{r})\, n(\mathbf{r})\ \mathrm{d}\mathbf{r} + T[n] + \frac{1}{2}\int \frac{e^2 n(\mathbf{r})\, n(\mathbf{r}')}{4\pi\epsilon_0 |\mathbf{r}-\mathbf{r}'|}\ \mathrm{d}\mathbf{r}\ \mathrm{d}\mathbf{r}' + E_{\text{xc}}[n]\,. \tag{3.22}$$

[6] It was indeed this model that inspired Walter Kohn to look into the problem anew [15].

The second term on the right is the kinetic energy functional for non-interacting electrons. The third term is the so-called Hartree-term, which gives the electrostatic energy of the electrons in the mean-field approximation. The last term is the *exchange-correlation* functional. It is defined as the functional that takes into account all the many-particle effects not already covered by the other terms in the equation. From the Hohenberg-Kohn theorems, we know that such a functional must exist.

Kohn and Sham went on to show [16] that the density that minimizes this functional, and thus by the Hohenberg-Kohn theorems must be the ground state density, can be found by solving a self-consistent set of equations, known today as the *Kohn-Sham equations*. The Kohn-Sham equations are a set of coupled equations for single-particle states φ_i (the Kohn-Sham orbitals), that for a system of N electrons are stated as

$$\left(-\frac{\hbar^2}{2m}\nabla^2 + V_{\text{eff}}\left(\mathbf{r}\right)\right)\varphi_i\left(\mathbf{r}\right) = \epsilon_i\varphi_i\left(\mathbf{r}\right) \tag{3.23}$$

with

$$\begin{aligned} V_{\text{eff}}\left(\mathbf{r}\right) &= V_{\text{ext}}\left(\mathbf{r}\right) + \int \frac{e^2 n\left(\mathbf{r}'\right)}{4\pi\epsilon_0\left|\mathbf{r}-\mathbf{r}'\right|}\,\mathrm{d}\mathbf{r}' + V_{\text{xc}}\left(\mathbf{r}\right), \\ n\left(\mathbf{r}\right) &= \sum_{i=1}^{N}\left|\varphi_i\left(\mathbf{r}\right)\right|^2. \end{aligned} \tag{3.24}$$

The Kohn-Sham orbitals φ_i and their corresponding eigenenergies ϵ_i do not themselves have physical meaning. The term $V_{\text{xc}}\left(\mathbf{r}\right)$ is the so-called exchange-correlation potential, and can be expressed as a functional derivative of the exchange-correlation energy with respect to the electron density

$$V_{\text{xc}}\left(\mathbf{r}\right) = \frac{\delta E_{\text{xc}}\left[n\left(\mathbf{r}\right)\right]}{\delta n\left(\mathbf{r}\right)}. \tag{3.25}$$

The ground state energy can now be written as

$$E = \sum_i \epsilon_i + E_{\text{xc}}\left[n\left(\mathbf{r}\right)\right] - \int V_{\text{xc}}\left(\mathbf{r}\right) n\left(\mathbf{r}\right)\,\mathrm{d}\mathbf{r} - \frac{1}{2}\int \frac{e^2 n\left(\mathbf{r}\right) n\left(\mathbf{r}'\right)}{4\pi\epsilon_0\left|\mathbf{r}-\mathbf{r}'\right|}\,\mathrm{d}\mathbf{r}\,\mathrm{d}\mathbf{r}'. \tag{3.26}$$

The exchange-correlation energy is unfortunately unknown for all but a few highly idealized systems. The idea of the *local density approximation* is to assume that the exchange-correlation energy per electron is the same as for the homogeneous electron gas, a system for which an analytical solution exists for the exchange part. The exchange-correlation energy is then given by

$$E_{\text{xc}}^{\text{LDA}}\left[n\left(\mathbf{r}\right)\right] = \int n\left(\mathbf{r}\right)\varepsilon_{\text{xc}}\left[n\left(\mathbf{r}\right)\right]\,\mathrm{d}\mathbf{r}, \tag{3.27}$$

where $\varepsilon_{\mathrm{xc}}\left[n\left(\mathbf{r}\right)\right]$ is the exchange-correlation energy per electron in the homogeneous electron gas. It seems absurd that the local density approximation should be useful for atomic and molecular systems, where clearly the charge density is anything but homogeneous. Nevertheless, the local density approximation has proven to be very useful in most applications. A whole range of improvements to this approximation exist, the most important one being the *generalized gradient approximation* (GGA), where a non-local correction involving the gradient of $n\left(\mathrm{r}\right)$ is added to the exchange-correlation energy.

The formalism above breaks down in the presence of a vector potential (e.g. a magnetic field) and no mention has been made of the spin of the electron. I will conclude this section by reassuring the reader that it is possible to include these effects by various generalizations of density functional theory.

3.2.3 The Full Configuration Interaction Method

The Hartree-Fock method is an example of a mean-field theory, in which we assume that the particles move around independently in an effective particle-independent potential. While this approach has proven to be highly successful, we know that these methods do not account for all many-particle effects. A proper treatment of the electron correlation effects is especially important for quantum dots, since the two-dimensional nature of the confinement increases the relative strength of the Coulomb interaction. For density-functional theory we also have the unsatisfactory situation that there is no possibility to systematically improve the calculations or to estimate the size of the neglected effects. Another limitation of the two methods is that they only give us the ground state of the system. The *full configuration interaction method* (FCI) on the other hand, gives us both the ground state energy and the excxited states. The FCI method can also, in principle, be made to converge to the exact solution. Mathematically, the FCI method is an instance of the Rayleigh-Ritz variational method (Eq. 3.16). I will now outline the method:

Let us first consider the abstract case where we have a complete set of orthonormal basis vectors $|\varphi_k\rangle$ in terms of which we can expand the state vector $|\Psi\rangle$

$$|\Psi\rangle = \sum_{k=0}^{\infty} c_k \left|\varphi_k\right\rangle, \qquad c_k = \langle\varphi_k|\Psi\rangle\,. \tag{3.28}$$

Using this expansion, we can formulate the Schrödinger equation

$$H\left|\Psi\right\rangle = E\left|\Psi\right\rangle \tag{3.29}$$

as a matrix diagonalization problem. To see this we insert Eq. (3.28) into the equation above, and multiply on the left by $\langle\varphi_j|$, giving us

$$\begin{aligned}\sum_k \langle\varphi_k|\Psi\rangle \langle\varphi_j|H|\varphi_k\rangle &= E\sum_k \langle\varphi_j|\varphi_k\rangle \langle\varphi_k|\Psi\rangle \\ &= E\sum_k \delta_{jk} \langle\varphi_k|\Psi\rangle \\ &= \langle\varphi_j|\Psi\rangle .\end{aligned} \tag{3.30}$$

By defining a matrix $\mathbf{H}$ of elements $(\mathbf{H})_{jk} = \langle\varphi_j|H|\varphi_k\rangle$ and a column vector $\mathbf{c}$ of the expansion coefficients c_k , we see that we have recast the Schrödinger equation into a matrix problem

$$\mathbf{Hc} = E\mathbf{c}. \tag{3.31}$$

To find the eigenvalues and eigenfunctions (in terms of the basis vectors $|\varphi_k\rangle$) we need to diagonalize the matrix $\mathbf{H}$. The matrix is infinite-dimensional however, so before diagonalizing we must truncate the basis after a finite number of basis vectors. This truncated basis must be large enough to give a good approximation to the problem. One useful test of this is to add more basis vectors $|\varphi_k\rangle$ to the expansion and study the change in the eigenvalues as the basis size and the matrix dimensions are increased.

For the many-particle case we work in a basis of Slater determinants $|\Phi_i\rangle$. In calculations on quantum dots the single-particle functions of the Slater determinants are usually chosen as the eigenfunctions of the single-electron harmonic oscillator Hamiltonian[7]. In computations in chemistry however, it is common practice to use the spin-orbitals resulting from Hartree-Fock calculations. One important question is how to build up the determinants that are used in the basis, and where to truncate the basis. We typically define some energy cut-off value, either for the single-particle functions or for the system as a whole, and include all Slater determinants up to this value. Each of the determinants, in which a number of particles are excited from the lowest-energy Slater determinant, is referred to as a a configuration state function. This is the origin of the "configuration"-part, in the name of this method. "Full configuration interaction", as opposed to only "configuration interaction", refers to the fact that we are considering determinants of more than one or two excited particles.

The full configuration interaction method is in principle exact, in the sense that it converges to the exact solution when increasing the number of basis functions of Slater determinants. The real advantage of the FCI method is that, in addition to the ground-state energy and wave function, all low-lying excited states are computed with essentially no extra cost or reduction of accuracy. The main drawback of the method is that it scales almost exponentially with the number of particles. This is referred to as the *curse of dimensionality*, and for the quantum dot, accurate calculations are currently limited to systems of about 6 electrons [14, 19].

[7] For examples of large scale diagonalization in the 1D and 2D harmonic oscillator basis, see Refs. [17, 18, 19].

To give a feeling for just how rapidly the basis size grows with the number of particles, let us look at a concrete example. Consider a system of N electrons in a two-dimensional quantum dot given by the Hamiltonian of Eq. (3.6). We want to do configuration interaction calculations in a basis of Slater determinants of (single-particle) solutions to the two-dimensional harmonic oscillator Hamiltonian. When this eigenproblem is solved in polar coordinates the eigenfunctions are given by the so-called Fock-Darwin orbitals ψ_{nm}^{FD} specified by the quantum numbers n (the nodal quantum number) and m (the azimuthal quantum number). The eigenvalues of these states are

$$E_{nm} = \hbar\omega_0 \left(2n + |m| + 1\right). \tag{3.32}$$

States of equal energy are said to be in the same shell, so we define $R = 2n + |m|$ as the *shell number*. Including the degree of freedom due to the electron spin, each shell has a degeneracy of $2\left(R+1\right)$. To define the truncation of the many-particle basis, we say that we will include all Slater determinants with single particle energy less than or equal to[8] $E/\hbar\omega = 6$. Hopefully, this will be good enough to capture most of the physics involved. This corresponds to a shell number of $R = 5$. The number of Fock-Darwin orbitals with shell number of $R = 5$ or less is (including the degeneracy due to the electron spin)

$$N_{\mathrm{basis}} = \left(R+2\right)\left(R+1\right) = 42. \tag{3.33}$$

For N electrons, the number of Slater determinants we need to include is then

$$\binom{N_{\mathrm{basis}}}{N} = \frac{N_{\mathrm{basis}}!}{(N_{\mathrm{basis}} - N)!\, N!} = \frac{42!}{(42-N)!\, N!} \tag{3.34}$$

For $N = 2$ electrons, we must include 861 basis states. For $N = 4$ this number has grown to 111930, and when this number is doubled again, to $N = 8$, we must include more than 10^9 states! Clearly, we cannot diagonalize matrices of this size. The dimensionality can be lowered by symmetry considerations [18], but the basis size will still scale almost exponentially with the number of particles.

3.2.4 Other approaches

Holding the key to understanding so many different phenomena in nature, a plethora of approximation techniques have been devised for solving the many-body Schrödinger equation, despite the formidable difficulties it represents. I will mention a few more of them here:

Möller-Plesset: Rayleigh-Schrödinger perturbation theory (Eq. (3.18)) applied to a systems of several interacting particles is generally called *many-body perturbation theory.*

[8] This basis is often called the *direct product space*. For a discussion, see [4].

In Möller-Plesset perturbation theory, Rayleigh-Schrödinger perturbation theory is applied to the the Hartree-Fock solutions for the system.

Coupled-Cluster: The coupled-cluster method was originally developed for the problem of the strongly interacting nucleons by Coester and Kummel around 1960. Today it is one of the most powerful methods for obtaining the ground state of many-body systems. In contrast to most other many-body methods, it is not built on a variational principle. This makes it difficult to analyze mathematically.

Quantum Monte Carlo: The main idea of this class of methods is to is to use the Monte Carlo method to handle the many-dimensional integrals that arise in solving the Schrödinger equation. Quantum Monte Carlo makes it possible to represent the many-body effects in the wave function directly, at the cost of statistical uncertainty that can be reduced by increasing the simulation time. The two most common approches are *variational monte carlo*, and *diffusion monte carlo*.

3.3 Atomic Units

When discussing numerical methods later in this thesis, the *atomic unit system* and the *reduced atomic unit system* will be used. This serves two purposes. Firstly, it makes manipulating equations easier by allowing us to set most of the constants equal to 1. Secondly, it is important that the units one makes use of are scaled to the size typically encountered in the problem. The numerical values of some of the quantities involved in atomic physics is typically either very large or very small in SI units ($\hbar$ for example having the minuscule value of 1.05×10^{-34} Js), and making use of such quantities directly in numerical calculations may lead to loss of numerical precision. The atomic unit system is defined by setting $m_e = e = \hbar = 4\pi\epsilon_0 = 1$ (Table 3.1).

Quantity	**Symbol**	**SI equivalent**
Electron mass	m_e	$9.109 \cdot 10^{-31}\,\mathrm{kg}$
Electron charge	e	$1.602 \cdot 10^{-19}\,\mathrm{C}$
Reduced Planck's constant	$\hbar$	$1.055 \cdot 10^{-34}\,\mathrm{Js}$
Permittivity	$4\pi\epsilon_0$	$1.113 \cdot 10^{-10}\,\mathrm{C^2J^{-1}m^{-1}}$

Table 3.1: *The basic units of the atomic unit system.*

There are other ways of defining the atomic unit system which gives the same result. In fact, it is sufficent to set any four of the six quantities $\{m_e, e, \hbar, 4\pi\epsilon_0, E_h, a_0\}$ equal to unity. The unit of energy E_h is called a *Hartree*, and is equal to twice the ionization energy of atomic hydrogen, $E_h = 27.211\ \mathrm{eV}$. It is common practice however, to convert the energy to electron volts (eV).

When working on problems involving electrons confined in quantum dots it is an advantage to modify this system somewhat. We define the *reduced atomic unit system* by

Quantity	Expression	SI equivalent
Energy	$E_h = m_e c^2 \alpha^2$	$4.359 \cdot 10^{-18}\,\mathrm{J}\,(= 27.211\,\mathrm{eV})$
Length	$a_0 = \hbar/\left(m_e c \alpha\right)$	$5.292 \cdot 10^{-11}\,\mathrm{m}$
Time	$\tau_0 = \hbar/E_h$	$2.419 \cdot 10^{-17}\,\mathrm{s}$
Electric field strength	$E_0 = e/\left(4\pi\epsilon_0 a_0^2\right)$	$5.142 \cdot 10^{11}\,\mathrm{Vm}^{-1}$
Velocity	$v_0 = a_0 E_h/\hbar$	$2.188 \cdot 10^{6}\,\mathrm{ms}^{-1}$
Angular frequency	$\omega_0 = v_0/\left(2\pi a_0\right)$	$6.580 \cdot 10^{15}\,\mathrm{s}^{-1}$
Force	$F_0 = E_h/a_0$	$8.238 \cdot 10^{-8}\,\mathrm{N}$

Table 3.2: *Some derived units of the atomic unit system.*

setting the unit of energy equal to the strength of the confining potential $\hbar\omega_0 = 1$, setting the unit of mass equal to the effective electron mass $m^* = 1$ and by setting $\hbar = e = 1$ (see Table 3.2). For our purposes, we need to know what the units of length, time, magnetic field strength and electric field strength correspond to in SI units. These can be obtained from the following expressions [20]:

$$\begin{aligned} U_{\mathrm{Time}} &= \frac{\hbar}{U_{\mathrm{Energy}}} & U_{\mathrm{Length}} &= \left(U_{\mathrm{Energy}} U_{\mathrm{Time}}^2 U_{\mathrm{Mass}}^{-1}\right)^{1/2} \\ U_{\mathrm{Magnetic}} &= \frac{U_{\mathrm{Mass}}}{U_{\mathrm{Time}} U_{\mathrm{Charge}}} & U_{\mathrm{Electric}} &= \frac{U_{\mathrm{Mass}}}{U_{\mathrm{Time}}^2 U_{\mathrm{Charge}}} \end{aligned} \tag{3.35}$$

As an example, consider a system with the effective mass set to that of an electron in GaAs, $m^* = 0.067 m_e$, and with a confinement strength of $\hbar\omega_0 = 1\ \mathrm{meV}$. This gives us a unit of time of $0.66\ \mathrm{ps}$, a unit of length of $34\ \mathrm{nm}$, a unit of magnetic field strength of $0.6\ \mathrm{T}$ and the unit of electric field strength corresponding to $30\ \mathrm{kVm}^{-1}$.

Chapter 4

Solving the Time-Dependent Schrödinger Equation

Time-dependent problems have in quantum mechanics traditionally been treated by perturbation methods. Such methods have limitations however, and in complex systems the only way to investigate the time evolution of the system might be to solve the Schrödinger equation directly. Since this is in most cases quite impossible to do by analytical means, numerical methods must be used. Due to the requirement of conservation of probability of the wave function, solving the Schrödinger equation numerically does present some extra difficulties. In this chapter, I will give a thorough derivation of a number of the most widely used methods for this task. I will also look at a relatively new numerical scheme, and see if this offers any advantages over the other methods. Numerical experiments are carried out to compare the performance of the methods.

4.1 The Time Evolution Operator

For all but the most simple time-dependent Hamiltonians the Schrödinger equation is not analytically solvable. We will for the time being however ignore the exact form of the Hamiltonian and investigate a formal expression for the solution of the Schrödinger equation.

We introduce an operator U which carries our initial state $\Psi(t_0)$ into the final state $\Psi(t)$,

$$\Psi(t) = U(t, t_0)\Psi(t_0), \qquad U(t_0, t_0) = I. \tag{4.1}$$

Conservation of probability requires that $\langle\Psi(t)|\Psi(t)\rangle = \langle\Psi(t_0)|\Psi(t_0)\rangle$. Substituting Eq. (4.1) into this equation gives us

$$\langle\Psi(t)|\Psi(t)\rangle = \Big\langle \Psi(t_0)|U^\dagger(t,t_0)U(t,t_0)|\Psi(t_0)\Big\rangle \tag{4.2}$$

from which it follows that $U^\dagger(t,t_0)U(t,t_0) = I$. Similarly we can show that $U(t,t_0)U^\dagger(t,t_0) = I$. From these two equations we conclude that $U(t,t_0)$ is a unitary operator, that is, an operator which satisfies $U^{-1} = U^\dagger$. We now substitute Eq. (4.1) into the Schrödinger equation and get

$$i\frac{\partial}{\partial t}U\left(t,t_0\right)\Psi(t_0) = HU\left(t,t_0\right)\Psi(t_0). \tag{4.3}$$

This holds for all $\Psi(t_0)$ so that

$$i\frac{\partial U}{\partial t} = H(t)U. \tag{4.4}$$

By integrating this we get an implicit expression for the time evolution operator

$$U(t,t_0) = I - i\int_{t_0}^{t} H(t_1)U(t_1)\,\mathrm{d}t_1. \tag{4.5}$$

This equation can be iterated. Iterating once gives us

$$\begin{aligned} U(t,t_0) &= I - i\int_{t_0}^{t} H(t_1)\left[I - i\int_{t_0}^{t_1} H(t_2)U(t_2)\,\mathrm{d}t_2\right]\,\mathrm{d}t_1 \\ &= I - i\int_{t_0}^{t} H(t_1)\,\mathrm{d}t_1 + (-i)^2\int_{t_0}^{t}\int_{t_0}^{t_1} H(t_1)H(t_2)U(t_2)\,\mathrm{d}t_1\,\mathrm{d}t_2. \end{aligned} \tag{4.6}$$

The successive iterations are given by replacing $U(t_n)$ with Eq. (4.5). To get rid of the integral over the solution itself we will have to perform infinitely many iterations

$$U(t,t_0) = \sum_{n=0}^{\infty}(-i)^n\int_{t_0}^{t}\mathrm{d}t_1\int_{t_0}^{t_1}\mathrm{d}t_2\ldots\int_{t_0}^{t_{n-1}}\mathrm{d}t_n H(t_1)H(t_2)\ldots H(t_n). \tag{4.7}$$

If the Hamiltonian at different times commutes, we can write this as

$$U(t,t_0) = \sum_{n=0}^{\infty}\frac{(-i)^n}{n!}\int_{t_0}^{t}\mathrm{d}t_1\int_{t_0}^{t}\mathrm{d}t_2\ldots\int_{t_0}^{t}\mathrm{d}t_n H(t_1)H(t_2)\ldots H(t_n). \tag{4.8}$$

This is not always the case however, as time-dependent Hamiltonians have no reason in general to be equal at different times. We are forced to introduce the time ordering operator $\mathcal{T}$. For the Hamiltonian at two different times $H(t_1)$ and $H(t_2)$ it is defined as

$$\mathcal{T}[H(t_1)H(t_2)] = H(\max\{t_1,t_2\})H(\min\{t_1,t_2\}) \tag{4.9}$$

For n different times $t_1, t_2, \ldots, t_n$ this generalizes in the obvious way by recursion. This gives us a formal expression for the time evolution operator

$$\begin{aligned} U(t,t_0) &= \sum_{n=0}^{\infty} \frac{(-i)^n}{n!} \mathcal{T} \int_{t_0}^{t} \mathrm{d}t_1 \int_{t_0}^{t} \mathrm{d}t_2 \ldots \int_{t_0}^{t} \mathrm{d}t_n H(t_1)H(t_2)\ldots H(t_n) \\ &= \mathcal{T} \exp\left(-i \int_{t_0}^{t} H(t)\, \mathrm{d}t\right). \end{aligned} \tag{4.10}$$

In the interaction picture this is most often called the Dyson series. If the Hamiltonian is time-independent, this reduces to

$$U(t,t_0) = \exp\left[-i\,(t-t_0)\,H\right]. \tag{4.11}$$

4.2 Numerical solution to the Schrödinger equation

We are given an initial state $\Psi(x,0)$ and asked to find the future state $\Psi(x,t)$. How do we solve this problem on a computer? The problem is that the spatial domain of the wave function extends to infinity, and that the wave function lives on a continuum. To implement this on a computer we need to discretize time and space.

In our way of attacking the problem we separate between time and space. This is connected with our physical way of thinking. We represent the wave function by its values on a finite number of points $x_j, \quad j = 1, 2, \ldots, N$, which we set to be equidistant. We also need to find a representation of the Hamiltonian on this finite grid. Thinking of it, we can see that this spatial discretization leads to an N-dimensional matrix formulation of the original Schrödinger equation. It is an approximation to the complete system, but is in itself a case of a completely general N-dimensional quantum system.

Defining a vector $\mathbf{c}(t)$ of the function values of $\Psi(x,t)$ at the grid points, $(\mathbf{c}(t))_j = \Psi(x_j,t)$, we get a semi-discrete Schrödinger equation of the form

$$\frac{\mathrm{d}}{\mathrm{d}t}\mathbf{c}(t) = \mathbf{H}\mathbf{c}(t) \tag{4.12}$$

where $\mathbf{H}$ now is an $N \times N$ Hermitian matrix.

This is now a system of N first order differential equations, for which many solution methods have been devised. One of the standard methods of attacking this problem would be to use for example a fourth-order Runge-Kutta method. So why not apply this

to solving the Schrödinger equation? Unfortunately most such methods are ill-suited for the Schrödinger equation, as most of them fail to preserve unitarity. We will discuss better time propagation schemes at length in the following sections. First, however, we need to resolve the issue of how to represent the Hamiltonian in our discretized version of the Schrödinger equation.

A word on notation: The different time-propagation schemes are not directly connected to the spatial discretization of the wave function. They will therefore be discussed in the context of the continuous wave function $\Psi(x,t)$. When a point needs to be made on the spatially discretized wavefunction, a boldface type will be used to denote the vector $\mathbf{\Psi}$ of the function values of the wave function on the grid points $(\mathbf{\Psi})_j = \Psi(x_j)$. This applies to the semi-discrete as well as the time-discretized wave function.

4.2.1 The Finite Difference Approximation

The conceptually simplest way of approximating differential operators is by using finite differences. The effect of an operator on the wave function at a given grid point is typically given by expressions involving the value of the wave function at the grid point and on the neighbouring grid points. Partial derivatives are approximated with difference expressions derived from considerations of Taylor expansions of the original function.

Let us define the grid as

$$x_m = x_0 + \frac{mL}{N+1} \equiv x_0 + m\Delta x, \quad m = 1, 2, ..., N, \tag{4.13}$$

where L is the length of the discretization interval. It might be confusing that we are dividing by $N+1$ and not by $N-1$, but this will all be clear in a moment. We will approximate the differential operator $\frac{\partial^2}{\partial x^2}$ in the finite difference approximation at a grid point x_m by

$$\frac{\partial^2}{\partial x^2}\Psi(x_m) = \frac{1}{\Delta x^2}\left[\Psi(x_{m+1}) - 2\Psi(x_m) + \Psi(x_{m-1})\right] + O(\Delta x^2). \tag{4.14}$$

The error in using this approximation is of second order in Δx. It is possible to improve upon this by using two additional points to get a fourth-order approximation (a so-called five-point stencil)

$$\frac{\partial^2}{\partial x^2}\Psi(x_m) = \frac{1}{12\Delta x^2}\left[-\Psi\left(x_{m+2}\right) + 16\Psi\left(x_{m+1}\right) - 30\Psi\left(x_m\right) + 16\Psi\left(x_{m-1}\right) - \Psi\left(x_{m-2}\right)\right] + O(\Delta x^4). \tag{4.15}$$

While offering increased accuracy this does however slow down the numerical methods in most cases. In the simpler case of using the three-point stencil of Eq. (4.14), the Hamiltonian matrix becomes tri-diagonal, which in many cases offers computational advantages.

Physically, limiting our wave function to a finite region sets the potential to ∞ outside this region since the particle is not allowed to be there (it is thus the same as the particle in a box). So even though we only defined the wave function at N points, we really specified its values at $N+2$ points, the values at the end points being $\Psi(x_0) = \Psi(x_{N+1}) = 0$. This is also the reason why we divided by $N+1$ and not by $N-1$ in Eq. (4.13).

The potential energy operator $V(x)$ is of course trivial to compute in the finite difference approximation, being simply $V(x_m)$. In matrix formulation, the action of the discrete Hamiltonian on $\mathbf{\Psi}$ becomes

$$\begin{aligned}(\mathbf{H\Psi})_m &= [(\mathbf{T}+\mathbf{V})\,\mathbf{\Psi}]_m \\ &= \frac{1}{\Delta x^2}\left[\Psi(x_{m+1}) - 2\Psi(x_m) + \Psi(x_{m-1})\right] + V(x_m)\,\Psi_m + \mathcal{O}\left(\Delta x^2\right), \quad 1 \le m \le N,\end{aligned} \tag{4.16}$$

where it is easily seen that $\mathbf{H}$ is tridiagonal.

The semi-discrete Schrödinger equation is thus

$$i\frac{\mathrm{d}}{\mathrm{d}t}\mathbf{\Psi}(t) = \mathbf{H}(t)\,\mathbf{\Psi}(t), \qquad + \text{boundary condition.} \tag{4.17}$$

As mentioned before this is a set of coupled ordinary differential equations.

4.2.2 The Spectral Method

The finite difference approximation given in the previous section is very simple, but suffers from a large error of order $\mathcal{O}(\Delta x^2)$, for the kinetic energy term. Based on the discrete Fourier transform (DFT) we may reduce this error to $\mathcal{O}(\Delta x^N)$, where N is the number of grid points on the spatial domain [21]. If we increase N inside our chosen boundary, this will cause the error to rapidly decrease, even in the case of using the finite difference method. But for the spectral method, the order of the method also increases when we increase the number of grid points! The error is actually decreasing exponentially with N. Using the spectral method has other virtues as well. When high resolution is needed in simulations we cannot simply increase the number of grid points indefinitely, otherwise we will run out of main memory. By the help of spectral methods we can reduce the number of grid points needed to meet the required accuracy.

The idea behind the spectral method is that differentiation is a diagonal operator in the frequency domain. The Fourier transform of $\psi(x)$ is given by

$$\phi(k) = \mathcal{F}\left[\psi(x)\right](k) = \int_{-\infty}^{\infty} \psi(x) \mathrm{e}^{-ikx} \, \mathrm{d}x \tag{4.18}$$

and the inverse Fourier transform is

$$\psi(x) = \mathcal{F}^{-1}\left[\phi(k)\right](x) = \frac{1}{2\pi} \int_{-\infty}^{\infty} \phi(k) \mathrm{e}^{ikx} \, \mathrm{d}k. \tag{4.19}$$

What we have done here is of course really nothing else than representing the wave function in momentum space, $p = k$ being the momentum. For the Fourier transform one should be aware of that there are several conventions in use (see Appendix A).

Differentiating $\psi(x)$ we get

$$\frac{\mathrm{d}}{\mathrm{d}x}\psi(x) = \frac{1}{2\pi} \int_{-\infty}^{\infty} ik\phi(k) \mathrm{e}^{ikx} \, \mathrm{d}k. \tag{4.20}$$

The Fourier transform of the differentiated function is

$$\mathcal{F}\left[\psi'(x)\right](k) = ik\mathcal{F}\left[\psi\right] = ik\phi(k). \tag{4.21}$$

Thus, differentiation becomes multiplication (with ik) in the frequency domain. The effect of $\frac{\mathrm{d}^2}{\mathrm{d}x^2}$ is easily seen to be multiplication by $-k^2$. Differentiation, and thus the kinetic energy term, is a diagonal operator.

To make use of this idea we represent our wave function on a finite grid as before, but use the discrete Fourier transform to transform to the frequency domain before computing the action of the kinetic energy operator. The spatial discretization must be modified somewhat, to incorporate periodic boundary conditions, as DFT is only valid for periodic functions. We will unfortunately get a somewhat artificial behaviour, as the one-dimensional particle suddenly lives on a circle. The solution to this problem is to extend the domain so the wave function never reaches the edges in the course of the simulation.

The expression for the grid points in the spectral method becomes

$$x_m = x_0 + \frac{mL}{N} = x_0 + m\Delta x, \quad 0 \leq m \leq N-1. \tag{4.22}$$

Note that because the discrete Fourier transform enforces periodic boundary conditions on the wave function $\Psi_0 = \Psi_N$.

4.3 Time Integration Methods

4.3.1 The Forward Euler Method

Perhaps the simplest possible numerical scheme for propagating the Schrödinger equation in time follows from approximating the time derivative by a forward difference. That is, the time derivative at time t_n is approximated as

$$\frac{\mathrm{d}}{\mathrm{d}t}\Psi\left(t_n\right) \approx \frac{\Psi\left(t_{n+1}\right) - \Psi\left(t_n\right)}{\Delta t} \equiv \frac{\Psi^{n+1} - \Psi^n}{\Delta t}. \tag{4.23}$$

Here time is discretized by an evenly spaced grid in the same vein as for the spatial discretization, $t_n = n\Delta t + t_0,\ n = 0, 1, 2, \ldots$. Inserting Eq. (4.23) into the Schrödinger equation we get an explicit expression for the wave function at the next time step

$$\Psi^{n+1} = \Psi^n - i\Delta t H^n \Psi^n. \tag{4.24}$$

This is known as the forward Euler method, or simply, the Euler method.

Is this a good method of solving the Schrödinger equation numerically? First of all, what defines a good method? Factors we need to take into consideration when discussing this includes accuracy, stability and computational cost. Clearly, when the time step Δt becomes smaller then our scheme should behave more and more like the solution of the continuous equation. But since a computer can only do a certain number of operations per second, we have to compromise on some smallest Δt.

How large is then the error in taking just one time step Δt? We find this error by inserting the solution of the continuous Schrödinger equation into our discretized version. The residual τ we are left with, is the error of the time-stepping scheme.

Inserting a solution Ψ_{Ex} of the continuous problem into the discretized equation and Taylor expanding Ψ_{Ex}^{n+1} around Ψ_{Ex}^n gives us

$$\begin{aligned}
\tau &= \Psi_{\mathrm{Ex}}^{n+1} - \Psi_{\mathrm{Ex}}^n + i\Delta t H^n \Psi_{\mathrm{Ex}}^n \\
&= \sum_{j=0}^{\infty} \frac{\Delta t^j}{j!} \frac{\partial^j \Psi_{\mathrm{Ex}}^n}{\partial t^j} - \Psi_{\mathrm{Ex}}^n + i\Delta t H^n \Psi_{\mathrm{Ex}}^n \\
&= \Delta t \frac{\partial \Psi_{\mathrm{Ex}}^n}{\partial t} + \frac{\Delta t^2}{2} \frac{\partial^2 \Psi_{\mathrm{Ex}}^n}{\partial t^2} + O(\Delta t^3) + i\Delta t H^n \Psi_{\mathrm{Ex}}^n
\end{aligned} \tag{4.25}$$

Since $-iH^n\Psi_{\mathrm{Ex}}^n = \frac{\partial \Psi_{\mathrm{Ex}}^n}{\partial t}$, the error for the forward Euler scheme is

$$\tau = \frac{\Delta t^2}{2} \frac{\partial^2 \Psi_{\mathrm{Ex}}^n}{\partial t^2} + O(\Delta t^3). \tag{4.26}$$

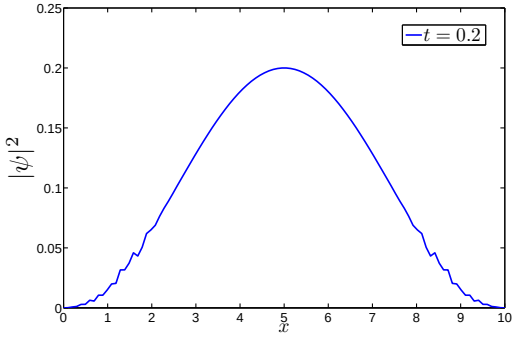

Figure 4.1: $N = 100$ *inner grid points.* $\Delta t = 0.001$.

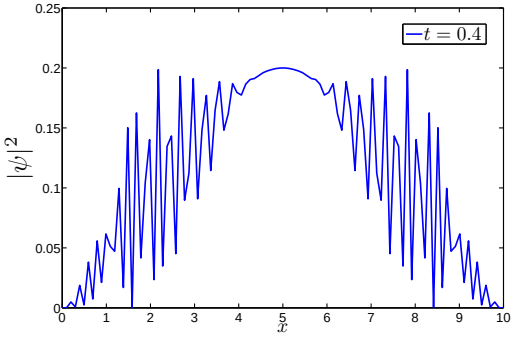

Figure 4.2: $N = 100$ *inner grid points.* $\Delta t = 0.001$.

This method is therefore a first order method[1]. While this is hardly impressive (we will explore methods of second and fourth order in the following sections), the error in each time step can of course be made arbitrarily small by decreasing Δt. Unfortunately, the forward Euler method is a lost cause for our purposes. The scheme is unstable, meaning that small errors build up over time.

As an example of this, see Figure 4.1. Here we have the familiar example of a particle in a box, in the finite difference approximation. The initial state is chosen as the ground state. We see that small instabilities around the edges of the box quickly build up, soon making the norm grow exponentially.

I have included this method to illustrate, especially for the physics student with little prior knowledge of numerical methods, that solving the Schrödinger equation requires more sophistication than simply finding an algorithm and starting the number crunching. The challenge is on to find stable, norm-conserving methods of higher order!

We finally note that all the numerical time-stepping schemes presented here can be seen as approximations to the exact time-evolution operator of Eq. (4.10). In the case of the forward Euler method we can see this by ignoring the time-ordering operator, approximating the exponential by the two first terms of its Taylor expansion, and by approximating the remaining integral by the rectangle rule:

$$\begin{aligned} \Psi^{n+1} &= \mathcal{T} \exp\left(-i \int_t^{t+\Delta t} H(s)\, \mathrm{d}s\right) \Psi^n \\ &\approx \left[1 - i \int_t^{t+\Delta t} H(s)\, \mathrm{d}s\right] \Psi^n \\ &\approx (1 - i\Delta t H^n)\Psi^n. \end{aligned} \tag{4.27}$$

[1] A method is said to be of nth order if the error is of order $n + 1$.

4.3.2 The Crank-Nicolson Method

We seek to find a method for solving the time-dependent Schrödinger equation that is stable. By only a minor modification of the method above this can be achieved. By approximating the time derivative by a backward difference,

$$i\left(\frac{\Psi^{n+1}-\Psi^n}{\Delta t}\right) = H^{n+1}\Psi^{n+1}, \tag{4.28}$$

we get a method that is stable. This method is called the backward Euler method. Unfortunately this method has the undesirable property that the wave function is dampened, and the scheme is thus non-unitary. As we see, Ψ^{n+1} is now defined implicitly, which means that we will have to solve a system of linear equations for every time step.

It turns out that we can do much better than this. Recognizing that $U\left(t_n-\Delta t, t_n\right)$ is an operator that propagates the state a step backwards in time, we get by using the approximation to the time evolution operator $U(t_n+\Delta t, t_n) \approx 1 - i\Delta t H(t_n)$ that

$$\begin{aligned} U\left(t_{n+1}-\Delta t, t_n\right)\Psi^{n+1} &= U\left(t_n+\Delta t, t_n\right)\Psi^n \\ \left[1+\frac{i}{2}\Delta t H^{n+1}\right]\Psi^{n+1} &= \left[1-\frac{i}{2}\Delta t H^n\right]\Psi^n. \end{aligned} \tag{4.29}$$

By solving for Ψ^{n+1} we get a scheme that is stable and conserves unitarity to a high degree. The resulting scheme is called the Crank-Nicolson method[2]. We can think of this as being midway between the forward Euler and the backward Euler methods. Thinking about it, since the forward Euler scheme makes the solution unstable in the sence that the norm is growing and the backward Euler scheme behaves in the opposite way, it is not unnatural to expect that these effects are balanced out.

The system is implicit however, and for each time step a system of linear equations has to be solved. In the finite difference approximation the matrix is tridiagonal and can be solved efficiently [22].

How accurate is this scheme? As before this is given by the residue we are left with when substituting a solution to the continuous equation into our discretized version. Rewriting Eqn. (4.29)

$$\left(\Psi^{n+1}-\Psi^n\right) + \frac{i}{2}\Delta t\left(H^n\Psi^n + H^{n+1}\Psi^{n+1}\right) = 0, \tag{4.30}$$

we insert the exact solution Ψ_{Ex} and Taylor expand the $n+1$ terms around n.

The first term in the equation becomes[3]

[2] After John Crank and Phyllis Nicolson.

[3] When using that $-iH^n\Psi^n_{\mathrm{Ex}} = \frac{\partial \Psi^n_{\mathrm{Ex}}}{\partial t}$

$$\begin{aligned}\left(\Psi_{\mathrm{Ex}}^{n+1}-\Psi_{\mathrm{Ex}}^{n}\right) &= \left(\sum_{j=0}^{\infty}\frac{\Delta t^{j}}{j!}\frac{\partial^{j}\Psi_{\mathrm{Ex}}^{n}}{\partial t^{j}}-\Psi_{\mathrm{Ex}}^{n}\right)\\ &= \Delta t\frac{\partial\Psi_{\mathrm{Ex}}^{n}}{\partial t}+\frac{\Delta t^{2}}{2}\frac{\partial^{2}\Psi_{\mathrm{Ex}}^{n}}{\partial t^{2}}+\frac{\Delta t^{3}}{6}\frac{\partial^{3}\Psi_{\mathrm{Ex}}^{n}}{\partial t^{3}}+\mathcal{O}\left(\Delta t^{4}\right).\end{aligned} \tag{4.31}$$

The second term becomes

$$\begin{aligned}\frac{i}{2}\Delta t\left(H^{n}\Psi_{\mathrm{Ex}}^{n}+H^{n+1}\Psi_{\mathrm{Ex}}^{n+1}\right) &= \frac{i}{2}\Delta tH^{n}\Psi_{\mathrm{Ex}}^{n}+\frac{i}{2}\Delta t\left(H^{n}\Psi_{\mathrm{Ex}}^{n}+\Delta t\frac{\partial}{\partial t}\left(H^{n}\Psi_{\mathrm{Ex}}^{n}\right)\right.\\ &\qquad\left.+\frac{\Delta t^{2}}{2}\frac{\partial^{2}}{\partial t^{2}}\left(H^{n}\Psi_{\mathrm{Ex}}^{n}\right)+\ldots\right)\\ &= -\Delta t\frac{\partial\Psi_{\mathrm{Ex}}^{n}}{\partial t}-\frac{\Delta t^{2}}{2}\frac{\partial^{2}\Psi_{\mathrm{Ex}}^{n}}{\partial t^{2}}-\frac{\Delta t^{3}}{4}\frac{\partial^{3}\Psi_{\mathrm{Ex}}^{n}}{\partial t^{3}}+\mathcal{O}\left(\Delta t^{4}\right)\end{aligned} \tag{4.32}$$

Inserting these results in Eq. (4.30) we get for the error of a time step Δt

$$\tau=-\frac{\Delta t^{3}}{12}\frac{\partial^{3}\Psi_{\mathrm{Ex}}^{n}}{\partial t^{3}}+\mathcal{O}\left(\Delta t^{4}\right) \tag{4.33}$$

So we see that this scheme is in fact of second order. But does the error accumulate over time as in the case of the forward Euler method? Here we need to investigate the stability of the method.

The unitarity of the time evolution operator should be reflected in the numerical solution of our discretized Schrödinger equation, i.e. in the numerical time evolution operator. The updating rules for the various schemes are in reality approximations to the time evolution operator U. In particular, for the Crank Nicolson rule we have that

$$U_{\mathrm{CN}}^{n}=\left(1+\frac{i}{2}\Delta tH^{n+1}\right)^{-1}\left(1-\frac{i}{2}\Delta tH^{n}\right). \tag{4.34}$$

If the scheme is to be perfectly unitary and thus norm-conserving, then $(U_{\mathrm{CN}}^{n})^{\dagger}U_{\mathrm{CN}}^{n}$ must be the identity operator. In the case of the time-dependent Hamiltonian the analysis of whether this is true is laborious to carry out, but is simplified in the case of a constant Hamiltonian: We note that if ϵ_n are the discrete eigenvalues of H, then the eigenvalues of U_{CN} are[23]

$$\lambda_{n}=\frac{1+\frac{i}{2}\Delta t\epsilon_{n}}{1-\frac{i}{2}\Delta t\epsilon_{n}}, \tag{4.35}$$

and the eigenvectors coincide with those of H. Furthermore, the norm of the eigenvalues are

$$|\lambda_n| = \left[\frac{1+\frac{1}{4}\Delta t^2\epsilon_n^2}{1+\frac{1}{4}\Delta t^2\epsilon_n^2}\right]^{1/2} = 1. \tag{4.36}$$

This means that this scheme is unconditionally stable in the time-independent case. For the time-dependent case the analysis is more complicated, so I will simply state the result. For a full derivation see Ref. [23].

In the time-dependent case the result is[23]

$$(U_{\mathrm{CN}}^n)^\dagger U_{\mathrm{CN}}^n = 1 - \frac{\Delta t^3}{4}\left[H^n\frac{\partial H^n}{\partial t} + \frac{\partial H^n}{\partial t}H^n\right] + \mathcal{O}\left(\Delta t^4\right), \tag{4.37}$$

which means that we have secured unitarity to second order in the general case, and to at least third order in the time-independent case.

4.3.3 The Leap-Frog Method

Is it possible to find a simple explicit scheme that is also norm-conserving? In the early days of numerical computation of the Schrödinger equation the method typically used was the (implicit) Crank-Nicolson method. In 1978 Askar and Cakmak published a paper proving that by only a simple modification of the methods I have been discussing so far you will get a method that is explicit, stable and easy to implement [24].

We recognize that the problem with our previous explicit method, the forward Euler method, is that the approximation to the time derivative is not centered. It is this non-centered aspect that causes the instability of the numerical scheme.

The Leap-Frog scheme itself is very simple. We simply use a centered difference for the time derivative and evaluate the right hand side in-between

$$\frac{1}{2\Delta t}\left(\Psi^{n+1} - \Psi^{n-1}\right) = -iH^n\Psi^n, \tag{4.38}$$

giving an explicit scheme as promised

$$\Psi^{n+1} = \Psi^{n-1} - 2i\Delta t H^n\Psi^n. \tag{4.39}$$

Note that we need two earlier wave functions Ψ^n and Ψ^{n-1} to find the new wave function Ψ^{n+1}, i.e. twice the information needed in the previous schemes[4]. In reality we do not need this double information. If we separate the real and imaginary parts of the wave function

$$\Psi^n = R^n + iI^n, \tag{4.40}$$

substitute this into Eqn. (4.39) and collect real and imaginary terms, we obtain

$$\begin{aligned} R^{n+1} &= R^{n-1} + 2\Delta t H^n I^n \\ I^{n+1} &= I^{n-1} - 2\Delta t H^n R^n. \end{aligned} \tag{4.41}$$

If H^n applied to a real vector is a real vector we have created an algorithm to update R and I separately. As we see when looking closely at the scheme, it is only necessary to know each component at every second grid point. We say that we are using a staggered grid. This implementation has the advantage that we do not have to work directly with complex numbers.

Let us find the accuracy of this scheme. We insert the exact solution Ψ_{Ex} to the continuous problem and Taylor expand $\Psi_{\text{Ex}}^{n\pm1}$ around t_n. This gives us the truncation error

$$\begin{aligned} \tau &= \frac{1}{2}\left(\Psi_{\text{Ex}}^{n+1} - \Psi_{\text{Ex}}^{n-1}\right) + 2i\Delta t^2 H^n \Psi_{\text{Ex}}^n \\ &= \frac{1}{2}\left[\sum_{m=0}^{\infty} \frac{\Delta t^{2m+1}}{(2m+1)!} \frac{\partial^{2m+1}\Psi_{\text{Ex}}^n}{\partial t^{2m+1}}\right] + 2i\Delta t^2 \frac{\partial \Psi_{\text{Ex}}^n}{\partial t} \\ &= \frac{\Delta t^3}{6}\frac{\partial^3 \Psi_{\text{Ex}}^n}{\partial t^3} + \mathcal{O}\left(\Delta t^4\right). \end{aligned} \tag{4.42}$$

The Leap-Frog scheme is thus also a second order method. Regarding the norm-conserving properties of the scheme, the result is that for the discretized time evolution operator we get[23]

$$\left(U_{\text{LF}}^n\right)^\dagger \left(U_{\text{LF}}^n\right) = 1 + \Delta t^3 \left(H^n \frac{\partial H^n}{\partial t} + \frac{\partial H^n}{\partial t} H^n\right) + \mathcal{O}\left(\Delta t^4\right). \tag{4.43}$$

We have secured unitarity to second order in the general case and for time independent problems to at least third order.

[4]When implementing this method the question arises of what to do with the first time step. Given the initial wave function Ψ^0 we need both this and Ψ^1 to calculate Ψ^2. The answer of course, is to use some other method to propagate the fist time step. We will make use of the Crank Nicolson method.

The Leap-Frog method is stable, but not unconditionally so. It can be shown that for the method to be stable, we must choose the time step Δt smaller than the inverse of the largest eigenvalue $\epsilon_{\max}$ of the discretized Hamiltonian,

$$\Delta t \leq \frac{1}{\epsilon_{\max}}. \tag{4.44}$$

I will not prove this here, so the interested reader should look at Ref. [23]. In the finite difference approximation, for a particle living on our discretized domain, the higher the energy of the particle (i.e. the larger the energy eigenvalue) the more the problem will resemble that of the square well. The energy eigenvalues of the infinite square well (of unit length) are given by $\epsilon_n = \frac{4}{\Delta x^2}\sin^2\left(n\pi\Delta x/2\right)$ in the finite difference approximation. From this we get a stability criterion for the Leap-Frog scheme in the finite difference approximation

$$\Delta t \leq \frac{1}{\epsilon_{\max}} = \frac{\Delta x^2}{4\sin^2\left(N\pi\Delta x/2\right)} = \frac{\Delta x^2}{4}. \tag{4.45}$$

4.3.4 The Pseudospectral Method

Is it possible to use the formal expression for the time evolution operator Eqn. (4.10) directly in a numerical method, that is, without using some form of Taylor expansion of this expression? Assume for now that the Hamiltonian is independent of time. The time-evolution operator is then given exactly as $U(t,t_0) = \exp\left[-i\left(t-t_0\right)H\right]$. So given our discretized Hamiltonian $\mathbf{H}$ and initial state $\mathbf{\Psi}\left(t_0\right)$, if we can find some way of calculating the exponential of a matrix we could in principle go directly from the initial state to the final state

$$\mathbf{\Psi}\left(t\right) = \exp\left[-i\left(t-t_0\right)\mathbf{H}\right]\mathbf{\Psi}\left(t_0\right). \tag{4.46}$$

That this should replace all our complicated time stepping schemes seems too good to be true, and in most cases this is indeed so. For a Hermitian matrix $\mathbf{A}$ and a number s, $\exp(is\mathbf{A})$ is in general only possible to calculate accurately for small s. Keeping the time step Δt small, it is still possible to use the direct calculation of matrix exponentials in a workable scheme as follows

$$\mathbf{\Psi}^{n+1} = \exp\left(-i\Delta t\mathbf{H}\right)\mathbf{\Psi}^{n}. \tag{4.47}$$

For a time-independent Hamiltonian, this method is in principle exact. We will encounter a method that makes use of this "brute force" computation of matrix exponentials in the next section. For the time being we note that evaluating matrix exponentials

this way involves much more computational effort than for the methods in the previous sections. The time needed for computing matrix exponentials depends strongly on the size of the matrix, on the size of its elements and if it is sparse. For the case of spectral discretization, $\mathbf{H}$ is dense, so that $\exp(-i\Delta t\mathbf{H})$ is only practical to compute for relatively small matrices.

We can find a much quicker way of calculating the exponential by splitting up the Hamiltonian into the kinetic and potential term, $H = T + V$. The idea is to split up the matrix exponential in a similar fashion. But unfortunately, in general

$$U(\Delta t) = \exp[-i\Delta t(T+V)] = \exp(-i\Delta tT)\exp(-i\Delta tV) \quad \Longrightarrow \quad [T,V] = 0. \tag{4.48}$$

The converse is also true. Since T and V are known not to commute, the splitting introduces an error. Just how large is this error? Expanding the exact time propagator and our split version

$$\begin{aligned} U(\Delta t) &= \exp[-i\Delta t(T+V)] \\ &= 1 - i\Delta t(T+V) - \frac{\Delta t^2}{2}\left(T^2+V^2+TV+VT\right) + \mathcal{O}\left(\Delta t^3\right) \\ U_{\text{split}}(\Delta t) &= \exp(-i\Delta tT)\exp(-i\Delta tV) \\ &= \left(1 - i\Delta tT - \frac{\Delta t^2}{2}T^2 + \mathcal{O}\left(\Delta t^3\right)\right)\left(1 - i\Delta tV - \frac{\Delta t^2}{2}V^2 + \mathcal{O}\left(\Delta t^3\right)\right) \\ &= 1 - i\Delta t(T+V) - \frac{\Delta t^2}{2}\left(T^2+V^2+2TV\right) + \mathcal{O}\left(\Delta t^3\right) \end{aligned} \tag{4.49}$$

the difference becomes

$$U(\Delta t) - U_{\text{split}}(\Delta t) = \Delta t^2[T,V] + \mathcal{O}\left(\Delta t^3\right). \tag{4.50}$$

Clearly, this method is of first order in the time step. By the following trick, the error introduced by the splitting can be reduced to $\mathcal{O}\left(\Delta t^3\right)$

$$U(\Delta t) = \exp(-i\Delta tV/2)\exp(-i\Delta tT)\exp(-i\Delta tV/2) + \mathcal{O}\left(\Delta t^3\right). \tag{4.51}$$

This can easily be shown by expanding the expression as in Eq. (4.49). The splittings introduced here[5] of course also carry over to the discretized problem. This method offers no improvement over what we had in Eq. (4.47), actually, quite the contrary. So why bother splitting up the exponential? We first note that the exponential $\exp(-i\Delta t\mathbf{V}/2)$

[5]Note that T and V can switch places while still keeping the error term to third order.

is trivial to compute because $\mathbf{V}$ is diagonal. In the frequency representation however, we know that $\mathbf{T}$ is diagonal. So if we Fourier transform the wave function before computing the action of $\exp(-i\Delta t\mathbf{T})$, computing the matrix exponentials would be trivial! With $\mathcal{F}$ being the discrete Fourier transform and $\mathcal{F}^{-1}$ the inverse, we have

$$\mathbf{\Psi}^{n+1} = \exp(-i\Delta t\mathbf{V}/2)\,\mathcal{F}^{-1}\left\{\exp(-i\Delta t\mathbf{T})\,\mathcal{F}\left[\exp(-i\Delta t\mathbf{V}/2)\,\mathbf{\Psi}^{n}\right]\right\}. \tag{4.52}$$

This particular combination of Eq. (4.51) and the discrete Fourier transform is often called the *pseudospectral method*, or split-step FFT, the latter referring to the fact that the discrete Fourier transform is almost invariably implemented by FFT. Since the FFT requires only $\mathcal{O}(N\log N)$ operations it scales favourably with the number of grid points compared with our previous methods. The pseudo-spectral method has excellent stability properties, and is in fact the first of our methods that conserves the norm exactly. We can show this as follows:

It is the unitarity of the time evolution operator U that secures the norm conservation of the wave function. Given $\mathbf{\Psi}^{n+1} = \mathbf{U}\mathbf{\Psi}^{n}$ where $\mathbf{U}$ is unitary, we see that

$$\left\|\mathbf{\Psi}^{n+1}\right\|^2 = \left(\mathbf{\Psi}^{n}\mathbf{U}\right)^{\dagger}\left(\mathbf{\Psi}^{n}\mathbf{U}\right) = \mathbf{\Psi}^{n\dagger}\mathbf{U}^{\dagger}\mathbf{U}\mathbf{\Psi}^{n} = \mathbf{\Psi}^{n\dagger}\mathbf{\Psi}^{n} = \left\|\mathbf{\Psi}^{n}\right\|^2. \tag{4.53}$$

The converse, that norm conservation implies unitarity, is also true. The adjoint matrix of $\mathbf{U} = \exp(-i\Delta t\mathbf{V}/2)\exp(-i\Delta t\mathbf{T})\exp(-i\Delta t\mathbf{V}/2)$, is

$$\mathbf{U}^{\dagger} = \exp(i\Delta t\mathbf{V}/2)\exp(i\Delta t\mathbf{T})\exp(i\Delta t\mathbf{V}/2). \tag{4.54}$$

Here we have used that for a general matrix $\mathbf{A}$ we have $\exp(\mathbf{A})^{\dagger} = \exp\left(\mathbf{A}^{\dagger}\right)$ and that $\mathbf{T}$ and $\mathbf{V}$ are Hermitian. Using that the inverse of $\exp(\mathbf{A})$ is $\exp(-\mathbf{A})$, we can easily see that we get $\mathbf{U}^{\dagger}\mathbf{U} = \mathbf{I}$. The split propagator is unitary and thus norm conserving.

But what about the case where H is time-dependent? Can we be sure that Eq. (4.51) is still of second order in the time step? And where should $V(t)$ be evaluated? We will first prove that $U_1(t_n+\Delta t, t_n) = \exp(-i\int_{t_n}^{t_n+\Delta t} H(s)\ \mathrm{d}s)$ gives us a second order approximation,

$$U(t_n+\Delta t, t_n) = \exp\left(-i\int_{t_n}^{t_n+\Delta t} H(s)\ \mathrm{d}s\right) + \mathcal{O}\left(\Delta t^3\right). \tag{4.55}$$

We do this by expanding U_1 and the exact time evolution operator U, and computing

the difference. Expanding to second order in the time step we get

$$\begin{aligned} U_1\left(t_n+\Delta t,t_n\right) &= I+\int_{t_n}^{t_n+\Delta t} H\left(s\right)\ \mathrm{d}s+\frac{1}{2}\int_{t_n}^{t_n+\Delta t}\int_{t_n}^{t_n+\Delta t} H\left(s_1\right)H\left(s_2\right)\ \mathrm{d}s_1\ \mathrm{d}s_2+\mathcal{O}\left(\Delta t^3\right) \\ U\left(t_n+\Delta t,t_n\right) &= I+\int_{t_n}^{t_n+\Delta t} H\left(s\right)\ \mathrm{d}s+\frac{1}{2}\int_{t_n}^{t_n+\Delta t}\int_{t_n}^{t_n+\Delta t} \mathcal{T}\left[H\left(s_1\right)H\left(s_2\right)\right]\ \mathrm{d}s_1\ \mathrm{d}s_2+\mathcal{O}\left(\Delta t^3\right), \end{aligned} \tag{4.56}$$

which gives us the difference

$$U_1-U=\frac{1}{2}\int_{t_n}^{t_n+\Delta t}\int_{t_n}^{s_2}\left[H\left(s_1\right),H\left(s_2\right)\right]\ \mathrm{d}s_1\ \mathrm{d}s_2+\mathcal{O}\left(\Delta t^3\right). \tag{4.57}$$

Now, the commutator $\left[H\left(s_1\right),H\left(s_2\right)\right]$ is of order $\mathcal{O}\left(s_1-s_2\right)$, as we can see from Taylor expanding $H\left(s_2\right)$ around s_1

$$\begin{aligned} \left[H\left(s_1\right),H\left(s_2\right)\right] &= \left[H\left(s_1\right),H\left(s_1\right)+\left(s_2-s_1\right)H'\left(s_1\right)+\ldots\right] \\ &= \left(s_2-s_1\right)\left[H\left(s_1\right),H'\left(s_1\right)\right]+\mathcal{O}\left(\left(s_2-s_1\right)^2\right) \\ &= \mathcal{O}\left(s_2-s_1\right). \end{aligned} \tag{4.58}$$

The integral of the commutator on the domain of area $\frac{1}{2}\Delta t^2$ in Eq. (4.57) must therefore have an error of order $\mathcal{O}\left(\Delta t^3\right)$.

Now, as we have seen, in order to implement this effectively we have to use splitting methods. Then we note, since the method is only of second order, there is no need to evaluate the integrals to more than second order either. We evaluate the integrals with midpoint and trapezoidal quadratures

$$\begin{aligned} \int_{t_n}^{t_n+\Delta t} H\left(s\right)\ \mathrm{d}s &= \int_{t_n}^{t_n+\Delta t} T\left(s\right)\ \mathrm{d}s+\int_{t_n}^{t_n+\Delta t} V\left(s\right)\ \mathrm{d}s \\ &= \Delta t T^{n+1/2}+\frac{\Delta t}{2}\left(V^n+V^{n+1}\right)+\mathcal{O}\left(\Delta t^3\right). \end{aligned} \tag{4.59}$$

Using the same reasoning as for the splitting in Eq. **??** we see that we get a third order method

$$U\left(t_n+\Delta t,t_n\right)=\exp\left(-\frac{i}{2}V^{n+1}\right)\exp\left(-iT^{n+1/2}\right)\exp\left(-\frac{i}{2}V^n\right)+\mathcal{O}\left(\Delta t^3\right). \tag{4.60}$$

This answers the question of where to evaluate $V\left(t\right)$ in the case of a time-dependent potential, and proves that this method is still of second order. For a Hermitian matrix $H(t)$ integrals of the form $\int H(t)\ \mathrm{d}s$ are still Hermitian, so $\exp\left(\int H(t)\ \mathrm{d}s\right)$ is still unitary and the method is norm-conserving.

4.3.5 A Fourth-Order Method

The methods investigated in the previous sections are easy to implement, have low computational cost and, especially in the case of the splitting method, have good stability properties. If there is something left to be desired it is greater accuracy in the time step. We will now look into a relatively new scheme first proposed by S. Blanes and P.C. Moan in 1999, giving a fourth order method in the time step. For the original article see Ref. [1].

Derivation of the method is unfortunately, due to the use of mathematical tools such as graph theory and the theory of free Lie algebras, beyond the scope of this thesis. A short overview of the basis for the method will be given, along with the results.

The method is based on the so-called Magnus expansion of the time evolution operator. It was introduced by W. Magnus in 1954 [25] in the context of quantum field theory and provided a way of approximating the time evolution operator by an exponential

$$U(t,t_0) = \exp\left(\Omega\left(t,t_0\right)\right), \qquad \Omega\left(t_0\right) = 0, \tag{4.61}$$

of a series of multiple integrals of nested commutators,

$$\Omega\left(t,t_0\right) = \sum_{k=1}^{\infty} \Omega_k\left(t,t_0\right). \tag{4.62}$$

A very important feature of the Magnus expansion is that, no matter where the series is truncated, the scheme remains unitary [26, 27]. This is a property not shared by the expansion of the time evolution operator in Eqn. (4.7).

It can be shown [26] that the terms in the Magnus expansion satisfy[6]

$$\Omega_k\left(t,t_0\right) = \sum_{j=0}^{n-1} \frac{B_j}{j!} \int_{t_0}^{t} S_k^j\left(\tau\right)\, \mathrm{d}\tau, \quad k \geq 1, \tag{4.63}$$

with S_k^j being given by the recurrence relation

$$\begin{aligned} S_1^0 &= -iH, \quad S_k^0 = 0, \quad k \geq 1, \\ S_k^j &= \sum_{m=1}^{k-j} \left[\Omega_m, S\right], \quad 1 \leq j \leq k-1. \end{aligned} \tag{4.64}$$

The first three terms in the Magnus series are then

[6] The B_j's are the Bernoulli numbers.

$$\begin{aligned}
\Omega_1(t,t_0) &= -i\int_{t_0}^{t} H(t_1)\,\mathrm{d}t_1 \\
\Omega_2(t,t_0) &= -\frac{1}{2}\int_{t_0}^{t}\mathrm{d}t_1\int_{t_0}^{t_1}\mathrm{d}t_2\,[H(t_1),H(t_2)] \\
\Omega_3(t,t_0) &= \frac{i}{6}\int_{t_0}^{t}\mathrm{d}t_1\int_{t_0}^{t_1}\mathrm{d}t_2\int_{t_0}^{t_2}\mathrm{d}t_3\,([H(t_1),[H(t_2),H(t_3)]]+[H(t_3),[H(t_2),H(t_1)]])\,.
\end{aligned} \tag{4.65}$$

In general, Ω_k is a k-dimensional integral of nested commutators of H evaluated at different times, and quickly becomes prohibitively expensive to evaluate with increasing k.

Used as a basis for a time integration scheme for our discretized Schrödinger equation, truncating the Magnus expansion after the first term gives a second order method, truncating after the second term a fourth order method, and so on:

$$\Psi^{n+1} = U\left(\Delta t + t_n, t_n\right)\Psi^n \approx \exp\left(\sum_{k=1}^{j}\Omega_k\right)\Psi^n + \mathcal{O}\left(\Delta t^{2j+1}\right). \tag{4.66}$$

Indeed, keeping only the first term in the Magnus expansion gives us Eqn. (4.55) exactly, a method we proved to be of second order. The multidimensional integrals in Eqn. (4.65) remain a major hurdle for implementing the higher order methods efficiently. In a paper by Blanes, Cacas and Ros [26] it is shown how to reduce these integrals to single-dimensional integrals and how to reduce the number of commutators involved. Blanes and Moan then applies this to the Schrödinger equation, see Ref. [1]. When restricting ourselves to the fourth-order case the conclusion is that the first two terms in the Magnus expansion can be written as

$$\begin{aligned}
\Omega_1 &= M_1 \\
\Omega_2 &= [M_1, M_2]\,,
\end{aligned} \tag{4.67}$$

where M_1 and M_2 are given as

$$\begin{aligned}
M_1 &= -i\int_{t_n}^{t_n+\Delta t} H\left(s\right)\,\mathrm{d}s \\
M_2 &= \frac{i}{\Delta t}\int_{t_n}^{t_n+\Delta t}\left(s-\left(\frac{\Delta t}{2}-t_n\right)H\left(s\right)\,\mathrm{d}s = \frac{i}{\Delta t}\left[\int_{t_n}^{t_n+\Delta t} sH\left(s\right)\,\mathrm{d}s\right] + \left(\frac{\Delta t}{2}-t_n\right)M_1.
\end{aligned} \tag{4.68}$$

We observe that if the Hamiltonian is independent of time M_2 vanishes identically. Our time stepping scheme becomes

$$\Psi^{n+1} = \mathrm{e}^{\Omega_1+\Omega_2}\Psi^n + \mathcal{O}(\Delta t^5) = \mathrm{e}^{M_1+[M_1,M_2]}\Psi^n + \mathcal{O}(\Delta t^5). \tag{4.69}$$

If the integrals of the form $\int H(s)\ \mathrm{d}s$ and $\int sH(s)\ \mathrm{d}s$ cannot be evaluated analytically, we must resort to numerical integration with a sufficient accuracy. I will use gaussian quadrature when implementing this method later in this chapter.

It is possible to get rid of the commutators using splitting methods for the exponential, while the method remains of fourth order. By using the Baker-Cambell-Hausdorff formula it can be shown that

$$\begin{aligned} U(t_n + \Delta t, t_n) &= \mathrm{e}^{\Omega_1+\Omega_2+O(\Delta t^5)} \\ &= \mathrm{e}^{\frac{M_1}{2}-2M_2}\mathrm{e}^{\frac{M_1}{2}+2M_2} + O(\Delta t^5) \\ &= \mathrm{e}^{-M_2}\mathrm{e}^{M_1}\mathrm{e}^{M_2} + \mathcal{O}(\Delta t^5). \end{aligned} \tag{4.70}$$

In the current form there is no "clever" way to evalute the matrix exponentials with the discrete Fourier transform as in the case of the pseudospectral method, and the matrix exponentials will have to be calculated by brute force. In the following sections I will investigate if we in some way can make up for this extra computational effort by increasing the time-step Δt.

4.4 Numerical Experiments

I will now conduct a short series of experiments to test the numerical methods described above. To gauge the accuracy of the methods the exact solutions to the time-dependent Schrödinger equation are needed. Of course this limits the choice of a test system somewhat. Since some of the methods are better suited to time-dependent problems than others, I will include tests with both time-dependent and time-independent Hamiltonians.

4.4.1 An Analytically Solvable Time-Dependent System

For the case of a time-dependent Hamiltonian there are precious few systems that can be solved exactly. In real-world applications such systems have traditionally been treated with perturbation theory or by numerical methods. But it so happens that for the following Hamiltonian,

$$H(t) = -\frac{1}{2}\frac{\mathrm{d}^2}{\mathrm{d}x^2} + E(t)x, \tag{4.71}$$

an exact solution can be found[7]. Inserting this into the Schrödinger equation we get

$$\frac{\partial}{\partial t}\Psi(x,t) = \frac{i}{2}\frac{\mathrm{d}^2}{\mathrm{d}x^2}\Psi(x,t) - iE(t)\Psi(x,t). \tag{4.72}$$

By considering the same problem in momentum space, it turns out that it is possible to find a closed form solution to this equation (for a discussion on momentum space see for example [28]). Here the Hamiltonian becomes

$$H\left(t\right) = \frac{1}{2}p^2 + iE\left(t\right)\frac{\mathrm{d}}{\mathrm{d}p}, \tag{4.73}$$

and the Schrödinger equation in momentum space is

$$\frac{\partial}{\partial t}\Phi(p,t) - E(t)\frac{\partial}{\partial p}\Phi(p,t) = -i\frac{p^2}{2}\Phi(p,t). \tag{4.74}$$

The position and momentum representations of the wave function, $\Psi(x,t)$ and $\Phi(p,t)$, are related via a Fourier transform

$$\begin{aligned} \Psi(x,t) = &\quad \frac{1}{2\pi}\int_{-\infty}^{\infty} \mathrm{e}^{ipx}\Phi(p,t)\mathrm{d}p \\ \Phi(p,t) = &\quad \int_{-\infty}^{\infty} \mathrm{e}^{-ipx}\Psi(x,t)\mathrm{d}x. \end{aligned} \tag{4.75}$$

We note that this is not the convention normally used in most quantum mechanics texts, where there is a factor of $1/\sqrt{2\pi}$ in front of each of the integrals. Our convention is chosen to conform with the way the fast Fourier transform most often is implemented (in fact, we will have to make even a few more changes before transforming between the two representations). In this convention the wave function in position space $\Psi(x,t)$ is normalized to 1 whereas the momentum space wave function $\Phi(p,t)$ is normalized to 2π, that is, $\int_{-\infty}^{\infty}|\Phi(p,t)|^2\mathrm{d}p = 2\pi$. These factors are not of physical significance since the Schrödinger equation is linear.

Our problem is to solve Eq. (4.74) given an initial state $\Phi(p,0)$. We will use the method of characteristics. For a first-order partial differential equation, the method of characteristics discovers trajectories (the so-called characteristic curves) along which the partial differential equation becomes an ordinary differential equation . This can be solved using standard techniques and then transformed into a solution of the original equation.

[7] This solution is due to Simen Kvaal.

We will thus follow a "particle" along a curve $\Gamma(t)$ in the pt-plane. Let $\Gamma(t)$ have the inital condition $\Gamma(0) = p_0$ and assume that $\Phi(p,t)$ is a solution to the Schrödinger equation (4.74) with the correct initial state. Define the function $z(t) \equiv \Phi(\Gamma(t),t)$, where we evaluate $\Phi(p,t)$ along the curve $\Gamma(t)$. Differentiation with respect to t gives

$$\begin{aligned} \frac{\mathrm{d}}{\mathrm{d}t}z(t) = &\quad \frac{\partial}{\partial t}\Phi(\Gamma,t) + \frac{\mathrm{d}}{\mathrm{d}t}\Gamma(t)\frac{\partial}{\partial \Gamma}\Phi(\Gamma,t) \\ = &\quad \frac{\partial}{\partial t}\Phi(p,t) + \frac{\mathrm{d}}{\mathrm{d}t}\Gamma(t)\frac{\partial}{\partial p}\Phi(p,t). \end{aligned} \tag{4.76}$$

We see that if $\Gamma(t)$ satisfies the differential equation $\Gamma'(t) = -E(t)$, we get

$$\frac{\mathrm{d}}{\mathrm{d}t}z(t) = \frac{\partial}{\partial t}\Phi(p,t) - E(t)\frac{\partial}{\partial p}\Phi(p,t) = -\frac{i}{2}\Gamma(t)^2 z(t). \tag{4.77}$$

The expression for $\Gamma(t)$ then becomes

$$\Gamma(t) = \Gamma(0) + F(t) = p_0 + F(t), \qquad F(t) \equiv -\int_0^t E(s)\mathrm{d}s. \tag{4.78}$$

We can now solve the differential equation for $z(t)$. The result is $z(t) = z(0)\mathrm{e}^{-\frac{i}{2}\int_0^t \Gamma(s)^2 \mathrm{d}s}$, which is the same as writing

$$\Phi(p_0 + F(t), t) = \Phi(p_0, 0)\, \mathrm{e}^{-\frac{i}{2}\int_0^t (p_0 + F(s))^2 \mathrm{d}s}. \tag{4.79}$$

Since we are free to choose p_0 to our liking, we set $p_0 = p - F(t)$, where p is arbitrary. This gives the exact solution in terms of the momentum wave function

$$\Phi(p,t) = \Phi(p - F(t), 0)\mathrm{e}^{-\frac{i}{2}f(p,t)}. \tag{4.80}$$

Here we have defined the phase function $f(p,t)$ as

$$f(p,t) \equiv \int_0^t \left(p - F(t) + F(s)\right)^2 \mathrm{d}s. \tag{4.81}$$

When using this result it can be useful to rewrite this function slightly. One possible way is

$$\begin{aligned} f(p,t) &= \int_0^t (p - F(t))^2 \mathrm{d}s + 2\int_0^t (p - F(t))F(s)\mathrm{d}s + \int_0^t F(s)^2 \mathrm{d}s \\ &= (p - F(t))^2 t + 2(p - F(t))\int_0^t F(s)\mathrm{d}s + \int_0^t F(s)^2 \mathrm{d}s \\ &= (p - F(t))^2 t + 2(p - F(t))G(t) + J(t), \end{aligned} \tag{4.82}$$

with the definitions

$$G(t) = \int_0^t F(s)\ \mathrm{d}s, \qquad\qquad J(t) = \int_0^t F(s)^2\ \mathrm{d}s. \tag{4.83}$$

The Initial State $\Phi\,(p,0)$

We choose a gaussian wave packet centered around $p = 0$ as our initial state

$$\Phi(p,0) = \sqrt{\frac{2}{\sigma}}\pi^{1/4}\mathrm{e}^{-\frac{p^2}{2\sigma^2}}. \tag{4.84}$$

In position space the initial state is given as

$$\Psi(x,0) = \frac{1}{2\pi}\int_{-\infty}^{\infty}\Phi(p,0)\mathrm{e}^{ipx}\mathrm{d}p = \frac{\sqrt{\sigma}}{\pi^{1/4}}\mathrm{e}^{-\frac{1}{2}\sigma^2 x^2}. \tag{4.85}$$

Incidentally, for the case where $E\,(t) \equiv 0$, i.e. the free particle, the analytical solution is trivial to obtain [28] and is given explicitly as

$$\Psi\,(x,t) = \frac{1}{\pi^{1/4}}\sqrt{\frac{\sigma}{1 + i\sigma^2 t}}\exp\left(-\frac{\sigma^2 x^2/2}{1 + i\sigma^2 t}\right). \tag{4.86}$$

The Time-Dependent Term $E\,(t)$

For the time-dependent part of the Hamiltonian I will use a modulated sinusoidal pulse of the form

$$E\,(t) = E_{\max}\sin^2\left(\frac{\pi t}{T}\right)\sin\left(\omega t\right). \tag{4.87}$$

This choice is motivated by the fact that it serves as a good model for a short laser pulse [29]. Sometimes it will be an advantage to use a slightly simpler time-dependence, so I will also use a function of the form

$$E(t) = E_{\max} \cos\left[\omega\left(t + \delta\right)\right]. \tag{4.88}$$

Computing the integrals in Eq. (4.83) with the function in Eq. (4.87) by hand would be a gargantuan task, so we will use Maple to do the integrals for us. We are not finished here however, as our solution given by Eq. (4.80) is still given in momentum space. Using the exact definition in Eq. (4.75) to transform to position space is impractical, if not impossible, and when comparing the results of our numerical experiments with the exact solution we will use FFT to transform between the two representations.

Using Ehrenfest's Theorem to Verify the Correctness of the Solution

An important gauge of the accuracy of our numerical methods is how well they reproduce the expectation values of properties such as position, momentum and energy. This we can check quickly against our analytical solutions by using Ehrenfest's theorem.

For a general operator A it can be proven from the basic axioms of quantum mechanics that [11]

$$\frac{\mathrm{d}}{\mathrm{d}t}\langle A\rangle = \frac{1}{i\hbar}\langle[A, H]\rangle + \left\langle\frac{\partial A}{\partial t}\right\rangle. \tag{4.89}$$

Applying this to a Hamiltonian of the form

$$H(x, p, t) = \frac{p^2}{2m} + V(x, t), \tag{4.90}$$

we get the relations

$$\begin{aligned}\frac{\mathrm{d}}{\mathrm{d}t}\langle x\rangle &= \langle p\rangle \\ \frac{\mathrm{d}}{\mathrm{d}t}\langle p\rangle &= \langle -\nabla V\rangle.\end{aligned} \tag{4.91}$$

These relations are known as *Ehrenfests theorem*[8]. These important relations justifies our sometimes classical mental image of a quantum-mechanical wave packet: The wave packet obeys the equations of motion of the corresponding classical particle when the position, momentum, and force acting on the particle are replaced by the expectation values of these quantities. Applied to our system Ehrenfest's theorem gives us

[8]Sometimes in the literature, the more general relation of Equation (4.89) is referred to as Ehrenfests theorem.

$$\langle p\,(t)\rangle = p_0 - \int_0^t E(s)\mathrm{d}s = F(t) \tag{4.92}$$

$$\langle x\,(t)\rangle = x_0 + \int_0^t F(s)\mathrm{d}s = G(t) \tag{4.93}$$

$$\langle T\,(t)\rangle = \frac{\langle p\rangle^2}{2} = \frac{1}{2}\left(\langle p^2\rangle + \left\langle (p-\langle p\rangle)^2\right\rangle\right) = \frac{1}{2}\langle p^2\rangle - \frac{\sigma^2}{4} \tag{4.94}$$

The last equation follows from the fact that for the gaussian wave packet the variance is $\frac{1}{2}\left\langle (p-\langle p\rangle)^2\right\rangle$.

4.4.2 An Analytically Solvable Time-Independent Model

It is interesting to compare the time stepping methods in the case of a time-independent Hamiltonian as well. When the time-dependent part of the system described in the previous section is turned off the system reduces to that of the free particle. This is not a very interesting system as nothing much happens, except for the spreading of the wave packet. Another problem is that if we want to extend the time frame of our simulation the dispersion of the wave packet will eventually give rise to unphysical effects due to the periodic boundary conditions defined in the Fourier transformation.

Our solution is to place the wave packet in a confining potential, where we choose that of the harmonic oscillator, so that our Hamiltonian becomes

$$H = -\frac{1}{2m}\frac{\mathrm{d}^2}{\mathrm{d}x^2} + \frac{1}{2}m\omega_0^2 x^2. \tag{4.95}$$

The stationary solutions to this Hamiltonian are well known and are given as

$$\psi(x)_n = \left(\frac{\omega_0}{\pi}\right)^{1/4}\frac{1}{\sqrt{2^n n!}}H_n\left(\sqrt{\omega_0}x\right)\mathrm{e}^{-\omega_0 x^2/2}, \tag{4.96}$$

where H_n are the Hermite polynomials. To create interesting time dependencies (other than just a complex phase) we can form linear combinations of these eigenstates. But it turns out also that for an initial state of the form

$$\Psi(x,0) = \left(\frac{\omega_0}{\pi}\right)^{1/4}\mathrm{e}^{-\frac{\omega_0}{2}(x-x_0)^2} \tag{4.97}$$

an analytical solution can be found [13]:

$$\Psi(x,t) = \left(\frac{\omega_0}{\pi}\right)^{1/4} \exp\left[-\frac{1}{2}i\omega_0 t\right] \exp\left[-\frac{1}{4}\omega_0 x_0^2\left(1-\mathrm{e}^{-2i\omega_0 t}\right)\right] \exp\left[-\frac{1}{2}\omega_0\left(x-x_0\mathrm{e}^{-i\omega_0 t}\right)^2\right]. \tag{4.98}$$

This particular solution is known as the *coherent state*. It is the system whose behaviour most closely resembles that of a classical harmonic oscillator system. At all times, the wave packet retains its initial shape. The motion of the expectation value of x follows that of a classical oscillator

$$\langle x\rangle = x_0\cos\left(\omega_0 t\right). \tag{4.99}$$

4.4.3 The Implementation

All the numerics in this thesis has been done using MATLAB. Some of the scripts written can be found in Appendix B. The programs have quite probably not been implemented in the most efficient way, but since most of the simulations have been of a relatively small scale this is not critical.

The time propagation schemes are implemented as function M-files: `LeapFrog.m`, `CrankNicolson.m`, `PseudoSpectral.m` and `FourthOrderMethod.m`. They are called from a main script file: `CompareMethods.m`. In the main script the form of $E(t)$, $\Psi(x,0)$ and $V(x)$ is specified. They are given as function handles which are then passed on to the time propagation functions. Thus we can simulate just about any one-dimensional system. Other important parameters such as the number of grid points N, the length of the simulation t_{final} and the number of time steps t_{steps}, are specified in the main script file as well. The time propagation functions compute the mean energy, mean x-position and norm of the wave packet at regular intervals. These quantities are computed using the Simpson quadrature, implemented as a function M-file. The wave function itself is recorded at a number of time steps specified in the main script file.

To compare with the analytical solution a similar function M-file has been written: `ExactSolution.m`. This gives much of the same data as the time propagation schemes, but with the important difference that here the exact solution is known. In the case of the time-dependent Hamiltonian discussed in Section 4.4.1 the closed-form solution is given in momentum space, so the fast Fourier transform is used to transform this to position space.

All of the methods are implemented using the spectral method of representing the operators. It is possible to use finite differences of second or fourth order instead, by changing the parameter `'fourier'` to `'second` or `'fourth'` in the main file `CompareMethods.m`. Details on the implementations specific to the different methods are given below.

The Leap-Frog Scheme The Leap-Frog scheme does not tell us how to compute the first time step. I have implemented it using the Crank-Nicolson method. MATLAB is quite capable of handling complex arithmetic, so there is no need to separate the scheme into real and imaginary parts as in Eq. (4.41).

The Pseudospectral Method The splitting used is the one given by Eq. (4.60).

The Fourth-Order Method I have not made use of splitting methods for the exponential as in Eq. (4.70), that is, the commutators in the exponential of Eq. (4.69) are computed directly. The integrals Eq. (4.68) over the discretized Hamiltonian I have implemented with gaussian quadratures, as this gives us the maximum accuracy with the least effort. When computing the matrix exponentials, I do not make use of MATLAB's built-in function `expm`. These have instead been implemented using the Expokit package [30], as it is significantly more efficient for the type of problems we are encountering. The name of the Expokit function is `expv`.

4.4.4 Some Considerations Before Beginning the Simulations

Before comparing the accuracy of the different time stepping schemes it is interesting to investigate how the computation time depends on the number of spatial grid points N. The total simulation time for a system of the form given in Section 4.4.1 is shown in Figure 4.3. The parameters used are:

$$E_{\max} = 1 \quad \omega = 1 \quad \delta = 0 \quad \sigma = \tfrac{1}{4} \quad L = 100 \quad t_{\text{final}} = 0.5 \quad N_{\text{tSteps}} = 100$$

Here, L is the length of the discretization domain which is always taken to be centered around $x = 0$. The number of time steps is denoted by N_{tSteps}. As expected, the fourth-order method and the Crank-Nicolson method use vastly more time than the other methods as they involve calculating matrix exponentials and solving systems of linear equations, respectively. As we increase the number of grid points the differences become quite pronounced. For the $N = 1024$ case, the Fourth-Order method has a total simulation time of $t_{\text{sim}} = 1.512 \cdot 10^3$ (in seconds), which should be contrasted to that of the Leap-Frog method of $t_{\text{sim}} = 0.028$. The fourth-order method here requires $\sim 5 \cdot 10^5$ times the computational effort of the leap-frog method[9].

Performing a simple regression analysis on this data set it is found that the simulation time for the leap-frog and pseudospectral methods scale with the number of grid points N as $\mathcal{O}\left(N^{0.7}\right)$. The Crank-Nicolson shows the dependency $\mathcal{O}\left(N^{2.6}\right)$ and the

[9] All simulations in this thesis are performed on my slightly aged laptop powered by a Pentium M 1.86GHz CPU.

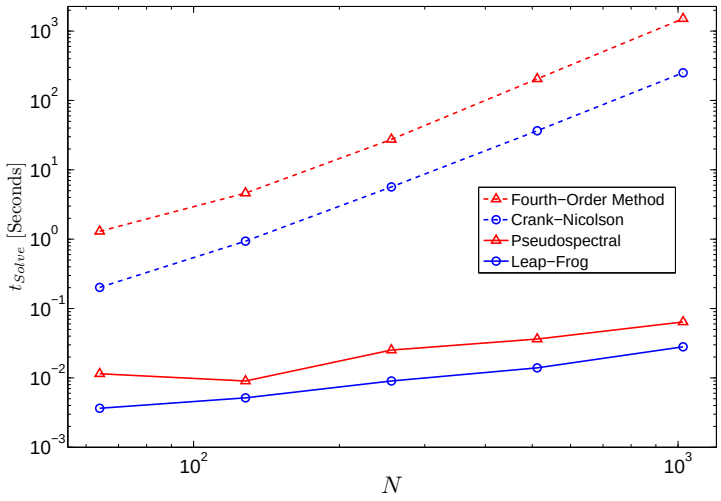

Figure 4.3: *Total computation time for 100 time steps with a grid size of* $N = 64$, $N = 128$, $N = 256$, $N = 512$ *and* $N = 1024$ *points.*

forth-order method, when removing the $N = 64$ point which for some inexplicable reason takes longer than the $N = 128$ case, shows the dependency $\mathcal{O}\left(N^{2.8}\right)$. The simulation time for the latter methods thus scale almost with the cube of the number of grid points. To illustrate the fallacy of relying blindly on computational power when performing simulations with such methods: Say we are simulating a three-dimensional quantum system and need to double the number of grid points in each direction to obtain sufficient accuracy. If the original simulation took one hour, the new simulation will take $\left(2^3\right)^{2.8} \cdot 1\text{h} = 337.79\text{h}$, which is the equivalent of two weeks.

The Crank-Nicolson method with the spectral discretization is a rather unfortunate combination, since we are no longer able to utilize the $\mathcal{O}(N \log N)$ behaviour of the FFT algorithm, and instead must live with the $\mathcal{O}(N^2)$ complexity of solving linear systems. Similarly, the fourth-order method requires exponentiating dense matrices. Ideally, the matrix-vector products utilized in Expokit should be implemented using the FFT directly and not dense representations of these.

I have done a small study see how the `expv` function depends on the size of the time step Δt. The result is shown in Figure 4.4. The system is essentially the same as in the previous simulation, but with $N = 256$ grid points. From this we see that the computation time increases only weakly until a step size of $\Delta t = 0.1$, by which time we would no longer expect `expv` to yield accurate results anyway. So for our purposes, `expv` does not depend on the step size Δt in a significant manner.

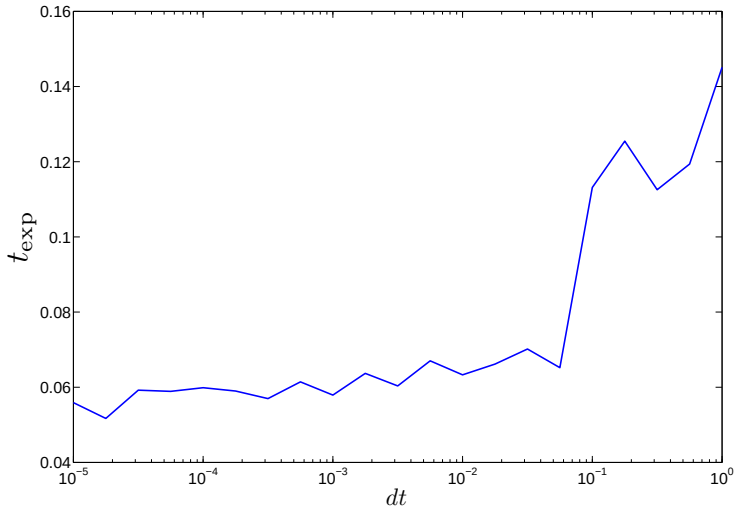

Figure 4.4: *Computation time for **expv** as a function of step length Δt .*

4.4.5 The Free Particle

For completeness, I include a simulation of one of the simplest systems imaginable: the free particle. The initial state is chosen as a gaussian wave packet, given on the form

$$\Psi(x,0) = \frac{\sqrt{\sigma}}{\pi^{1/4}} \mathrm{e}^{-\frac{1}{2}\sigma^2 x^2}. \tag{4.100}$$

In Section 4.4.1 a closed form solution of the time development of this state is stated. The parameters used in the simulation are:

$$\sigma = 1 \quad L = 30 \quad N = 512 \quad t_{\text{final}} = 1 \quad N_{\text{tSteps}} = 1500 \quad \Delta t = 0.00067$$

Before starting any simulation it is of interest to see if we have satisfied the stability criterion of the Leap-Frog scheme given by Eq. (4.45). This criterion tells us that in order for the Leap-Frog scheme to be stable, we must have

$$\frac{4\Delta t}{\Delta x^2} \leq 1. \tag{4.101}$$

For the chosen simulation parameters, we get $4\Delta t/\Delta x^2 = 0.78$, so we should be one the safe side. A plot of the probability density of the wave function at different times is seen in Figure 4.5a, where we see the spreading of the wave packet as dictated by Heisenberg's uncertainty principle. A plot of the devation of the simulated wave functions from the exact solution is shown in Figure 4.5. This shows a behaviour we will see a lot

more of: the fourth-order method wins hands down, followed by the pseudospectral method, the Crank-Nicolson method, and the leap-frog method. In that order.

In Figure 4.6 a plot of the deviation from the expectation value of x against time is shown. Perhaps surprisingly, it is the Leap-Frog method that gives the most accurate results. The deviation is very low for all the methods, below 10^{-14}. We clearly need to look at a more complicated system.

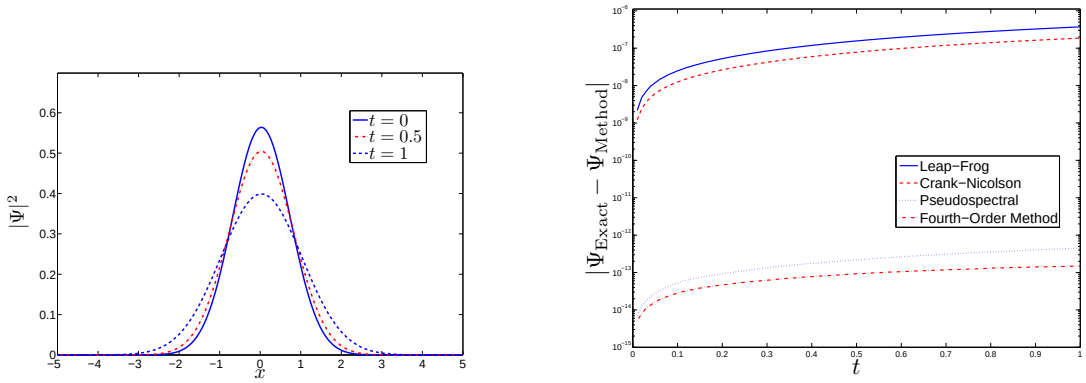

(a) Snapshots of the wave packet.

(b) Deviation from the exact wave function.

Figure 4.5: *The free particle: Probability density at three different times (left). Accuracy in reproducing the wave function (right).*

4.4.6 The Coherent State

As discussed in Section 4.4.2 the coherent state is a system for which an exact solution for the time-dependency can be found. We place a gaussian wave packet in a harmonic potential. For a specific width of this wave packet, it its initial shape and rocks back and forth with the classical oscillator frequency. The parameters used in the simulation are:

$$\omega_0 = 0.5 \quad L = 40 \quad N = 256 \quad t_{\text{final}} = 14 \quad N_{\text{tSteps}} = 5000 \quad \Delta t = 0.0028$$

Here we have that $4\Delta t/\Delta x^2 = 0.47$, so the stability of the Leap-Frog scheme is secured. The total time for the simulation was $t_{\text{sim}} = 477.2$. A plot of the expectation value of x is shown in Figure 4.7a. We have simulated for little over a period of the classical period of the harmonic oscillator.

A plot of the deviation from the expectation value of x (Figure 4.7b) reveals that the fourth-order method is about eight orders of magnitude more accurate than the next best method. The devation from the exact wave function (Figure 4.9) shows much of

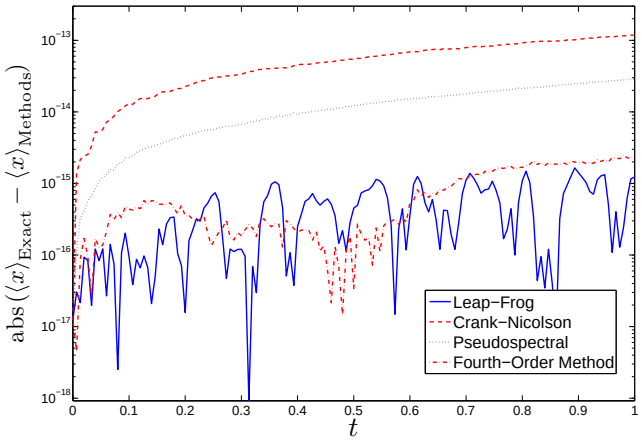

Figure 4.6: *The free particle: deviation from the mean value of position.*

the same behaviour as for the free particle, but with the difference in accuracy between the pseudospectral method and the fourth-order method now becoming apparent. The plot of the deviation from unitarity (Figure 4.8) shows that the fourth-order method conserves unitarity to machine precision, while the leap-frog method is showing rather large fluctuations.

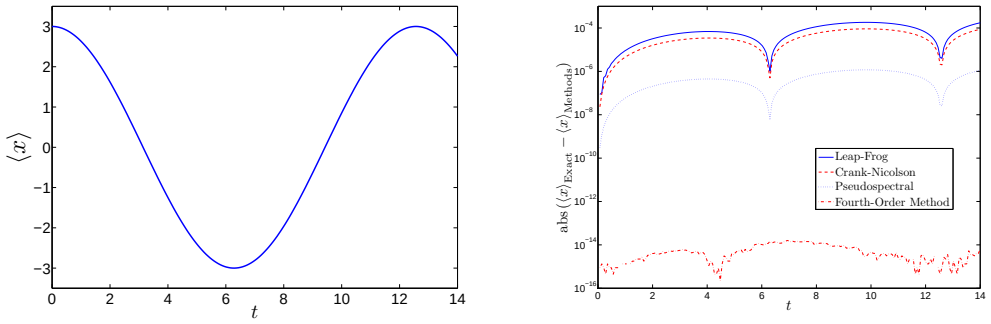

(a) Expectation value of position. **(b)** Deviation from the expectation value of position.

Figure 4.7: *The coherent state: The mean value of position (left). Deviation from mean value of position (right).*

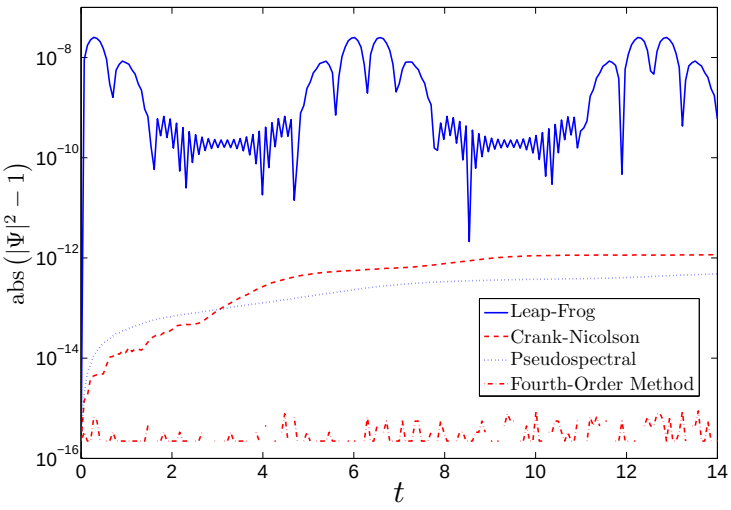

Figure 4.8: *The coherent state: deviation from unitarity.*

4.4.7 The Time Dependent External Field

Numerical methods for solving the time-dependent Schrödinger equation are typically intended to be used to solve problems involving time-dependent perturbations. The simulation of a system with a time-dependent potential will thus reveal more about under which conditions the methods are accurate enough for real-world applications. As discussed in Section 4.4.1, for the Hamiltonian

$$H(t) = -\frac{1}{2}\frac{\mathrm{d}^2}{\mathrm{d}x^2} + E(t)\,x, \tag{4.102}$$

an exact solution can be found. For the time-dependent term $E(t)$ we will use a modulated sinusoidal pulse of the form

$$E(t) = E_{\max}\sin^2\left(\frac{\pi t}{T}\right)\sin(\omega t), \tag{4.103}$$

and use a gaussian initial state of the form

$$\Psi(x,0) = \frac{\sqrt{\sigma}}{\pi^{1/4}}\mathrm{e}^{-\frac{1}{2}\sigma^2 x^2}. \tag{4.104}$$

The parameters used in the simulation are:

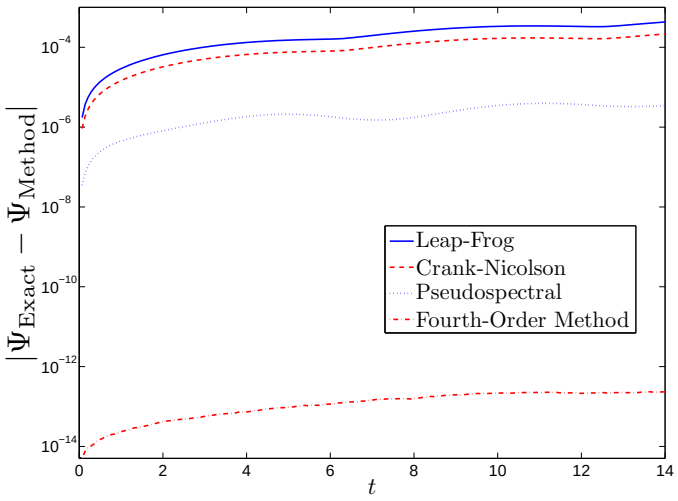

Figure 4.9: *The coherent state: deviation from the exact solution.*

$$E_{\max} = 3 \quad \omega = 2 \quad T = 10 \quad \sigma = \tfrac{1}{4} \quad L = 100$$
$$N = 512 \quad t_{\text{final}} = 10 \quad N_{\text{tSteps}} = 2500 \quad \Delta t = 0.004$$

We have here that $4\Delta t/\Delta x^2 = 0.42$, so the stability of the Leap-Frog scheme should be secured. The total run time for the simulation was $t_{\text{sim}} = 5.77 \cdot 10^3$. In Figure 4.10 some of the quantities that characterizes the system are shown, such as the form of the external pulse and the mean energy of the wave packet. In Figure 4.10d the deviation from the mean value of x is shown. The fourth-order seems capable of simulating this quantity almost to machine precision. In Section 4.3.3 and 4.3.2 we saw that for time-dependent systems the unitarity was conserved only to second order, and that the leading term in the error contained the derivative of the Hamiltonian. We can clearly see the consequences of this in Figure 4.12, where the deviation from unitarity is seen to fluctuate with the frequency of $E(t)$.

Fourth-Order Method versus Pseudospectral

In the course of the simulation in the previous sections, we have clearly established that fourth-order method is superior to the other methods in terms of accuracy. We have also seen that for the three other methods, in every test the pseudospectral method has come out on top. In Section 4.4.4 it was shown that the fourth-order method uses vastly computation resources than the pseudospectral method. It is therefore interesting to compare if we in the pseudospectral method can make up for the lack of accuracy (as

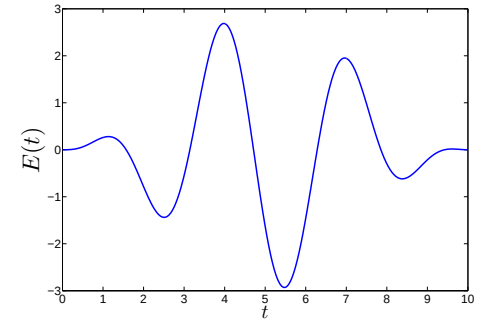

(a) $E(t)$.

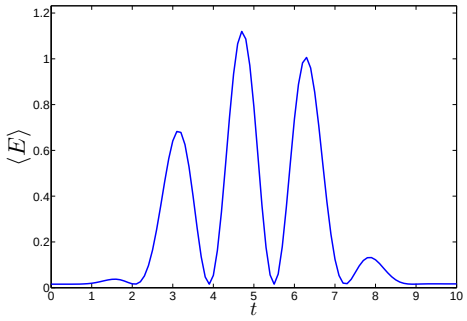

(b) Mean energy of the wave packet

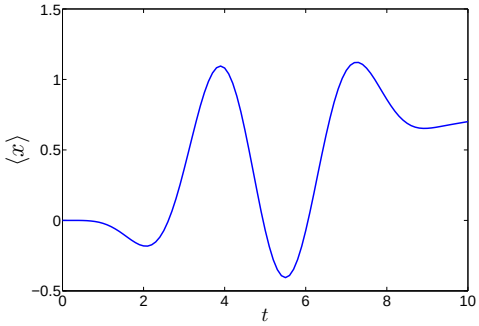

(c) The expectation value of position.

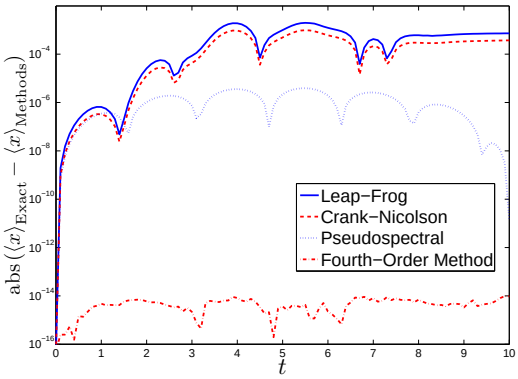

(d) Deviation from the expectation value of position.

Figure 4.10: *The time dependent external field: various simulation data.*

compared to the fourth order method) by taking smaller time steps. If we allow the two methods to use the same total simulation time, who will win?

We will simulate a time-dependent system similar to that in the previous secion. The simulation parameters used are

$$E_{\max} = 3 \quad \omega = 2 \quad T = 10 \quad \sigma = \tfrac{1}{4} \quad L = 100 \quad N = 512 \quad t_{\text{final}} = 10$$

The parameters specific to the fourth-order method are

$$N_{\text{tSteps}} = 10^3 \quad \Delta t = 0.01$$

and those specific to the pseudospectral method are

$$N_{\text{tSteps}} = 7000 \cdot 10^3 \quad \Delta t = 1.43 \cdot 10^{-6}$$

The length of the time step for the fourth-order method is 7000 that of the pseudospec-

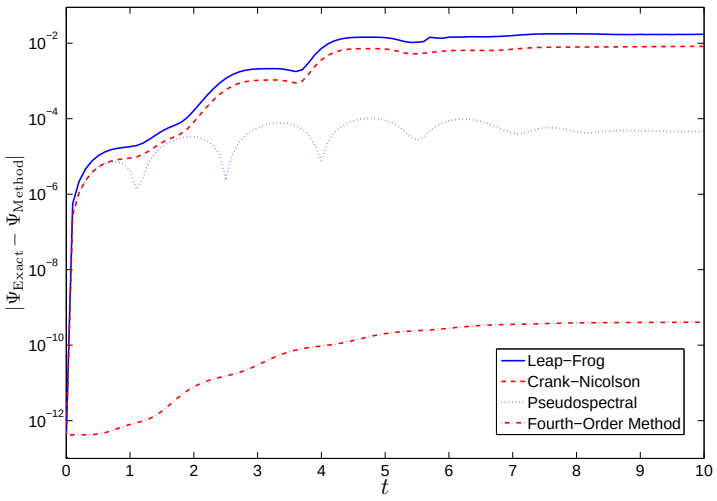

Figure 4.11: *The time dependent external field: deviation from the exact wave function.*

tral method. But amazingly, they use just about the same total simulation time. The pseudospectral method has a total run time of $t_{\mathrm{sim}} = 2.176 \cdot 10^3$ while the fourth-order method has a total run time of $t_{\mathrm{sim}} = 2.041 \cdot 10^3$.

For the expectation value of x, where the deviation from this is plotted in Figure 4.13a, by now taking $\sim 10^3$ times the number of time steps than in the simulation in the previous section, the pseudospectral fares slightly better with the error now reduced by three orders of magnitude. But still it is no match for the fourth-order method, which calculates this quantity, again, almost to machine precision. The deviation from the exact wave function is shown in Figure 4.13b. The pseudospectral method does actually reproduce the wave function slightly better than the fourth-order method, after a simulation time of $t = 2.5$.

4.4.8 Discussion

A number of experiments were carried out to test the methods discussed in detail in the first part of this chapter. In many ways we confirmed what we expected from the discussion of the methods. The fourth-order method was indeed proven to be the most accurate method. It was particularly striking how well it reproduced the one observable recorded in the simulations; the mean value of position. It was perhaps not so clear from the derivation how the Crank-Nicolson method, leap-frog method and the pseudospectral method would compare against each other, other than that the pseudospectral method should conserve unitarity. The results were quite unaminous: The

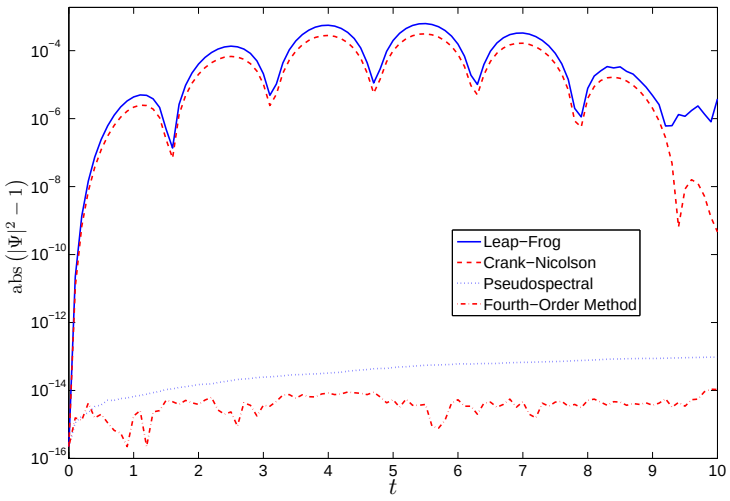

Figure 4.12: *The time dependent external field: deviation from unitarity.*

pseudospectral method outperformed the two others in terms of accuracy, and the leap-frog method performed slightly better than the Crank-Nicolson method. Because of the way the spectral discretization was been implemented, a system of linear equations requiring $\mathcal{O}(N^2)$ operations had to be solved at every time step. It was therefore several orders of magnitude slower than the leap-frog and pseudospectral methods. In a contest of accuracy versus computation cost, this method was no longer a contender. The pseudospectral method requires $\mathcal{O}(N \log N)$ operations per time step against that of $\mathcal{O}(N)$ operations for the leap-frog method, which for practical purposes is about equal. In the current implementation it was therefore interesting to compare the pseudospectral method against the fourth-order method, and see which method would perform better when allowing them the same computation time. (The fourth-order method is very slow in its current implementation, because an exponential of a dense matrix must be calculated at each time step.) The results from this test were inconclusive. The pseudospectral method was the best at reproducing the wave function, and the fourth-order method the best at reproduced the expectation value of position. The tests did unfortunately not test the methods to their extremes. It would be interesting to see for just how large a time step, and how rapid oscillations of the external field, the fourth order method can give accurate results.

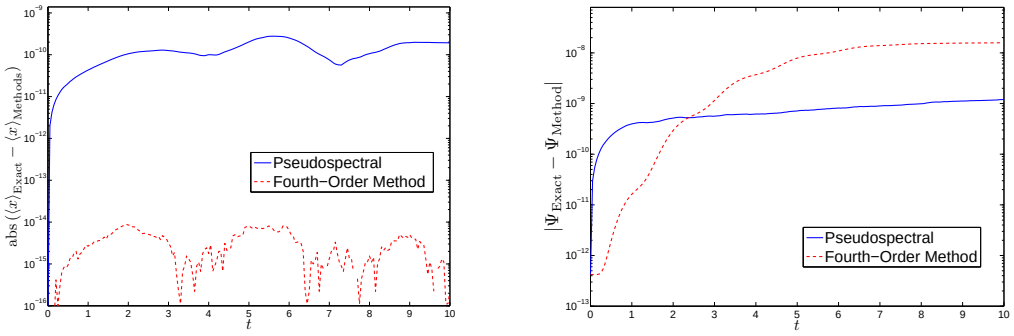

(a) Devation from the expectation value of x.

(b) Deviation from the exact solution.

Figure 4.13: *Testing the performance of the fourth-order method against that of the pseudospectral method, on the premise that the two methods are allowed the same total computation time. Devation from the expectation value of position (left). Deviation from the exact wave function (right).*

Suggestions for Future Work

One of the supposed advantages of the fourth-method is that it enables us to use larger time steps without losing accuracy, whereby the simulation time can be decreased significantly. While the simulations certainly indicated that the fourth-order method is more accuracy than the other time-stepping schemes, we did not fully reach a conclusion as to whether the fourth-order method can help us speed up numerical simulations. If the work in this chapter is to be extended it would first and foremost be of interest to investigate thoroughly if the greater accuracy of the fourth-order method enables it to out-perform the other methods, when the methods are allowed the same simulation time.

Chapter 5

Time Evolution in a Two-Electron Coupled Quantum Dot

In this chapter, the fourth-order method time stepping scheme discussed in Chapter 4 is applied to a simple one-dimensional model of a quantum dot molecule with two interacting particles under the influence of a time-dependent electric field. I must confess at once the temptation to put the term quantum dot in quotation marks when discussing this model. It is undeniably an over-simplification of the complicated dynamics that takes place in real quantum dots. However, even this simple model shows many of characteristics that are observed in experiments on coupled quantum dots.

The original intention of this thesis was to look at the dynamics of several interacting particles (possibly as many as 5-6) in a two-dimensional quantum dot model using a newly developed FCI code at UiO. However, mid-way through the thesis it was realized that when applied to our model system, the program would slow down considerably. It turned out that our choice of the Hamiltonian broke many of the symmetries that the program exploited to speed up the diagonalization. To solve the eigenproblem to the required accuracy, the code would need to be re-written to facilitate parallel execution. According to the author of the program, this would require several months of hard labour, and this effectively ruled out that option. To still have something to show for in this thesis, a simpler diagonalization routine for solving interacting two-particle systems in one dimension has been used. Looking at such a simple system is not as silly as it may seem. We are in any event simulating the dynamics of a system that is not well-understood. It makes sense to first look at a model where we can visualize the wave functions, and that is much less computationally intensive than what the simulation of the full problem would have been.

I will begin this chapter by discussing some of the theoretical models used to study quantum dots. I will describe the necessary topics from quantum mechanics, including how we can adequately model the effects of electromagnetic radiation on our quantum

system. An outline of how one can modify the time-stepping schemes to simulate systems of two or three dimensions and of several particles will then be given, before I turn to the simulation of the two-particle quantum dot.

5.1 Modelling the Physics of Quantum Dots

A quantum dot is really a very complicated system. The electrons we are interested in studying in reality move in a complicated background of vibrating lattice ions. By making some simplifying assumptions however, we can model and understand much of the physics involved. I will briefly describe the most commonly adopted models for describing quantum dots.

5.1.1 Shape of the Confining Potential

Experimental and theoretical evidence suggests that we to a good approximation can make two simplifying assumptions about the confining potential in quantum dots:

1. The finite thickness of the dot, which is much smaller than its lateral extent, can be neglected. The problem can be considered to be two-dimensional in the spatial coordinates
2. The potential is essentially that of an isotropic harmonic oscillator.

The potential adopted in most calculations on quantum dots is of the form

$$V(x,y) = \frac{1}{2} m^* \omega_0^2 \left(x^2 + y^2\right), \tag{5.1}$$

where m^* is the effective mass of the electron. This potential is as I discussed in Section 2.4.1 responsible for the shell-structure seen in conductance spectra of quantum dots, analogous to that set up by the electrons in atoms or nucleons in nuclei.

Much work has been done to delineate the situations where these approximations are valid. It has been shown that for the lateral quantum dot the confinement has a symmetry very close to circular, even if the confinement was formed by a square-shaped metallic gate pattern [31]. The potential strength of the isotropic oscillator is not completely independent of the number of electrons in the dot [8], and the assumption of a parabolic potential becomes less accurate for high numbers ($N > 20$) of electrons [14]. The deviation from a pure two-dimensional system is found in [32] to effectively take the form of an extra anharmonic potential term ($\sim r^4$).

For a system of N particles, we have then the Hamiltonian

$$H = \sum_{i=1}^{N} \left[-\frac{\hbar^2}{2m^*}\nabla_i^2 + \frac{1}{2}m^*\omega_0^2\left(x_i^2 + y_i^2\right)\right] + \frac{1}{2}\sum_{i,j,i\neq j}^{N} \frac{e^2}{4\pi\epsilon_r\epsilon_0}\frac{1}{r_{ij}}, \tag{5.2}$$

where ϵ_r is the relative permittivity. For the most commonly used quantum dot material, GaAs, this value is $\epsilon_r \approx 12$.

5.1.2 Quantum Dot Molecules

For two closely spaced quantum dots, it is possible to get a situation where electrons can move between the two dots. By adjusting the distance between the dots we can effectively control the coupling between the two dots, and we can e.g. get a situation where an electron is quasi-stationary in one of the dots and have to tunnel through a relatively high barrier to get to the other dot. Controlling this transition by external electric or magnetic field is interesting for quantum information processing applications, and is currently a much researched topic.

Extending the analogy between atoms and quantum dots, systems of coupled quantum dots are often called *quantum dot molecules*. A system of two coupled quantum dots with one electron would then be the quantum dot analogue of the H_2^+ ion. The confining potential for systems of two coupled quantum dots is often modelled by

$$V(x,y) = \frac{1}{2}m^*\omega_0^2 \min\left[\left(x-\frac{d}{2}\right)^2 + y^2, \left(x+\frac{d}{2}\right)^2 + y^2\right]. \tag{5.3}$$

The distance between the centre of the wells is given by d. The ground state $\varphi_1(\mathbf{x})$ and first excited state $\varphi_2(\mathbf{x})$ of a single-particle system with this double-well potential are approximately degenerate since the barrier approximately decouples the system into two individual harmonic oscillators. $\varphi_1(\mathbf{x})$ is symmetric, while $\varphi_2(\mathbf{x})$ is anti-symmetric. $\psi_\pm(\mathbf{x}) = \varphi_1(\mathbf{x}) \pm \varphi_2(\mathbf{x})$ is localized in different wells depending on the sign $\pm$. These two are then approximate eigenfunctions which are approximately degenerate.

For two particles which are not interacting, the symmetric wave functions $\psi_+(\mathbf{x}_1)\psi_+(\mathbf{x}_2)$, $\psi_-(\mathbf{x}_1)\psi_-(\mathbf{x}_2)$, and $\psi_+(\mathbf{x}_1)\psi_-(\mathbf{x}_2) + \psi_-(\mathbf{x}_1)\psi_+(\mathbf{x}_2)$ are all approximately degenerate eigenfunctions. If we turn on interactions, however, it is easy to see that the two first are no longer approximate eigenfunctions since the interactions are strong for electrons localized in the same well.

5.1.3 Electromagnetic Fields

The classical electromagnetic field is described by electric and magnetic field vectors $\mathbf{E}$ and $\mathbf{B}$, which obey Maxwell's equations, and which can be generated from the scalar

potential φ and the vector potential $\mathbf{A}$ by

$$\begin{aligned} \mathbf{E}(\mathbf{r},t) &= -\nabla\varphi(\mathrm{r},t) - \frac{\partial}{\partial t}\mathbf{A}(\mathbf{r},t) \\ \mathbf{B}(\mathbf{r},t) &= \nabla\times\mathbf{A}(\mathbf{r},t). \end{aligned} \tag{5.4}$$

These equations do not uniquely define the potentials. We are free to impose extra confitions on φ and $\mathbf{A}$, as long as $\mathbf{E}$ and $\mathbf{B}$ are left unchanged. In particular, for any scalar function $\chi(\mathbf{r},t)$ the electric and magnetic fields are not affected by the transformations

$$\begin{aligned} \mathbf{A} &\rightarrow \mathbf{A}' = \mathbf{A} + \nabla\chi \\ \varphi &\rightarrow \varphi' = \varphi - \frac{\partial\chi}{\partial t}. \end{aligned} \tag{5.5}$$

Such transformations are known as *gauge transformations*. The connection to Newton's laws of motion is given by the Lorentz force law

$$\mathbf{F} = q\mathbf{E} + q\frac{\mathbf{v}}{c}\times\mathbf{B}. \tag{5.6}$$

The incorporation of electromagnetism into quantum mechanics is a lot more subtle. By means of the *minimal coupling*[1] we can find a semiclassical theory of electrodynamics. For a "free" particle of charge q, the minimal coupling dictates that Hamiltonian is

$$H = \frac{1}{2m}\left(-i\hbar\nabla - q\mathbf{A}\right)^2 + q\varphi. \tag{5.7}$$

Our challenge is then to deduce meaningful solutions for the problem from the Schrödinger equation

$$i\hbar\frac{\partial}{\partial t}\Psi(\mathbf{r},t) = \left[-\frac{\hbar^2}{2m}\nabla^2 + i\hbar\frac{q}{2m}\left(\mathbf{A}\cdot\nabla + \nabla\cdot\mathbf{A}\right) + \frac{q^2}{2m}\mathbf{A}^2 + q\varphi\right]\Psi(\mathbf{r},t). \tag{5.8}$$

As we saw, the function χ has no physical meaning in classical electrodynamics. Is the semiclassical theory of electrodynamics also invariant under the gauge transformations of Eq. (5.5)? Looking at the Schrödinger equation (5.8) it seems far from obvious that this should be so, as the potentials $\mathbf{A}$ and φ appear explicitly in the equation. It can be shown however, that the wave function Ψ' that satisfies the gauge transformed Schrödinger equation

[1] The term *minimal coupling* is mostly used in the context of the Dirac equation and its application to relativistic field theories.

$$i\hbar\frac{\partial}{\partial t}\Psi'(\mathbf{r},t)=\left[\frac{1}{2m}\left(-i\hbar\nabla-q\mathbf{A}'\right)^2+q\varphi'\right]\Psi'(\mathbf{r},t)\,, \tag{5.9}$$

differs from the wave function Ψ of the original problem by nothing more than a phase factor [11]

$$\Psi'=\exp\left(iq\chi/\hbar\right)\Psi. \tag{5.10}$$

Generally, it can be shown that imposing a unitary transformation (of which $\exp\left(iq\chi/\hbar\right)$ is a special case) on the state function, corresponds to a *picture transformation*. Such transformations do not change the physical content of the theory [33].

In many situations the electromagnetic field can be adequately described as monochromatic plane waves, or linear combinations thereof. In the Coulomb gauge, where we have used the gauge freedom to set $\nabla\cdot\mathbf{A}=0$, a monochromatic plane wave of polarized light is given in terms of the vector potential $\mathbf{A}$ as [28]

$$\mathbf{A}(\mathbf{r},t)=A_0(\omega)\,\hat{\epsilon}\cos\left(\mathbf{k}\cdot\mathbf{r}-\omega t+\delta\right), \tag{5.11}$$

where $\hat{\epsilon}$ is the polarization vector, and $\mathbf{k}$ is in the direction of propagation. In atomic and molecular physics, the systems under consideration have a size typically much smaller than the wavelength of radiation. For instance, red light has a wavelength of about $700\,\mathrm{nm}$, while a typical size of a molecule is about $1\,\mathrm{nm}$. It follows that the electromagnetic field can be taken to be uniform over the whole system. This is referred to as the *dipole approximation*. In most situations of interest the dipole approximation is valid for quantum dots as well, since we would typically manipulate them using radiation of longer wavelength. In the dipole approximation, the vector potential reduces to

$$\mathbf{A}(\mathbf{r},t)=A_0(\omega)\,\hat{\epsilon}\cos\left(\omega t+\delta\right). \tag{5.12}$$

For a single particle in an external potential $V(x,t)$ under the influence of a radiation field $\mathbf{A}$, the Schrödinger equation is given in the Coulomb gauge as

$$i\hbar\frac{\partial}{\partial t}\Psi(\mathbf{r},t)=\left[-\frac{\hbar^2}{2m}\nabla^2+V(x,t)+i\hbar\frac{q}{m}\mathbf{A}\cdot\nabla+\frac{q^2}{2m}\mathbf{A}^2\right]\Psi(\mathbf{r},t)\,. \tag{5.13}$$

It is of interest to get rid of the term quadratic in the field, $\mathbf{A}^2$, because it complicates calculations and in most situations gives only a negligible contribution [11]. By performing a gauge transformation specified by setting $\chi(\mathbf{r},t)=\mathbf{A}(t)\cdot\mathbf{r}$, we see from Equations (5.5) and (5.10) that

$$\begin{aligned} \mathbf{A}' &= 0 \\ \varphi' &= \frac{\partial}{\partial t}\mathbf{A}(t) \cdot \mathbf{r} = -\mathbf{E}(t)(\mathbf{r}) \cdot \mathbf{r} \\ \Psi'(\mathbf{r},t) &= \Psi(\mathbf{r},t) \exp\left(\frac{iq}{\hbar}\mathbf{A}(t) \cdot \mathbf{r}\right). \end{aligned} \tag{5.14}$$

The Schrödinger equation for $\Psi(\mathbf{r},t)$ is now

$$i\hbar\frac{\partial}{\partial t}\Psi'(\mathbf{r},t) = \left(-\frac{\hbar^2}{2m}\nabla^2 + V(\mathbf{r},t) - q\mathbf{E}\cdot\mathbf{r}\right)\Psi'(\mathbf{r},t), \tag{5.15}$$

which is said to be given in the *length gauge* due to the fact that the interaction term now couples the electric field $\mathbf{E}$ to the position operator $\mathbf{r}$. The interaction term happens to have the same form as the potential energy of a dipole of charges $\pm q$, separated by the vector $\mathbf{r}$, in an electric field $\mathbf{E}$. This is the reason why the approximation where the electromagnetic field is assumed to be uniform over the system is referred to as the dipole approximation.

For the sake of completeness: In the *velocity gauge*, another frequently used gauge in the dipole approximation, the Schrödinger equation becomes [28]

$$i\hbar\frac{\partial}{\partial t}\Psi'(\mathbf{r},t) = \left(-\frac{\hbar^2}{2m}\nabla^2 + V(\mathbf{r},t) + \frac{i\hbar q}{m}\mathbf{A}\cdot\nabla\right). \tag{5.16}$$

The origin of the name *velocity gauge* stems from the fact that the interaction term couples the vector potential $\mathbf{A}$ to the velocity operator $-i\hbar\nabla/m$. In the velocity gauge, the vector potential $\mathbf{A}$ is independent of spatial coordinates [34], and there can then be no magnetic field[2]. For the length gauge, there clearly is no magnetic field either. So by performing these gauge transformations we are effectively saying that the magnetic field can be neglected.

5.2 Time Propagation for Systems of Several Dimensions and Particles

So far we have discussed time integration of the Schrödinger equation only for the simple case of a single particle in one dimension. To be able to simulate more realistic systems we must learn how the time stepping schemes can be modified to handle two or three spatial dimensions, and more than one particle.

[2]From $\mathbf{B} = \nabla \times \mathbf{A}$ this follows directly.

5.2.1 Generalizing the Time-Stepping Schemes to Two or More Dimensions/Particles

With some difficulty, all the methods discussed in Chapter 4 can be generalized to two, three, or more dimensions. This applies to the finite difference approximation as well as for the spectral approximation. With the exception of symmetry requirements, extending the methods to several particles is quite analogous to extending the number of spatial dimensions, so the following discussion applies to this case as well. For simplicity I will only discuss the two-dimensional case.

For the finite difference approximation in two dimensions, we discretize the domain by the grid

$$(x_j, y_k) = (x_0, y_0) + \frac{L}{N+1}(j,k), \qquad 1 \leq j,k \leq N. \tag{5.17}$$

Here, L is the length of each of the sides of the discretization domain, which here is taken to be quadratic. The wave function is now represented by an $N \times N$ matrix. The question now arises of what to do with the operator $T = T_x + T_y$. Clearly, it cannot be a matrix. It is now an operator that maps matrices into matrices, that is, a tensor. This can be quite confusing when one first encounters it. To implement the finite difference method in two dimensions it is easiest to work element by element[3]. The action of T_x and T_y on the discretized wave function then becomes (when writing $\Psi_{j,k} \equiv \Psi(x_j, y_k)$)

$$\begin{aligned} T_x \Psi_{j,k} &= -\frac{1}{\Delta x^2}\left(\Psi_{j+1,k} - \Psi_{j,k} + \Psi_{j-1,k}\right) \\ T_y \Psi_{j,k} &= -\frac{1}{\Delta y^2}\left(\Psi_{j,k+1} - \Psi_{j,k} + \Psi_{j,k-1}\right) \end{aligned} \tag{5.18}$$

We can work with matrices directly if we map the indices j and k onto a single index l defined by

$$l = N(j-1) + k. \tag{5.19}$$

Of course, there are many ways of defining such mappings. The wave function is now a vector of length N^2. It is also not too difficult to show that the Hamiltonian becomes an $N^2 \times N^2$ matrix.

The spectral approximation can also be used in the two-dimensional case. Here we would keep the matrix representation of the wave function $\Psi_{j,k}$. To compute the action of T_x in the frequency domain we must apply the discrete Fourier transform to all rows

[3] For an example of the Leap-Frog scheme applied to a system of two particles in one dimension, see Ref. [35]

in succession, and then compute the action of the diagonal operator before transforming back again. The process is similar for T_y.

When increasing the dimensionality of the system the computational complexity increases drastically. For many of the simulations in Chapter 4 a grid of $N = 512$ points was used. If we were to use the same number of grid points in all directions for a three-dimensional problem, the wave function would consist of $N = 512^3 \approx 10^8$ points. This would in most cases not be possible to store in the main memory, not to mention the corresponding scaling of computation time needed. In practical calculations, we would have to use a significantly lower number of grid points in each direction. Some problems that are out of reach for the finite difference approximation can be tackled by the spectral approximation, since the memory requirements for the former is much greater than for the latter, when the same accuracy is required [21].

5.2.2 The Time Stepping Schemes in the Eigenvector Basis

When discussing the time stepping schemes in Chapter 4 we represented the wave function by its values on a finite grid. In reality, we could actually have used any orthonormal basis set to represent the wave function. The time stepping schemes were not really discussed in the context of any particular discretization, so they would retain their validity. Since we will of course have to truncate the basis after some finite number, we must be sure that this truncated basis captures most of the exact wave function.

Let us formulate this more accurately. Given a complete set of of orthonormal basis vectors $|\phi_k\rangle$, we expand the state vector $|\Psi\rangle$ in this basis, and truncate after the first N basis vectors

$$|\Psi\rangle = \sum_{k=1}^{N} c_k |\phi_k\rangle , \quad c_k = \langle \phi_k | \Psi \rangle . \tag{5.20}$$

Conversely, any coefficient vector $\mathbf{c}$ defines a unique wave function on this truncated basis. In the case where the basis vectors are labelled by several quantum numbers, we will have to define some mapping of these onto the single index k. The action of operators can now be viewed as matrix multiplication on the coefficient vector. That is, the action of an operator A on the state vector corresponds to $\mathbf{Ac}$, where the matrix elements of A in the basis of vectors $|\phi_k\rangle$ are given by

$$(\mathbf{A})_{jk} = \langle \phi_j | A | \phi_k \rangle . \tag{5.21}$$

In this basis the time-dependent Schrödinger equation may be written

$$i \frac{\mathrm{d}}{\mathrm{d}t} \mathbf{c}\,(t) = \mathbf{H}\mathbf{c}\,(t) . \tag{5.22}$$

This is the general case of the semi-discrete Schrödinger equation discussed in Section 4.12. If we use the eigenvectors $|\psi_k\rangle$ of the Hamiltonian as a basis, the problem becomes trivial when H is time-independent. In this basis H is diagonal, with the diagonal elements being the eigenvalues of H. Equation (5.22) decouples

$$i\frac{\mathrm{d}}{\mathrm{d}t}\mathbf{c}\left(t\right)=\mathbf{D}\mathbf{c}\left(t\right),\qquad\mathbf{D}=\mathrm{diag}\left(E_1,E_2,\ldots,E_N\right), \tag{5.23}$$

and the time development is given simply as $c_k\left(t\right)=\exp\left[-i(t-t_0)E_k\right]c_k\left(t_0\right)$. We now look at the case where H has a time-dependent perturbation $H_1\left(t\right)$

$$H\left(t\right)=H_0+H_1\left(t\right). \tag{5.24}$$

Here, H_0 is the stationary part of the Hamiltonian of an, as of yet, unspecified number of particles. For the rest of this section we will consider H_0 to be the full Hamiltonian of the many-body problem, including the two-particle Coulomb terms. We will use the eigenvectors $|\psi_k\rangle$ of H_0 as a basis to approximate the total Hamiltonian H. To find the eigenvectors of the many-body Hamiltonian, an approximation method that gives the ground state and the excited states up to some specified cut-off value must be used. The full configuration interaction method would be the natural candidate for this. Using the N first vectors $|\psi_k\rangle$ of the many-body basis, the matrix version of the Hamiltonian becomes

$$\mathbf{H}=\mathbf{H}_0+\mathbf{H}_1\left(t\right), \tag{5.25}$$

where

$$\mathbf{H}_0=\mathrm{diag}\left(E_1,E_2,\ldots,E_N\right),\qquad\left[\mathbf{H}_1\left(t\right)\right]_{jk}=\langle\psi_j|H_1|\psi_k\rangle. \tag{5.26}$$

The typical line of attack for solving the time-dependent problem is then to use Dirac's method of variation of constants (i.e. ordinary time-dependent perturbation theory). This approach has a number of limitations however, assuming among other things that the perturbation is in some sense small.

When discussing the time stepping schemes in Chapter 4 I made a point of separating between the spatial discretization and the time integration. This is to be contrased to most other introductory texts on solving the time-dependent Schrödinger equation, where the finite difference approximation is typically used, and time and spatial coordinates are both given explicitly. The beauty of not adhering to any particular spatial discretization is that now our time stepping schemes are valid for any basis!

There is one potential difficulty however: To use the eigenfunctions $|\psi_k\rangle$ of the unperturbed, stationary part of the Hamiltonian, we have to be able to calculate the matrix elements $\langle\psi_j|H_1\left(t\right)|\psi_k\rangle$. In the case of the many-particle Hamiltonian this can be prohibitively expensive. In most cases, this certainly rules out calculating these matrix

elements for each time step. In many cases, however, the time-dependent perturbation $H_1(t)$ can be written as a product of a function depending only on time, and a function of spatial coordinates. The form of perturbation of interest to us later, the electric field in the dipole approximation, is of this form. As an example: For a system of M particles of charge q exposed to monochromatic, polarized light, which in the dipole approximation can be written $\mathbf{E}(t) = E_0 \cos(\omega t - \delta)\,\hat{\epsilon}$, the perturbation is (see Section 5.1.3)

$$H_1 = q\mathbf{E}(t) \cdot (\mathbf{r}_1 + \mathbf{r}_2 + \ldots \mathbf{r}_M) = qE_0 \cos(\omega t - \delta)\,\hat{\epsilon} \cdot (\mathbf{r}_1 + \mathbf{r}_2 + \ldots \mathbf{r}_M). \tag{5.27}$$

Here, $\hat{\epsilon}$ is the polarization vector. We see that by calculating the matrix elements

$$\langle \psi_j | \hat{\epsilon} \cdot (\mathbf{r}_1 + \mathbf{r}_2 + \ldots \mathbf{r}_M | \, \psi_k \rangle \tag{5.28}$$

once and for all, we can obtain the matrix elements of $H_1(t)$ simply by multiplying by the time-dependent part $qE_0 \cos(\omega t - \delta)$. There is no need for doing the complete calculation for each time step.

Often, when the perturbation is not too strong, a system starting out in the ground state will only contain contributions from the ground state and the lowest lying states. For the quantum dot system, this is in particular true if we have an anharmonic term in the potential. We can therefore describe the system accurately by relatively small basis sizes. In Chapter 4, we saw that the fourth-order method triumphed over the other methods in terms of accuracy, but had the drawback of being computation intensive, and that the computation time increased rapidly with the number of basis vectors. For time propagation in the energy-eigenvector basis however, the situation is tilted in favour of the fourth-order method. That we could make use of fact that the kinetic energy operators are diagonal in the frequency domain, made the pseudospectral method attractive for the one-dimensional case. In the energy-eigenvector basis this is no longer the case, and we can obtain the added accuracy from the fourth-order method at essentially no extra cost (as compared to second order splitting methods).

5.3 Numerical Experiments

In this section I will apply the fourth-order time stepping scheme to a model system of two interacting particles in a one-dimensional quantum dot. The confining potential will be an anharmonic double well, and the system will be under the influence of an oscillating electric field polarized in the x-direction. Even though the one-dimensional quantum dot is a much studied system, advanced stepping schemes like the fourth-order method studied here have not yet been studied when applied to complicated quantum systems. Our model problem is simple, but retains many of the essential features of an N-electron quantum dot in two dimensions. It allows for visualization

of the wave-functions and relatively cheap computations. Therefore it is ideally suited for studying time-stepping schemes.

5.3.1 The Model Quantum Dot

In the numerical experiments we will consider a model of two coupled quantum dots described by a Hamiltonian of the form

$$H = -\frac{1}{2}\frac{\mathrm{d}^2}{\mathrm{d}x_1^2} - \frac{1}{2}\frac{\mathrm{d}^2}{\mathrm{d}x_2^2} + V_{\text{ext}}(x_1) + V_{\text{ext}}(x_2) + U(x_{12};\lambda,\delta) + H_1(\vec{x},t), \tag{5.29}$$

where $x_{12} \equiv x_1 - x_2$ and $\vec{x} = (x_1, x_2)$. The confining potential, V_{ext}, is chosen as an anharmonic double well

$$V_{\text{ext}} = \frac{1}{2d^2}\left(x - \frac{d}{2}\right)^2\left(x + \frac{d}{2}\right)^2, \tag{5.30}$$

where d is the distance between the well-centres. Restricting the motion of the particles to one dimension artificially strengthens the Coulomb interaction, so we will use a screened approximation $U(x_{12};\lambda,\delta)$ given by

$$U(x_{12};\lambda,\delta) = \frac{\lambda}{\sqrt{(x_1 - x_2)^2 + \delta^2}}, \tag{5.31}$$

where λ is the strength of the interaction and $\delta > 0$ is the screening parameter. The time dependent term of the Hamiltonian, $H_1(\vec{x},t)$, will in our model be representing an oscillating electric field which we take to be polarized in the direction along an axis running through centres of the dots (in the one-dimensional model we are considering there is only one axis of course, so this statement makes more sense if we think of our model as an approximation to a three-dimensional system). We assuming that the dipole approximation is valid for our system, and use the length gauge (see Section 5.1.3). The electric field then gives us the following term in the Hamiltonian

$$H_1(\vec{x},t) = E(t)(x_1 + x_2) = E_0 \sin(\omega t)(x_1 + x_2). \tag{5.32}$$

In general, the wave function of the system is a function of both position and spin coordinates, $\Psi = \Psi(x_1,\sigma_1,x_2,\sigma_2)$. The fact that the Hamiltonian does not contain the spin of the electrons explicitly allows us to separate the wave function and concentrate solely on the spatial part. If the Hamiltonian is independent of time, simultaneous eigenfunctions of H, $\mathbf{S}^2$ and S_z can be written as products of spatial eigenfunctions $\psi(x_1,x_2)$ satisfying the time-independent Schrödinger equation

$$H\psi\left(x_1, x_2\right) = E\psi\left(x_1, x_2\right), \tag{5.33}$$

and of two-electron spin functions $\chi\left(\sigma_1, \sigma_2\right)$, which are eigenfunctions of $\mathbf{S}^2$ and S_z. When combining two spin $1/2$ particles the total spin quantum number can take on the values $S = 0$ and $S = 1$. For $S = 0$ there is only one spin function, the singlet state χ_{singlet}, which is antisymmetric in interchange of the spin coordinates. For $S = 1$ there are three states, the triplet state χ_{triplet}, which is symmetric in interchange of the spin coordinates. The product of the spin and spatial parts of the wave function must be antisymmetric, which means that the spatial part must either be symmetric ψ^{S}, in case of the spin singlet, or antisymmetric ψ^{A}, in case of the spin triplet. When the Hamiltonian is time-dependent but does not depend explicitly on spin, as long as we start out with a state that is either a singlet or a triplet state (i.e. not a superposition of these), we can expect the system to remain in such a state since the transition matrix element between a singlet and triplet state is then zero.

We can therefore justify to work only with the spatial part of the wave funciton, $\psi\left(\vec{x}, t\right)$, and to impose the additional constraint that is should be either symmetric or antisymmetric under interchange of the two position coordinates. The problem we are facing for the numerical experiments, is then to solve the Schrödinger equation for the spatial part of the wave function

$$i\frac{\partial}{\partial t}\psi\left(\vec{x}, t\right) = \left\{\sum_{j=1}^{2}\left(-\frac{1}{2}\frac{\mathrm{d}^2}{\mathrm{d}x_j^2} + V_{\text{ext}}\left(x_j\right)\right) + \frac{\lambda}{\sqrt{x_{12}^2 + \delta^2}} + E_0 \sin\left(\omega t\right)\left[x_1 + x_2\right]\right\}\psi\left(\vec{x}, t\right), \tag{5.34}$$

given the initial state $\psi\left(\vec{x}, t\right)$ and the symmetry requirements on the wave function.

5.3.2 The Implementation

I will now apply the fourth-order time stepping scheme discussed in Chapter 4 to the one-dimensional quantum dot system described in the previous section. The fourth-order method will not be implemented by working directly with the wave function projected on some spatial grid, as in Chapter 4, but rather by expanding the wave function in the basis of eigenstates of the unperturbed problem.

I will first give a brief review of the fourth-order method and how to implement it in the eigenvector basis: We define a vector $\mathbf{\Psi}$ of expansion coefficients of the wave function in a truncated basis of eigenvectors $\varphi_j\left(x_1, x_2\right)$ of the time-independent Schrödinger equation for the unperturbed system

$$H_0\varphi_j\left(x_1, x_2\right) = E_j\varphi_j\left(x_1, x_2\right). \tag{5.35}$$

Here, H_0 is the time-independent part of the Hamiltonian of Eq. (5.29). As explained in the previous section, it is enough to consider only the spatial part of the wave function, and to impose the condition that it must be either symmetric or antisymmetric under interchange of the spatial coordinates. The fourth-order time stepping scheme is given by

$$\mathbf{\Psi}^{n+1} = \mathrm{e}^{\mathbf{M_1}+[\mathbf{M_1},\mathbf{M_2}]}\mathbf{\Psi}^{n}, \tag{5.36}$$

where $\mathbf{M_1}$ and $\mathbf{M_2}$ as defined in Eq. (4.68) consists of terms proportional to integrals of the form $\int \mathbf{H}(s)\ \mathrm{d}s$ and $\int s\mathbf{H}(s)\ \mathrm{d}s$. When applying a time-dependent perturbation, which in our case is given by Eq. 5.32, the Hamiltonian matrix $\mathbf{H}$ is in the eigenvector basis given by

$$\mathbf{H} = \mathbf{H}_0 + \mathbf{H}_1(t), \tag{5.37}$$

where $\mathbf{H}_0$ is a diagonal matrix of the energy-eigenvalues, $\mathbf{H}_0 = \mathrm{diag}(E_1, E_2, \ldots, E_N)$, and $\mathbf{H}_1(t)$ is given by

$$[\mathbf{H}_1(t)]_{jk} = E(t)\int_{-\infty}^{\infty}\int_{-\infty}^{\infty}\varphi_j^*(x_1,x_2)(x_1+x_2)\varphi_k(x_1,x_2)\ \mathrm{d}x_1\ \mathrm{d}x_2. \tag{5.38}$$

We see what we only need to feed the fourth-order method the matrix elements

$$\langle\varphi_j|x_1+x_2|\varphi_k\rangle \tag{5.39}$$

and the eigenvalues of the unperturbed problem, along with $E(t)$, in order to propagate the wave function in time. The most difficult part of using the eigenvector basis is undoubtedly to obtain the eigenvalues and matrix elements of the perturbation with sufficient accuracy in the first place.

The two-particle time-independent Hamiltonian is diagonalized using spectral methods. More specifically, we use the sine-series part of a FFT discretization to avoid periodic boundary conditions, see [36]. This gives a standard uniform grid with N points in the interval $-L/2 < x_j < +L/2$. The Matlab program that accomplished this is written by Simen Kvaal at the university of Oslo. The program returns the eigenfunctions $\varphi_j(x_1,x_2)$ for $0 \leq j < \mathrm{nev}$, where nev is a parameter specifying how many eigenfunctions the program should return, and the corresponding eigenvalues E_j of H_0. Also, the matrix of x_1+x_2 in this eigenfunction basis is returned.

5.3.3 Results

Two scenarios have been simulated: One where the electrons do not interact, and one where they interact via the screened Coulomb potential. This we do in order to assess

the impact of interactions on the time-evolutions of the system. For simplicitly I will only consider symmetric wave functions, i.e., a singlet state.

The parameters in the eigensolver program are:

$$L = 30 \quad N = 80 \quad \text{nev} = 100$$

For the double well

$$V_{\text{ext}} = \frac{1}{2d^2}\left(x - \frac{d}{2}\right)^2 \left(x + \frac{d}{2}\right)^2, \tag{5.40}$$

a distance between the wells of $d = 8$ has been chosen. The use of this potential was originally motivated by this paper [37]. For the screened Coulomb potential

$$U\left(x_1 - x_2; \lambda, \delta\right) = \frac{\lambda}{\sqrt{\left(x_1 - x_2\right)^2 + \delta^2}}, \tag{5.41}$$

a value of $\lambda = 0.6$ and $\delta = 0.1$ has been used.

For the time integration part, the parameters are:

$$t_{\text{final}} = 600 \quad N_{\text{tSteps}} = 20 t_{\text{final}} \quad \Delta t = 0.05$$

It is often difficult to see the physics of a two-variable complex function (three, counting time). It is helpful to introduce the *single-particle density* $\rho_i(x_i, t)$ defined by integrating the two-particle density, $\left|\psi\left(x_1, x_2, t\right)\right|$, over one of the particles

$$\rho_i\left(x_i, t\right) = \int_{\infty}^{\infty} \left|\psi\left(x_1, x_2, t\right)\right|^2 \, \mathrm{d}x_j, \qquad \left(i \neq j = 1, 2\right). \tag{5.42}$$

Since we are dealing with symmetric wave functions, the two single-particle densities ($i = 1, 2$) are equal. For all the plots of the probability density (not the single-particle), the x_1 axis runs from left to right, and the x_2 axis from the top to the bottom of the plot, as seen in Figure 5.3a.

Non-Interacting Particles

The ten lowest eigenvalues E_j of the stationary problem are:

0.9659 0.9661 0.9663 1.8421 1.8423 1.8566 1.8568 2.4665 2.4666 2.6604

A single-particle density plot of the ten lowest states are shown in Figure 5.4a. The ground state is three-fold degenerate. The first and second excited states are doubly degenerate, and are barely distinguishable in the single-particle density plot. An initial state localized to the left dot can be created by the combination

$$\psi\left(t{=}0\right) = \frac{1}{2}\varphi_1 + \frac{1}{\sqrt{2}}\varphi_2 + \frac{1}{2}\varphi_3, \tag{5.43}$$

where φ_1 is the first state from the eigensolver program, φ_2 is the second state, and so on. From the plots of the ground state in Figure 5.1, it is easy to see why this particular combination gives a state localized to the left well. The angular frequency of the electric field is set to $\omega = \Delta E = 0.8762$, where ΔE is the difference in energy between the ground state and first excited state. This gives a number of time steps per oscillation of

$$n = \frac{2\pi}{\omega \Delta t} = 143.4 \tag{5.44}$$

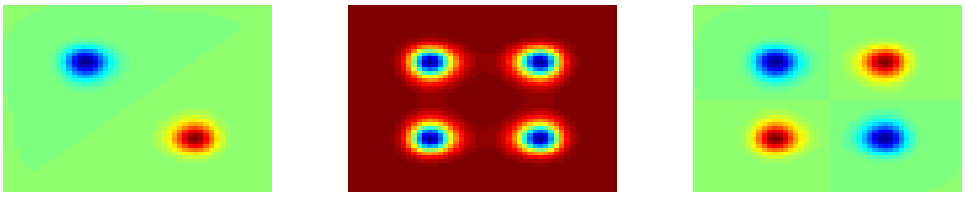

(a) φ_1 **(b)** φ_2 **(c)** φ_3

Figure 5.1: *Non-interacting particles: The three-fold degenerate ground state.*

Suffice it to say that this should be more than enough. The strength of the electric field is set to $E_0 = 0.1$. The probability of finding both particles as functions of the number of oscillations of the electric field is seen in Figure 5.3, where the initial particle density is also illustrated.

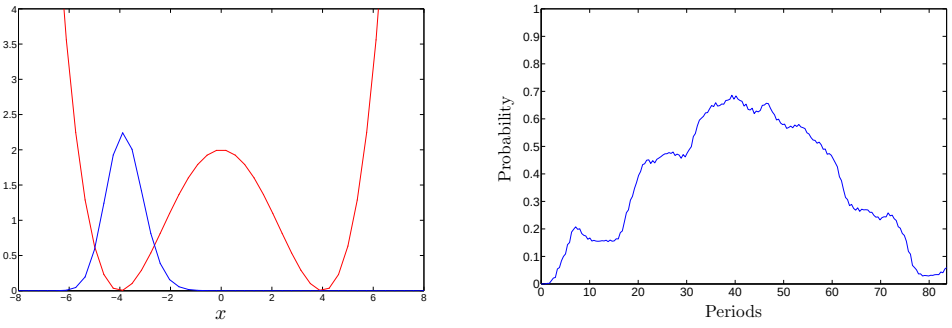

(a) Initial state

(b) Probability of finding both particles in the right well.

Figure 5.2: *Non-Interacting particles.*

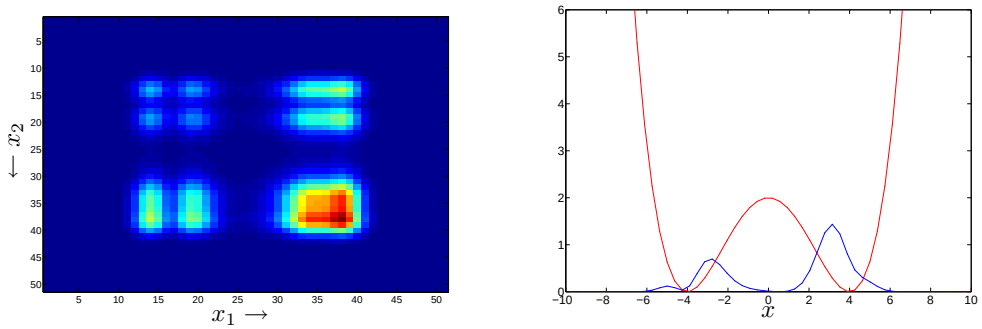

(a) Probability density

(b) Single-particle probability density.

Figure 5.3: *Non-Interacting particles: Midway through the simulation ($t = 300$). A significant proportion of the wave packet is here localized to the right well. The probability density (left) indicates that the wave function now contains substantial contributions from the excited states.*

Interacting Particles

The ten lowest eigenvalues E_j of the stationary problem are

1.0467	1.9369	1.9408	2.0321	2.0321	2.6059	2.6059	2.7961	2.7962	2.8351

As we see, the ground state is no longer degenerate, due to the interactions between the particles (see discussion in Section 5.1.2). A state localized to the left well can be created by setting

$$\psi\,(t{=}0) = \frac{1}{\sqrt{2}}\varphi_4 + \frac{1}{\sqrt{2}}\varphi_5. \tag{5.45}$$

Why this particular combination localizes the particle to the left well can be understood from Figure 5.5. Why there is no contribution from the three lowest states in Eq. (5.45) is evident from the probability density plot of these states in Figure 5.6, where we see that the electrons choose to reside in different wells.

I have repeated the simulations; this time with interactions turned on, for both $\omega = 0.8762$ as in the previous simulation, but also with $\omega = 0.5737$ corresponding to the spacing between the lowest-lying states in the interacting case. The number of time steps per oscillation is in the latter case

$$n = \frac{2\pi}{\omega\Delta t} = 219.02 \tag{5.46}$$

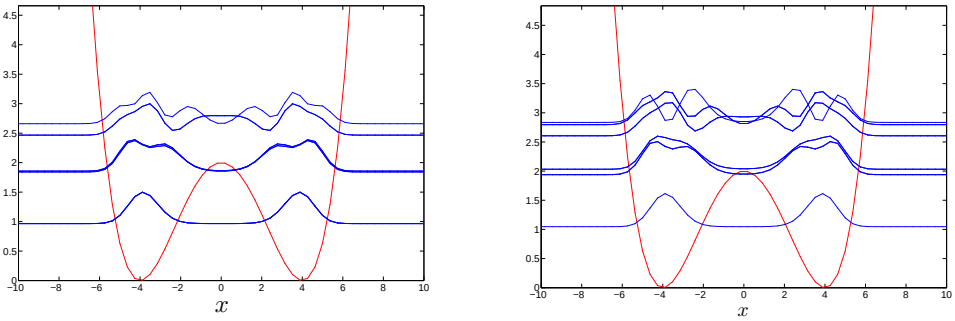

(a) Non-interacting particles. **(b)** Interacting particles.

Figure 5.4: *The ten lowest ground states.*

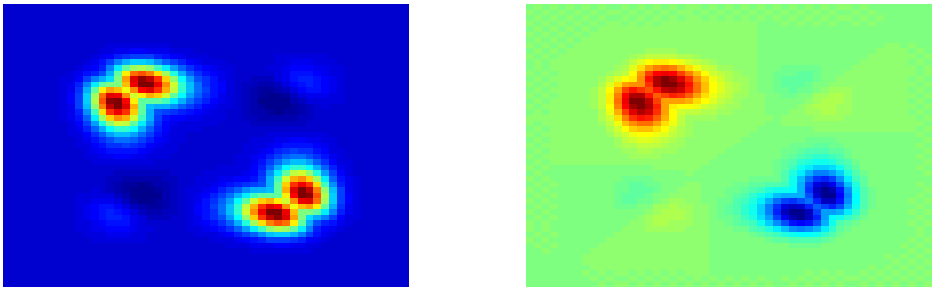

(a) Fourth excited state. **(b)** Fifth excited state.

Figure 5.5: *Interacting particles: Here the wave function is plotted.*

5.3.4 Discussion

For the simulation of the non-interacting system, after about 40 field cycles the probability of finding both electrons in the right dot reached a maximum of about 0.7. After 40 more field cycles the electrons are again (approximately) localized to the left dot. A further simulation study (not included) shows that this pattern repeats itself when extending the simulation time. We do not succeed in transferring the electrons to unit probability, but by tweaking the the distance between the well centres d, it might be tempting to think that a $100\ \%$ transfer can be achieved.

It is clear that when interaction is turned on, transport of the electrons becomes more difficult. The probabilities as function of time is very different in the two cases, with a much larger peak for the non-interacting case. This is a very interesting feature which should be investigated in more detail. By selecting a angular frequency of $\omega = 0.8762$

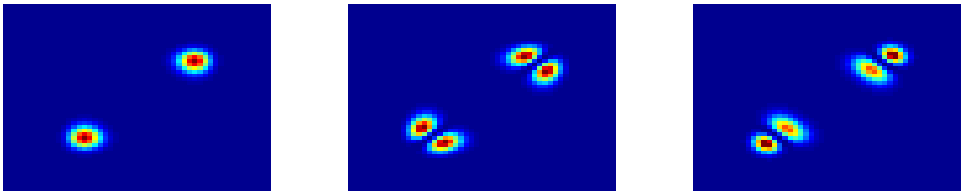

(a) Ground state. **(b)** First excited state. **(c)** Second excited state.

Figure 5.6: *Interacting particles: Probability densities.*

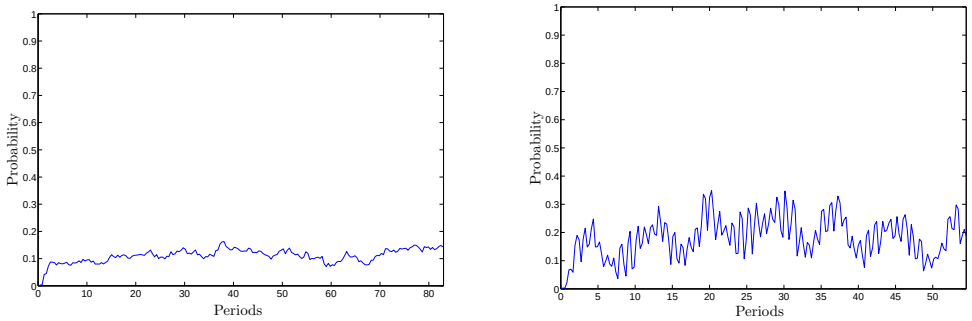

(a) $\omega = 0.8762$ **(b)** $\omega = 0.5737$

Figure 5.7: *Probability of finding both particles in the right dot, for a given angular frequency of the field.*

for the field, corresponding to the spacing in the non-interacting case, gives a completely different behaviour of the probability function than in the non-interacting case. We clearly hit some resonance phenomenon when we on the other hand set $\omega = 0.5737$ corresponding to the energy spacing in the interacting case.

Can we trust the simulations after this many cycles? This should be verified by using, e.g., using a larger basis size (larger nev) and increasing the accuracy of the spatial discretization. Nevertheless, we expect the interactions to profoundly alter the transport properties of the electric field.

Suggestions for future work

The first question that should be addressed before delving into a more serious study of this model, is whether we can trust the simulations. The properties and accuracy of the simulations should be studied when adjusting the size of the time step, the number of basis vectors, and the number of grid points in the spatial discretization.

For a given desired accuracy, it would be interesting to compare the cost of this scheme to a few of the other time-stepping schemes, e.g. the Crank-Nicolson scheme.

If we by adjusting the parameters in the simulation succeed in transferring the two electrons to the other dot, what happens when we turn off the field? Do they remain stationary there? If they "leak" over to the other well, for how long time are they approximately confined to the right well? How does it compare to the natural decoherence time observed in quantum dots? This last question is interesting when having applications for quantum information technology in mind.

In a more serious study of the transport properties of electrons in quantum dots it would be natural to look at a more realistic model of a quantum dot.

Chapter 6

Summary and Outlook

In this thesis the theoretical basis needed for a study of the electronic structure and the electron dynamics in quantum dots has been discussed, and a simple model illustrating electron transport between coupled quantum dots has been studied.

A short introduction to quantum dots was given in Chapter 2. More practical matters, such as how one can manufacture quantum dots, and experimental techniques for studying quantum phenomena in quantum dots, were also addressed. Methods for obtaining approximate solutions to the Schrödinger equation for several particles were discussed in Chapter 3. Methods for solving the time-dependent Schrödinger equation numerically were discussed in Chapter 4. Five different time stepping schemes were discussed in detail, of which four were put to test in several numerical experiments. One of these methods, referred to as the fourth-order method, was of relatively recent origin. It was of special interest, since it should give more accurate, and potentially less computationally demanding, simulations of time-dependent quantum systems. The numerical experiments revealed that the fourth-order method was indeed more accurate than the other methods to a significant degree, but failed to reach a conclusion as to whether the fourth-order could provide faster simulations at a desired accuracy.

In Chapter 5 the theoretical models used to study quantum dots were discussed, and a description of how one can modify the time-stepping schemes to simulate systems of two or three dimensions and of several particles was given. A one-dimensional model with two interacting electrons in a coupled quantum dot was studied numerically with the fourth-order time stepping scheme. The numerical experiment tried to reveal whether it would be possible, by applying an oscillating electric field to the system, to transport the electrons initially confined to one of the dots, to the other. It was shown that the interaction between the electrons had a negative impact on the possibility of transporting the two electrons between the dots.

There may be several ways of extending the work done in thesis. The question of whether the fourth-order method is better suited for studying physical phenomena

than more traditional methods when computation cost is taken into account, is still an open one. Conclusive tests should be carried out to verify or falsify this. It would further be interesting to look at more realistic models of quantum dots. If the fourth-order method is shown to be superior to the other methods, it would be the natural choice for studying time-dependent problems in quantum dots.

Bibliography

[1] S. Blanes and P. C. Moan. Splitting methods for the time-dependent schrödinger equation. *Physics Letters A*, 265(1-2):35 – 42, 2000.

[2] J. Singh. *Electronic and Optoelectronic Properties of Semiconductor Structures*. Cambridge University Press, 2003.

[3] L. Jacak. Semiconductor quantum dots - towards a new generation of semiconductor devices. *European Journal of Physics*, 21:487–497, November 2000.

[4] S. Kvaal. *Analysis of many-body methods for quantum dots*. PhD thesis, University of Oslo, 2008.

[5] S. Kiravittaya, A. Rastelli, and O. G Schmidt. Advanced quantum dot configurations. *Reports on Progress in Physics*, 72(4):046502 (34pp), 2009.

[6] D. Loss and D. P. DiVincenzo. Quantum computation with quantum dots. *Phys. Rev. A*, 57(1):120–126, Jan 1998.

[7] C. Marcus L. Kouwenhoven. Quantum dots. *Physics World*, June 1998.

[8] S. Tarucha, D. G. Austing, T. Honda, R. J. van der Hage, and L. P. Kouwenhoven. Shell filling and spin effects in a few electron quantum dot. *Phys. Rev. Lett.*, 77(17):3613–3616, Oct 1996.

[9] S. Tarucha, Austing, and L. P. Kouwenhoven. Few-electron quantum dots. *Reports on progress in physics*, (64):701–736, 2001.

[10] S. M. Reimann and M. Manninen. Electronic structure of quantum dots. *Rev. Mod. Phys.*, 74(4):1283–1342, Nov 2002.

[11] P. C. Hemmer. *Kvantemekanikk*. Tapir akademisk forlag, 1993.

[12] R. J. Bartlett and M. Musiał. Co.pled-cluster theor. in quantum chemistry. *Rev. Mod. Phys.*, 79(1):291, 2007.

[13] P. C. Hemmer. *Kvantemekanikk 2*.

[14] E. Waltersson and E. Lindroth. Many-body perturbation theory calculations on circular quantum dots. *Physical Review B (Condensed Matter and Materials Physics)*, 76(4):045314, 2007.

[15] W. Kohn. Nobel lecture: Electronic structure of matter—wave functions and density functionals. *Rev. Mod. Phys.*, 71(5):1253–1266, Oct 1999.

[16] W. Kohn and L. J. Sham. Self-consistent equations including exchange and correlation effects. *Phys. Rev.*, 140(4A):A1133–A1138, Nov 1965.

[17] S. Kvaal, M. Hjorth-Jensen, and H. M. Nilsen. Effective interactions, large-scale diagonalization, and one-dimensional quantum dots. *Physical Review B (Condensed Matter and Materials Physics)*, 76(8):085421, 2007.

[18] S. Kvaal. Open source fci code for quantum dots and effective interactions. *arXiv:0810.2644v1*.

[19] M. Rontani, C. Cavazzoni, D. Bellucci, and G. Goldoni. Full configuration interaction approach to the few-electron problem in artificial atoms. *J. Chem. Phys.*, 124:124102, 2006.

[20] V. Popsueva. *Structure and Dynamics of Few-Electron Quantum Dot Molecules*. PhD thesis, University of Bergen, 2007.

[21] J. P. Boyd. *Chebyshev and Fourier Spectral Methods*. DOVER Publications, Inc., 2000.

[22] Morten Hjorth-Jensen. Computational physics, lecture notes 2008.

[23] S. Kvaal. *A Critical Study of the Finite Difference and Finite Element Methods for the Time Dependent Schrödinger Equation*. Master's thesis, University of Oslo, 2004.

[24] A. Askar and A. S. Cakmak. Explicit integration method for the time-dependent schrodinger equation for collision problems. *The Journal of Chemical Physics*, 68(6):2794–2798, 1978.

[25] W. Magnus. On the exponential solution of differential equations for a linear operator. *Communications on Pure and Applied Mathematics*, 7(4):649–673, 1954.

[26] J. Ros S. Blanes, F. Casas. Improved high order integrators based on the magnus expansion. *BIT Numerical Mathematics*, 40(3):434–450, Sep 2000.

[27] J. A. Oteo and J. Ros. From time-ordered products to magnus expansion. *Journal of Mathematical Physics*, 41(5):3268–3277, 2000.

[28] B.H. Bransden & C.J. Joachain. *Quantum Mechanics (2nd Edition)*. Benjamin Cummings, 2000.

[29] L. B. Madsen. Gauge invariance in the interaction between atoms and few-cycle laser pulses. *Phys. Rev. A*, 65(5):053417, May 2002.

[30] R. B. Sidje. Expokit: a software package for computing matrix exponentials. *ACM Trans. Math. Softw.*, 24(1):130–156, 1998.

[31] U. Meirav, M. A. Kastner, and S. J. Wind. Single-electron charging and periodic conductance resonances in gaas nanostructures. *Phys. Rev. Lett.*, 65(6):771–774, Aug 1990.

[32] P. Matagne and J.-P. Leburton. Three-dimensional analysis of the electronic structure of cylindrical vertical quantum dots. *Phys. Rev. B*, 65(23):235323, Jun 2002.

[33] P. M. Mathews & K. Venkatesan. *A Textbook of Quantum Mechanics*. McGraw-Hill Companies, 1979.

[34] H. R. Reiss. Dipole-approximation magnetic fields in strong laser beams. *Phys. Rev. A*, 63(1):013409, Dec 2000.

[35] J. J.V. Maestri, R. H. Landau, and M. J. Páez. Two-particle schrödinger equation animations of wave packet–wave packet scattering. *American Journal of Physics*, 68(12):1113–1119, 2000.

[36] Vetterling Press, Teukolsky and Flannery. *Numerical Recipes in C++*. Cambridge, year = 2005.

[37] S. Selstø and M. Førre. Coherent single-electron transport between coupled quantum dots. *Physical Review B (Condensed Matter and Materials Physics)*, 74(19):195327, 2006.

Appendix A

The Discrete Fourier Transform

The motivation for the Fourier transform comes from the study of Fourier series. In the study of Fourier series, periodic functions of arbitrary shape can be written as the sum of sines and cosines. The Fourier transform can be seen as a limiting case of the Fourier series, where the period goes to infinity. A function can be thought of as having two equivalent representations, one in the familiar spatial representation and one in the frequency domain (the Fourier transform is most often discussed in the case of a time-dependent function, hence the use of the word frequency) . One changes between the two representations by the means of the Fourier transform equations,

$$\begin{aligned} H(f) &= \int_{-\infty}^{\infty} h(x) \mathrm{e}^{2\pi i f x} \, \mathrm{d}x \\ h(x) &= \int_{-\infty}^{\infty} H(f) \mathrm{e}^{-2\pi i f x} \, \mathrm{d}f. \end{aligned} \tag{A.1}$$

We note that there are other conventions in use as well. Describing the Fourier transform in term of the angular frequency $w \equiv 2\pi f$ gives

$$\begin{aligned} H(w) &= \int_{-\infty}^{\infty} h(x) \mathrm{e}^{iwx} \, \mathrm{d}x \\ h(x) &= \frac{1}{2\pi} \int_{-\infty}^{\infty} H(w) \mathrm{e}^{-iwx} \, \mathrm{d}w. \end{aligned} \tag{A.2}$$

Another popular convention is to split the factor of 2π evenly between the Fourier transform and its inverse, which leads to definitions

$$\begin{aligned} H(w) &= \frac{1}{\sqrt{2\pi}} \int_{-\infty}^{\infty} h(x) \mathrm{e}^{iwx} \, \mathrm{d}x \\ h(x) &= \frac{1}{\sqrt{2\pi}} \int_{-\infty}^{\infty} H(w) \mathrm{e}^{-iwx} \, \mathrm{d}w. \end{aligned} \tag{A.3}$$

This convention, incidentally, is equal to how we transform between the spatial and momentum representations of the wave function in quantum mechanics. It also restores the symmetry between the Fourier transform and its inverse.

The Discrete Fourier Transform Usually we are faced with the problem of determining the Fourier transform of a function $h(x)$ when the function values are only known at a discrete set of points. Let these points be equally spaced as $h_m = h(x_0 + m\Delta x)$, where $m = 0, 1, 2, \ldots, N-1$ [1][2]. With N numbers of input we are obviously going to produce no more than N independent numbers of output. We choose some maximum frequency f_c and seek estimates only at discrete points $f_n = nf_c$, where $n = -N/2, \ldots, N/2$. It can be shown that in order to avoid aliasing effects f_c must in general be chosen no larger than the Nyquist critical frequency, given by $f_c = \frac{1}{2\Delta x}$.

Approximating the Fourier transform by a sum gives us

$$H(f_n) = \int_{-\infty}^{\infty} h(x) \mathrm{e}^{2\pi i f_n x} \, \mathrm{d}x \approx \sum_{m=0}^{N-1} h_m \mathrm{e}^{2\pi i f_n x_m} \Delta x = \Delta x \sum_{m=0}^{N-1} h_m \mathrm{e}^{2\pi i n m/N}. \tag{A.4}$$

The final summation is called the discrete Fourier transform:

$$H_n \equiv \sum_{m=0}^{N-1} h_m \mathrm{e}^{2\pi i n m/N}. \tag{A.5}$$

The inverse Fourier transform, which recovers the points f_m exactly from the points H_n is given by

$$h_m = \frac{1}{N} \sum_{n=0}^{N-1} H_n \mathrm{e}^{-2\pi i n m/N}. \tag{A.6}$$

[1] We have assumed for simplicity that N is even

[2] There are evidently $N+1$ points here, but the transform is in fact periodic with $F_{N/2} = F_{-N/2}$, and thus there are only N independent numbers.

The Fast Fourier Transform The fast Fourier transform (FFT) is an efficient algorithm for computing the discrete Fourier transform and its inverse. Computing the discrete Fourier transform directly from the definition is often too slow to be practical. Using FFT we can speed up this calculation. Computing the discrete Fourier transform of N points using the definition directly, takes $\mathcal{O}(N^2)$ operations, while with the FFT we can compute the same result in only $\mathcal{O}(N \log N)$ operations. The difference in speed can be substantial, and in many cases the computation time can be reduced by several orders of magnitude. The improvement is roughly proportional to $N/\log(N)$. This huge improvement has made many algorithms based on the discrete Fourier transform practical. The Cooley-Tukey algorithm is the most common fast Fourier transform algorithm. As a result of the factorization approach taken by this method, the number of points that are transformed by the FFT is of the form 2^k.

Appendix B

Program Listings

In this appendix I will list some of MATLAB programs written for studying the time stepping schemes in Chapter 4. For brevity I will only include the code of one of the time stepping schemes, the fourth-order method. The programs have been described briefly in Chapter 4.

B.1 FourthOrderMethod.m

```
function [norm,meanX,energy,psiBM,psiFinal] = FourthOrderMethod(Psi0,E,Emax,Vstat,N,L,tFinal,tSteps,discretization,
    updateStep,savePsi,saveMeans)
% Calculates time propagation of a given initial wave packet in the
% position representation using a fourth order method first proposed by
% Moan & Banes. The matrix exponentials are calculated with the Expokit
% package.

% Grid properties
switch discretization
   case 'fourier'
        Xmax = L/2;
        Xmin = -Xmax;
        dx = (Xmax-Xmin)/N;
        x = linspace(Xmin, Xmax,N+1); % The wavefunction becomes periodic
        x = x(1:N);
        X = diag(x);
        k = ifftshift(-N/2:(N/2-1))/(Xmax-Xmin);
    otherwise
        Xmax = L/2;
        Xmin = -Xmax;
        x = linspace(Xmin,Xmax,N); % The wavefunction is zero at Xmax and Xmin
        dx = x(2)-x(1);
        X = diag(x);
end

% Time properties
dt = tFinal/tSteps;
meanX = zeros(1,tSteps/saveMeans+1);
norm = zeros(1,tSteps/saveMeans+1);
energy = zeros(1,tSteps/saveMeans+1);
psiBM = zeros(N,tSteps/savePsi+1);

% Initial wave packet
Psi = (Psi0(x)).'; % The wave function is a column vector

% External time-independent potential
Trap = Vstat(x);

% Matrix representation of H_0 (that is, the time independent part of the
```

```
% Hamiltonian)
switch discretization
   case 'second'
        % Setting up the matrix representation of T and V:
        d = 1/dx^2; % Diagonal elements in T
        e = -1/(2*dx^2); % Off-diagonal elements in T
        V = diag(Trap);
        T = diag(d*ones(1,N));
        T(2:(N),1:(N-1)) = diag(e*ones(1,(N-1))) + T(2:(N),1:(N-1));
        T(1:(N-1),2:N) = diag(e*ones(1,(N-1))) + T(1:(N-1),2:N);
        H = V + T;
        H = sparse(H);
        X = sparse(X);
   case 'fourth'
       % By using a so-called five point stencil we lower the error to
       % fourth order for the finite difference method.
       % Setting up the matrix representation of T and V:
        d = 30/(24*dx^2); % Diagonal elements in T
        e = -16/(24*dx^2); % Off-diagonal elements in T
        f = 1/(24*dx^2); % Off-diagonal elements in T
        V = diag(Trap);
        T = diag(d*ones(1,N));
        T(2:(N),1:(N-1)) = diag(e*ones(1,(N-1))) + T(2:(N),1:(N-1));
        T(1:(N-1),2:N) = diag(e*ones(1,(N-1))) + T(1:(N-1),2:N);
        T(3:(N),1:(N-2)) = diag(f*ones(1,(N-2))) + T(3:(N),1:(N-2));
        T(1:(N-2),3:N) = diag(f*ones(1,(N-2))) + T(1:(N-2),3:N);
        H = V + T;
        H = sparse(H);
        X = sparse(X);
    case 'fourier'
       T = diag(2*pi^2*k.*k); % Uncertain of numerical factors here...
       V = diag(Trap);
       M = ifft(T*fft(eye(N))); %M is a dense matrix
end

% Set plot properties
figure
psiPlot = plot(x,abs(Psi).^2);
hold on
%plot(x,Trap/max(abs(Trap)),'g');
title('Fourth-Order Method');
axis([Xmin,Xmax,0,max(abs(Psi).^2)*1.1]);
drawnow;

% Gaussian integration properties
n = 10; % Number of quadrature points
[abscissa,weights] = gauleg(n);

% Values to set before starting time propagation
meanX(1) = SimpsonsRule(abs(Psi.').^2.*x,dx);
norm(1) = SimpsonsRule(abs(Psi).^2,dx);
psiBM(:,1) = Psi;
switch discretization
   case 'fourier'
        energy(1) = SimpsonsRule(Psi'*(M+V)*Psi,dx);
    otherwise
        energy(1) = (Psi'*(H)*Psi)/(Psi'*Psi);
end

% Time propagation
switch discretization
    case 'fourier'
        for j = 1:tSteps
            tPrev = (j-1) / tSteps * tFinal;
            tNow = j / tSteps * tFinal;
            tGau = tPrev + (abscissa+1)*dt/2;
            wGau = weights*dt/2;
            H_0 = -i*dt*(M+V)-i*X*sum(E(tGau).*wGau);
            if Emax == 0 % For time-indep. Hamiltonians it is easy to show that H_1=0
                Omega4 = H_0;
            else
                Integrand = @(y) E(y).*(y-(tPrev+dt/2));
                H_1 = -i/dt*sum(Integrand(tGau).*wGau)*X;
                Omega4 = H_0-H_0*H_1+H_1*H_0;
            end
            Psi = expv( 1, Omega4, Psi);
            if mod(j,updateStep) == 0
                    set(psiPlot,'ydata',abs(Psi).^2);
                    drawnow;
            end
            if mod(j,saveMeans) == 0
                meanX(j/saveMeans+1) = SimpsonsRule(abs(Psi.').^2.*x,dx);
                norm(j/saveMeans+1) = SimpsonsRule(abs(Psi).^2,dx);
```

```
            energy(j+1) = (Psi'*(M+V)*Psi)/(Psi.'*Psi);
        end
        if mod(j,savePsi) == 0
            psiBM(:,j/savePsi+1) = Psi;
        end
    end
otherwise
    for j = 1:tSteps
        tPrev = (j-1) / tSteps * tFinal;
        tNow = j / tSteps * tFinal;
        tGau = tPrev + (abscissa+1)*dt/2;
        wGau = weights*dt/2;
        Integrand = @(y) E(y).*(y-(tPrev+dt/2));
        H_0 = -i*dt*H-i*X*sum(E(tGau).*wGau);
        H_1 = -i/dt*sum(Integrand(tGau).*wGau)*X;
        Omega4 = H_0-H_0*H_1+H_1*H_0;
        Psi = expv( 1, Omega4, Psi);
        if mod(j,updateStep) == 0
            set(psiPlot,'ydata',abs(Psi).^2);
            drawnow;
        end
        if mod(j,saveMeans) == 0
            meanX(j/saveMeans+1) = SimpsonsRule(abs(Psi.').^2.*x,dx);
            norm(j/saveMeans+1) = SimpsonsRule(abs(Psi).^2,dx);
            energy(j/saveMeans+1) = (Psi'*(H)*Psi)/(Psi'*Psi);
        end
        if mod(j,savePsi) == 0
            psiBM(:,j/savePsi+1) = Psi;
        end
    end
end
close;
psiFinal = Psi;
end
```

B.2 ExactSolution.m

```
function [norm,meanX,energy,psiExact,psiFinal] = ExactSolution(E,p0,N,L,tFinal,tSteps,updateStep,Emax,T,w,sigma,
    savePsi,saveMeans)
%EXACTSOLUTION From the analytical solution in momentum space, the same
%quantities that are calculated by the approxiate methods are produced. The
%transformation to position space is implemented with the fast Fourier
%transform.

Xmax = L/2;
Xmin = -Xmax;
dx = (Xmax-Xmin)/N;
x = linspace(Xmin, Xmax,N+1); % The wavefunction becomes periodic
x = x(1:N);

f_c = 1/(2*dx);
f = linspace(-f_c, f_c, N+1)';
f = ifftshift(f(1:N));
df = f(2)-f(1);

meanX = zeros(1,tSteps/saveMeans+1);
norm = zeros(1,tSteps/saveMeans+1);
energy = zeros(1,tSteps/saveMeans+1);
psiExact = zeros(N,tSteps/savePsi+1);

Pi = pi;
I = i;

% THE COMPLICATED ELECTRIC FIELD -> Emax*sin(pi*t/T).^2.*sin(w*t)
phiFunction = @(p,t) 2^(1/2)/sigma^(1/2)*Pi^(1/4)*exp(-1/2*(p-1/4*(-8*Pi^2+8*cos(w*t)*Pi^2-2*T*cos((w*T+2*Pi)/T*t)*w
    *Pi+2*T*cos((-w*T+2*Pi)/T*t)*w*Pi+T^2*cos((w*T+2*Pi)/T*t)*w^2+T^2*cos((-w*T+2*Pi)/T*t)*w^2-2*cos(w*t)*w^2*T^2)
    *Emax/w/(w*T+2*Pi)/(-w*T+2*Pi)).^2/sigma^2).*exp(-1/2*I*((p-1/4*(-8*Pi^2+8*cos(w*t)*Pi^2-2*T*cos((w*T+2*Pi)/T*
    t)*w*Pi+2*T*cos((-w*T+2*Pi)/T*t)*w*Pi+T^2*cos((w*T+2*Pi)/T*t)*w^2+T^2*cos((-w*T+2*Pi)/T*t)*w^2-2*cos(w*t)*w^2*
    T^2)*Emax/w/(w*T+2*Pi)/(-w*T+2*Pi)).^2*t-1/2*(p-1/4*(-8*Pi^2+8*cos(w*t)*Pi^2-2*T*cos((w*T+2*Pi)/T*t)*w*Pi+2*T*
    cos((-w*T+2*Pi)/T*t)*w*Pi+T^2*cos((w*T+2*Pi)/T*t)*w^2+T^2*cos((-w*T+2*Pi)/T*t)*w^2-2*cos(w*t)*w^2*T^2)*Emax/w
    /(w*T+2*Pi)/(-w*T+2*Pi))*Emax*(-8*Pi^2*t*w^3*T^2+32*Pi^4*t*w+16*w^2*T^2*sin(w*t)*Pi^2-32*Pi^4*sin(w*t)-4*w^3*T
    ^3*sin((w*T+2*Pi)/T*t)*Pi+4*w^2*T^2*Pi^2*sin((w*T+2*Pi)/T*t)-4*w^3*T^3*Pi*sin((-w*T+2*Pi)/T*t)-4*w^2*T^2*Pi^2*
    sin((-w*T+2*Pi)/T*t)+w^4*T^4*sin((w*T+2*Pi)/T*t)-w^4*T^4*sin((-w*T+2*Pi)/T*t)-2*w^4*T^4*sin(w*t))/w^2/(w*T+2*
    Pi)^2/(-w*T+2*Pi)^2+1/64*Emax^2*(1536*Pi^9*t*w+w^9*T^9*sin(4*Pi*t/T)-6*w^7*T^7*sin(2*(w*T+2*Pi)/T*t)*Pi^2-192*
    w^5*T^5*sin(2*Pi*t/T)*Pi^4+128*w^2*T^2*sin(2*t*(-w*T+Pi)/T)*Pi^7-96*w^5*T^5*sin(2*t*(-w*T+Pi)/T)*Pi^4-24*w^6*T
    ^6*sin(2*t*(-w*T+Pi)/T)*Pi^3+72*w^7*T^7*sin(2*Pi*t/T)*Pi^2+672*w^5*T^4*Pi^5*t-108*w^7*T^6*Pi^3*t-2112*w^3*T^2*
    Pi^7*t+12*w^9*T^8*t*Pi-1152*Pi^5*sin(w*t)*w^4*T^4-2*w^5*T^5*sin(2*(w*T+2*Pi)/T*t)*Pi^4+11*w^6*T^6*sin(2*(w*T
    +2*Pi)/T*t)*Pi^3-12*w^4*T^4*sin(2*(w*T+2*Pi)/T*t)*Pi^5+12*w^7*T^7*sin(2*t*(-w*T+Pi)/T)*Pi^2-9*w^7*T^7*sin(4*Pi
    *t/T)*Pi^2+192*w^3*T^3*sin(2*t*(w*T+Pi)/T)*Pi^6-128*w^2*T^2*sin(2*t*(w*T+Pi)/T)*Pi^7-70*sin(2*w*t)*Pi^3*w^6*T
    ^6+192*w^3*T^3*sin(2*t*(-w*T+Pi)/T)*Pi^6+8*w^3*T^3*sin(2*(-w*T+2*Pi)/T*t)*Pi^6-192*w^4*T^4*Pi^5*sin((w*T+2*Pi)
```

```
        /T*t)+4*w^8*T^8*sin(2*t*(-w*T+Pi)/T)*Pi+24*w^5*T^5*sin(4*Pi*t/T)*Pi^4-16*w^3*T^3*sin(4*Pi*t/T)*Pi^6+128*w^3*T
        ^3*sin(2*Pi*t/T)*Pi^6-256*Pi^7*w^2*T^2*sin((-w*T+2*Pi)/T*t)+128*Pi^3*sin(w*t)*w^6*T^6+8*w^3*T^3*sin(2*(w*T+2*
        Pi)/T*t)*Pi^6-96*w^5*T^5*sin(2*t*(w*T+Pi)/T)*Pi^4-4*w^8*T^8*sin(2*t*(w*T+Pi)/T)*Pi+24*w^6*T^6*sin(2*t*(w*T+Pi)
        /T)*Pi^3+12*w^7*T^7*sin(2*t*(w*T+Pi)/T)*Pi^2+256*w^2*T^2*Pi^7*sin((w*T+2*Pi)/T*t)-64*w^6*T^6*Pi^3*sin((w*T+2*
        Pi)/T*t)+288*sin(2*w*t)*Pi^5*w^4*T^4+6*sin(2*w*t)*Pi*w^8*T^8-480*sin(2*w*t)*Pi^7*w^2*T^2+192*Pi^5*w^4*T^4*sin
        ((-w*T+2*Pi)/T*t)-256*Pi^6*w^3*T^3*sin((-w*T+2*Pi)/T*t)-256*w^3*T^3*Pi^6*sin((w*T+2*Pi)/T*t)+256*w^5*T^5*Pi^4*
        sin((w*T+2*Pi)/T*t)+64*Pi^3*w^6*T^6*sin((-w*T+2*Pi)/T*t)+12*w^4*T^4*sin(2*(-w*T+2*Pi)/T*t)*Pi^5-6*w^7*T^7*sin
        (2*(-w*T+2*Pi)/T*t)*Pi^2-2*w^5*T^5*sin(2*(-w*T+2*Pi)/T*t)*Pi^4-2048*Pi^9*sin(w*t)+256*sin(2*w*t)*Pi^9-11*w^6*T
        ^6*sin(2*(-w*T+2*Pi)/T*t)*Pi^3+w^8*T^8*sin(2*(w*T+2*Pi)/T*t)*Pi+3072*Pi^7*sin(w*t)*w^2*T^2-8*w^9*T^9*sin(2*Pi*
        t/T)-w^8*T^8*sin(2*(-w*T+2*Pi)/T*t)*Pi+256*Pi^4*w^5*T^5*sin((-w*T+2*Pi)/T*t))/w^3/(w*T+2*Pi)^3/(-w*T+2*Pi)^3/
        Pi/(-w*T+Pi)/(w*T+Pi)));
meanXAnalytical = @(t) -1/4*Emax*(-8*Pi^2*t*w^3*T^2+32*Pi^4*t*w+16*w^2*T^2*sin(w*t)*Pi^2-32*Pi^4*sin(w*t)-4*w^3*T^3*
        sin((w*T+2*Pi)/T*t)*Pi+4*w^2*T^2*Pi^2*sin((w*T+2*Pi)/T*t)-4*w^3*T^3*Pi*sin((-w*T+2*Pi)/T*t)-4*w^2*T^2*Pi^2*sin
        ((-w*T+2*Pi)/T*t)+w^4*T^4*sin((w*T+2*Pi)/T*t)-w^4*T^4*sin((-w*T+2*Pi)/T*t)-2*w^4*T^4*sin(w*t))/w^2/(w*T+2*Pi)
        ^2/(-w*T+2*Pi)^2;

% THE SIMPLE ELECTRIC FIELD --> Emax*cos(w*t)
%phiFunction = @(p,t) 2^(1/2)/sigma^(1/2)*Pi^(1/4)*exp(-1/2*(p+Emax/w*sin(w*t)).^2/sigma^2).*exp(-1/2*I*((p+Emax/w*
        sin(w*t)).^2*t+2*(p+Emax/w*sin(w*t))*Emax*(-1+cos(w*t))/w^2+1/2*Emax^2*(-cos(w*t)*sin(w*t)+w*t)/w^3));
%meanXAnalytical = @(t) Emax*(-1+cos(w*t))/w^2;

% THE SIMPLE ELECTRIC FIELD --> Emax*sin(w*t)
%phiFunction = @(p,t) 2^(1/2)/sigma^(1/2)*Pi^(1/4)*exp(-1/2*(p-Emax*(-1+cos(w*t))/w).^2/sigma^2).*exp(-1/2*I*((p-
        Emax*(-1+cos(w*t))/w).^2*t-2*(p-Emax*(-1+cos(w*t))/w)*Emax*(w*t-sin(w*t))/w^2+1/2*Emax^2*(3*w*t-4*sin(w*t)+cos
        (w*t)*sin(w*t))/w^3));
%meanXAnalytical = @(t) -Emax*(w*t-sin(w*t))/w^2;

%Psi = (1/dx) * ifft( phiFunction(2*pi*f,0) );
%Psi = ifftshift(Psi);

% If Emax=0 we have explicit analytic solutions in the spatial representation
PsiElOff = @(x,t) pi^(-1/4)*sqrt(sigma/(1+i*sigma^2*t))*exp((i*p0*x-sigma^2*x.^2/2-i*p0^2*t/2)/(1+i*sigma^2*t));

% Initial state values
Psi0 = (1/dx) * ifft( exp(2*pi*i*f*Xmin) .* phiFunction(2*pi*f,0) );
meanX(1) = meanXAnalytical(0);
norm(1) = SimpsonsRule(abs(Psi0').^2,dx);
%energy(1) = E(0)*meanXAnalytical(0)+SimpsonsRule(0.5*(2*pi*f).^2.*abs(phiFunction(2*pi*f,0)).^2,df*2*pi);
switch Emax
    case 0
        psiExact(:,1) = PsiElOff(x,0);
    otherwise
        psiExact(:,1) = Psi0;
end

% Set plot properties
figure;
psiPlot = plot(x,abs(Psi0).^2);
hold on;
axis([Xmin,Xmax,0,max(abs(Psi0).^2)*1.1]);
title('Exact solution');
drawnow;

% Calculate Psi(x,t)
for j=1:tSteps
    tNow = j / tSteps * tFinal;
  Psi = (1/dx) * ifft( exp(2*pi*i*f*Xmin) .* phiFunction(2*pi*f,tNow) );

  if mod(j,updateStep) == 0
        set(psiPlot,'ydata',abs(Psi).^2);
        drawnow;
    end

    if mod(j,saveMeans) == 0
        meanX(j/saveMeans+1) = meanXAnalytical(tNow);
        norm(j/saveMeans+1) = SimpsonsRule(abs(Psi).^2,dx);
        %energy(j/saveMeans+1) = SimpsonsRule(0.5*(2*pi*f).^2.*abs(phiFunction(2*pi*f,tNow)).^2,df);
    end

  if mod(j,savePsi) == 0
         switch Emax
            case 0
                psiExact(:,j/savePsi+1) = PsiElOff(x,tNow);
            otherwise
                psiExact(:,j/savePsi+1) = Psi;
         end
  end

end

close;
psiFinal = Psi;
end
```

B.3 CompareMethods.m

```
N = 2*64; % Number of inner grid points (matrix size becomes N^2)
L = 40; % Length of discretization interval
tFinal = 1; % Propagate wave function to time tFinal
tSteps = 1000; % Number of time steps
discretization = 'fourier'; % Options: 'second', 'fourth', 'fourier'.
updateStep = 30; % How often to update the animation
savePsi = 10; % Save the wave function every savePsi steps. tSteps/savePsi must be an integer.
saveMeans = 10; % Save the meanX, norm, energy at every saveMeans steps. tSteps/saveMeans must be an integer.
t = linspace(0,tFinal,tSteps/saveMeans+1); % For the sake of plotting

% Initial wave function (Normalized gaussian wave packet)
sigma = 1/4;
x0 = 0;
k0 = 0;
p0 = 0;
Psi0 = @(x) sqrt(sigma)*pi^(-1/4)*exp(-0.5*sigma^2*x.^2);

% Trap potential
Vstat = @(x)0.0*x.^2;

% Time-dependent perturbation (of the form E(t)*x)
Emax = 3;
T = tFinal;
w = 2;
E = @(t) Emax*sin(pi*t/T).^2.*sin(w*t);

% The simulation
tic;
[normLF,meanXLF,energyLF,psiLF,psiFinalLF] = LeapFrog(Psi0,E,Vstat,N,L,tFinal,tSteps,discretization,updateStep,
    savePsi,saveMeans);
[normCN,meanXCN,energyCN,psiCN,psiFinalCN] = LeapFrogTest(Psi0,E,Vstat,N,L,tFinal,tSteps,discretization,updateStep,
    savePsi,saveMeans);
[normSS,meanXSS,energySS,psiSS,psiFinalSS] = PseudoSpectral(Psi0,E,Vstat,N,L,tFinal,tSteps,discretization,updateStep
    ,savePsi,saveMeans);
[normBM,meanXBM,energyBM,psiBM,psiFinalBM] = FourthOrderMethod(Psi0,E,Emax,Vstat,N,L,tFinal,tSteps,discretization,
    updateStep,savePsi,saveMeans);
[normExact,meanXExact,energyExact,psiExact,psiFinalExact] = ExactSolution(E,p0,N,L,tFinal,tSteps,updateStep,Emax,T,w
    ,sigma,savePsi,saveMeans);
timeOfSim = toc;
```